Linkages between Eurasian Snow Cover and Northern Hemisphere Winter-time Climate Variability

by

Kazuyuki Saito

B.Eng., Mathematical Engineering, University of Tokyo (1989)
M.Eng., Mathematical Engineering, University of Tokyo (1992)

Submitted to the Department of Earth, Atmospheric and Planetary Sciences in Partial Fulfillment of the Requirements for the Degree of Master of Science in Climate Physics and Chemistry

at the

Massachusetts Institute of Technology

June 2000

Signature of Author .....
Department of Earth, Atmospheric and Planetary Sciences
May 5, 2000

Certified by .....
Dara Entekhabi
Associate Professor
Thesis Supervisor

Accepted by .....
Ronald G. Prinn
Department Head

Linkages between Eurasian Snow Cover and
Northern Hemisphere Winter-time Climate Variability

by

Kazuyuki Saito

Submitted to the Department of Earth, Atmospheric and Planetary
Sciences on May 5, 2000 in partial fulfillment of the requirements
for the Degree of Master of Science in Climate Physics and Chemistry

Abstract

Recently it has been shown that the Eurasian snow cover in the prior autumn (ESC_{SON}) and the leading mode variability in the wintertime extratropical Northern Hemisphere (NH) atmospheric circulation have significant correlation. In this study, a linkage between the ESC_{SON} and the following wintertime NH climate variability was investigated.

Satellite data from the NOAA is used for snow cover, and NCEP/NCAR Reanalysis data are used for climate variables. The high latitudes sea-level pressure is quality-controlled by use of the IABP sea-level pressure dataset, which is derived from the buoy observations. Interannual variability of and association between ESC_{SON} and winter climate variables were surveyed by use of linear statistical analysis techniques; Empirical Orthogonal Function (EOF) analysis, and correlation/regression analysis.

The gravity current by the expansion of the cold, dense air over Siberia north- and westward remained one among the several possible mechanisms. The upper air mechanism may be active to connect the ESC_{SON} and the leading mode of DJF surface pressure variability. It is also suggested that the DJF sea-level pressure variations associated with the ESC_{SON} is considerably confined to the Atlantic side, and has only limited association with the linear trend and the Pacific side variations.

Future work may include reexamination of the results using the possible, longer data of the observation. The mechanism connecting the ESC_{SON} anomalies and the upper level circulation anomaly should be investigated further, for which one possible approach is analysis of the wave activity and energy propagation in the troposphere and stratosphere.

Thesis Supervisor: Dara Entekhabi
Title: Associate Professor

Acknowledgment

The author would like to express his gratitude to Prof. Dara Entekhabi and Dr. Judah Cohen for their persistent supervision, enthusiastic guidance and helpful suggestions in starting, progressing, and completing this thesis research.

He also thanks his wife, Kaoru, and his son, Hajime Zorg, for their support, patience, and encouragement.

Contents

List of Figures

List of Tables

Chapter 1

Introduction

Boreal winter (December-January-February, DJF) shows strong low-frequency variabilities on interannual, decadal, and interdecadal timescales. Due to their hemispheric spatial scale, these variabilities are usually captured as several teleconnection patterns. *Wallace and Gutzler (1981)* [71] and *Barnston and Livezey (1987)* [7] identify a number of teleconnection patterns prominent in the Northern Hemisphere (NH) winter using statistical analysis techniques such as correlation maps and principal component analysis, which is also known as Empirical Orthogonal Function (EOF) analysis. North Atlantic Oscillation (NAO) is the dominant mode of variability found in the NH wintertime, the existence of which has already been recognized since as early as the 1920s.

An NAO index may be defined by taking the pressure difference between the two stationary centers of mass over the Atlantic basin. The surface pressure difference between the Azore islands and Iceland is indicative of the intensities of the Icelandic low and Azores high. When the index indicates a strong pressure gradient, the Atlantic storm track is more active than normal and thus the weather over Europe and the Mediterranean region is affected.

Thompson and Wallace (1998) [64] document the leading EOF mode of sea-level pressure (SLP), which has one center of action over the polar cap and two flanking centers in the North Atlantic and the North Pacific, as the Arctic (or Annular) Oscillation (AO). The AO pattern can be seen as a hemispheric extension of the see-saw pattern of the NAO. They also show that this mode has considerably barotropic structure through the troposphere and

lower stratosphere, and is associated with such hemispheric-scale surface temperature trends as warming over land mass and cooling over the Oceans.

A key question is: What are the forcing mechanisms for the interannual and the decadal variabilities in the NAO (AO) pattern? Due to the timescales of variability in this leading mode of boreal winter climate variability, the oceans have been regarded as the causal mechanisms (e.g., *Deser and Blackmon (1993)* [15], *Kushnir (1994)* [38] *Rodwell et al. (1999)* [56], *Mehta et al. (2000)* [44]), *Robertson et al.. (2000)* [54]). However, there is not a clear lag-lead and cause-effect relation established to show, in a definitive manner, that the correlation between the NAO and regional SST patterns are indicative of the oceanic forcing of the atmosphere. On shorter timescales (intraseasonal variability), the NAO (AO) pattern has been statistically related to waves originating from polar stratosphere (*Perlwitz and Graf (1995)* [49], *Perlwitz et al. (1999)* [50], *Baldwin and Dunkerton (1999)* [2]). The interannual and decadal variability patterns associated with the NAO (AO) remain largely unexplained.

Recently it has been shown that the Eurasian snow cover in the prior autumn and the leading mode variability of NH atmospheric circulation in the following winter correlate significantly (*Cohen and Entekhabi (1999)* [13], *Watanabe and Nitta (1998)* [74], *Watanabe and Nitta (1999)* [75], *Bamzai (1999)* [4]). This significant linear association gives a possible, predictive potential of pre-season Eurasian snow cover on the following winter NH climate variability, although the mechanisms to connect the former to the latter, as well as the sources of variations in the former is not yet clear.

1.1 Low-frequency Northern Hemisphere wintertime climate variability

1.1.1 The role of ocean

Ocean-coupling is widely considered as a major component of interannual to decadal variability in the atmospheric circulation[1]. Deser and Blackmon (1993) show the dominant, decadal variability of a dipole pattern in sea surface temperature (SST) and surface air temperature

[1]Most ocean-atmosphere coupling studies have focused on the Pacific. However, there are important studies which show the Atlantic also to be important.

in the wintertime Atlantic sector. It corresponds well to the NAO-like variability mode. This dipole pattern is consistent with a local surface wind fluctuation, which, they argue, suggests a possible coupling between the Atlantic SST and atmospheric circulation on the timescale which local wind fluctuation induces the SST anomaly. Kushnir (1994) supports this coupling up to decadal, but he discusses that the interdecadal patterns of ocean and atmospheric patterns lack a coherent relationship.

Potential role of SST in atmospheric circulation variability is demonstrated by some of studies with aide of coupled general circulation models (GCMs) of different complexities and some of them are successful in reproducing the temporal history from the observed SST time series (e.g., Rodwell et al. (1999), Mehta et al. (2000), *Bretherton and Battisti (2000)* [9], *Latif et al. (1999)* [39], *Osborn et al. (1999)* [47], Robertson et al.. (2000), *Watanabe et al. (1999)* [76] etc.) Bretherton and Battisti (2000) give the caveat, however, that the model results on reproduced variabilities may possibly lack physical basis but merely stochastic outcome, and that predictability is limited to a few season.

1.1.2 Wintertime variability associated with the leading mode

Hurrell (1995, 1996) [26], [27] studied the wintertime Eurasian continent climate variability in the recent two decades with respect to the sea-level pressure change in the Atlantic sector, namely the NAO pattern, and documented that in high NAO index winter the Icelandic low and the Azores high are both intensified, and subsequently enhanced westerly over the North Atlantic brings moisture to the northern Europe where it is warmer-than-average at this extreme phase. In the opposite or negative NAO index winter, the westerly, and hence storm tracks, over the North Atlantic is shifted equatorward and brings moisture to the Mediterranean and North Africa, instead. *Rogers (1990)* [57] showed similar results.

Increase trend of surface air temperature over the land mass and decrease of sea surface temperature over the Oceans in the extratropical NH winter in the recent decades are documented in context of the global warming issue (*IPCC (1995)* [29]). Hurrell (1995) showed that there is evidence for that the wintertime warming over the land and cooling over the Ocean in the North Atlantic sector in a decade from the early 1980s are strongly related with the high NAO index. *Thompson et al. (2000)* argue that these temperature trend are up to

50% congruent to the fluctuation of the AO index.

Rogers and Mosley-Thompson (1995) [58], however, argue the regional mechanism in that the extreme warm phase of wintertime Siberian surface air temperature found in 80s have little conjunction with the large-scale variations such as the NAO, but is rather in association with an extended Arctic low into the Kara Sea and the European part of Russia and subsequent warm southwesterly flow into Central Asia.

More evidence of the relationship between the increasing trend of temperature on the Eurasian land mass and the change of the hemispheric-scale atmospheric circulation in the NH is given by *Przybylak (2000)* [53], who, using the several sources of observational data from the Arctic and sub-Arctic weather stations, documents that since 1975 decrease of the cold season diurnal temperature range in the Arctic has been led by large-scale changes in the circulation, that is, increase of the zonal circulation and decrease of the meridional circulation.

Low-frequency variability of the high-latitude climate is also investigated recently. *Mysak and Venegas (1998)* [45] identify an association of the sea ice concentration in the Arctic basin with NAO/AO, and propose a possible feedback loop of decadal cycle between sea ice concentration anomalies and the NAO. *Serreze et al. (1997)* [60] document the association of the Icelandic low cyclones and the NAO index: in positive phase cyclone counts in the Icelandic low region increase and in negative phase the area of cyclone activity moves southward to the mid-latitude Atlantic. Although they use NAO index in their study, their result on the recent relationship of the cyclone activity to the atmospheric circulation variability is suggestive of a relation of larger spatial scale, including the Arctic region, such as the Arctic Oscillation.

Polyakov et al. (1999) [51], *Proshutinsky and Johnson (1997)* [52], and *Johnson et al. (1999)* [30] propose different regimes of alternating extremes on interannual timescale over the Arctic basin based on the difference in wind-driven circulation in the upper Arctic Ocean which is derived from a two-dimensional, barotropic ocean model, and argue that the annular pattern of SLP anomaly found in the transition between the two extreme regimes suggests that the variation in the upper layer circulation of the Arctic Ocean is in response to the

atmospheric AO variation.

The Pacific-North American pattern (PNA) is another important teleconnection patterns in the winter NH circulation variability, and shows interannual and longer-scale variability (*Trenberth and Hurrell (1994)* [68]). *Overland et al. (1999)* [48] look at the low-frequency variability at the Pacific side of the Northern Hemisphere. They investigate the interannual to decadal variations of mean central pressure of the wintertime Aleutian low to show the association with the atmospheric circulation variability both with the AO-like mode over the polar cap and with the PNA mode over the Pacific side.

Recently, the evidence has been raised in supporting the view that the annular appearance of the "AO," that is, the leading mode of the DJF extratropical Northern Hemisphere variability of the tropospheric circulation anomaly is primarily a linear combination of the two different modes of regional variabilities in the Atlantic side and the Pacific side, whereby the variability of the both variabilities are neither intrinsicly linked nor coordinated but rather randomly superimposed (*Deser (2000)* [14], *Ting et al. (2000)* [67], *Ting et al. (1996)* [66]). Deser (2000) further concludes the dominant reflection of the Atlantic side on the AO mode.

1.1.3 The stratospheric connection

In the stratosphere the largest wintertime extratropical circulation variability is the polar-night jet. Additional to the theoretical suggestions (*Charney and Drazin (1961)* [11] and *Matsuno (1970)* [43]), recently several researches have been conducted on influence of the mean stratospheric circulation on the tropospheric circulation and heat flux (e.g., Perlwitz and Graf (1995), Perlwitz et al. (1999), Thompson and Wallace (1998), *Dunkerton et al. (1999)* [19], *Kodera and Koide (1997)* [35], *Kodera and Yamazaki (1994)* [33]) The structure and strength of stratospheric polar-night jet have an influence on the reflection and transmission properties of vertically propagating, planetary waves forced in the troposphere by orography and large-scale diabatic heating (e.g., *Boville (1984)* [8]). *Kodera et al. (1996)* [34] showed that the propagation of tropospheric stationary planetary waves is associated with variation of the leading, zonal mode of 50hPa geopotential height in the case of a strong stratospheric polar-night jet (strong polar vortex), the forced planetary waves propagate equatorward due to inhibition of upward and poleward propagation.

That inaccuracies in stratospheric characterization in GCMs will cause erroneous tropospheric circulation and climate is one supporting evidence of coupled variability of the stratosphere and the troposphere. *Shindell et al. (1999)* [62] recently showed that realistic implementation of stratosphere dynamics is important for GCMs to capture the linear trend congruent with AO and associated increase in surface air temperature.

Another probable importance of the stratospheric dynamics is suggested by Baldwin and Dunkerton (1999) and *Baldwin et al. (1999)* [3]. They showed, using lag-correlation of the "signature" AO time series that the variation associated with the AO pattern propagates downward from the lower stratosphere to the troposphere on a timescale of a few weeks.

1.2 Effect of snow cover on Climate

One of the important components of the global climate, especially in the extratropical winter hemisphere, is snow and ice. The effect of anomalous snow cover upon the climate system at the surface and in the troposphere is evident in numbers of previous observational studies as well as by simulations and numerical experiments using the general circulation models (GCMs), as mentioned in the following.

Important properties of snow and ice cover are high reflectivity and emissivity, strong thermal insulation, and those specific to water itself, e.g., latent heat. (*Cohen (1994)* [12], *Kuhn (1989)* [37]). Snow cover reduces the effective absorption of solar radiation at the surface, which may induce local temperature inversion and stabilize the boundary layers. It works as heat sink when melting due to latent heat absorption, and may cause delay of local temperature increase at the beginning of the warm season. It modifies water distribution in time and space. In the synoptic and planetary-scale atmospheric dynamics it works as large-scale differential heating at lower boundary in the winter hemisphere at mid- to high latitudes.

The effects of snow cover upon climate variations, local and remote, at the surface and in the atmosphere have been demonstrated both observationally and computationally. *Walsh et al. (1985)* [73] showed that anomalous snow cover has a strong cooling effect on local surface air temperature anomaly in the early winter over the US. Further, *Leathers and Robinson*

(1993) [40] displayed the remote effect of anomalous snow cover on temperatures in the North American winter. They also investigate the relations between anomalous snow, temperature perturbation and tropospheric circulation on regional scale to document the different intraseasonal relationships. In early winter (December) the circulation anomaly corresponds to the area of snow and temperature anomalies, but in late winter the area of strong fluctuations in snow and temperature is not necessarily coincidental to the strong tropospheric circulation fluctuations. On a larger scale, *Gutzler and Rosen (1992)* [24] observed the relationship between subcontinental scale snow cover anomaly and large-scale atmospheric circulation in the Northern Hemispheric winter, and noted that snow anomalies in western Eurasia are correlated with an NAO-like teleconnection pattern. *Serreze et al. (1998)* [61] describe a general, simultaneous relationship between snow cover variations and atmospheric circulation fluctuations over the wintertime US, namely, correspondence with the PNA pattern.

Walland and Simmonds (1997) [72] conducted a comparison experiment using GCM of January NH snow and show a considerable impact, not only local but remote, of snow cover on the mean climate state. Watanabe and Nitta (1998) investigate the relative impact of snow and the SST in the extreme winter NH atmospheric circulation of 1988/89. They suggest that the relative impact of snow is two-third in magnitude of that of SSTs.

Another issue of large-scale snow effect, recognized and surveyed from early days, is on the relation of Eurasian early spring snow cover to the monsoon activity in the following warm season (*Hahn and Shukla (1976)* [25], *Bamzai and Shukla (1999)* [5], *Kripalani and Kulkarni (1999)* [36]). Anomalously heavy (light) snow in western Eurasia in the prior winter/spring is followed by the weak (strong) South Asian monsoon. The basic mechanisms suggested are changes of land-sea temperature contrast due to cooling effect of anomalous snow. This snow–monsoon relation is also investigated by use of GCMs (e.g., *Barnett et al. (1989)* [6], *Douville and Royer (1996)* [18]). Those results reproduce successfully that heavier (lighter) pre-season snow changes the monsoon activity in the way observations state. Simulational studies, such as *Yasunari et al. (1991)* [79], *Yamazaki (1989)* [78], provided that the anomalous snow cover in spring influences, through thermodynamic, radiative, and hydrological mechanisms, not only locally but also further downstream until the end of warm season.

Studies on variations of the Siberian high, one of the most apparent wintertime atmo-

spheric phenomena thought to be affected by Eurasian snow cover, have been either regional or synoptic (*Sahsamanoglou et al. (1991)* [59], *Makrogiannis et al. (1981)* [42], *Ding and Krishnamurti (1987)* [16] and *Ding (1990)* [17]), and studies on climatological variabilities on interannual and longer timescale remain few partly due to insufficient and incoherent sets of observational data. Seasonal and climatological behavior of surface atmospheric circulation for each of several subregions of the former Soviet Union is described in detail by *Lydolph (1977)* [41]. Similarly, a detailed view of seasonal characteristics of near surface atmosphere over the Arctic Basin and surrounding Seas is provided by *Vowinckel and Orvig (1970)* [69]. *Sahsamanoglou et al. (1991)* [59] investigates the seasonal variations, on timescale longer than a year, of the center of the Siberian high in terms of geographical position, pressure intensity, and trend using the observational data longer than a century. They note a steady increase (ca. 3hPa/120yr) of wintertime mean pressure, and find also that the central pressure and mean 500-1000hPa thickness are negatively correlated during the winter months (November to February), from 1970s to late 80s. *Kanno and Matsumoto (1993)* [32] surveyed large-scale cold air anomalies (LCAs) in the lower troposphere (850hPa) formed in the winter Northern Hemisphere and identify phase-locked migration, through winter, of two centers of LCA offshore from northeastern part of Eurasia and North America, respectively. The relationship with continental snow cover is, however, not mentioned.

In order to delineate and deepen our understanding of the role snow plays on the large-scale climate, it is essential to have as a coherent and accurate dataset of snow observation, with large coverage in time and space, as possible. To this end, considerable efforts have been made to improve and reconstruct the snow-related data in terms of precipitation in high latitudes, snow cover or snow depth (*Brown (1997)* [10], *Frei and Robinson (1999)* [21], *Frei et al. (1999)* [22] etc.), or to describe their long-term variations over 100 years (e.g., *Fallot et al. (1997)* [20]). At the time of this study, the best available dataset of Eurasian autumn snow cover is the remotely sensed dataset by the National Oceanic and Atmospheric Administration (NOAA) (*Robinson et al. (1993)* [55]). This dataset was used in this study and will be explained in Section 2.1.

1.3 Eurasian snow cover and Northern Hemisphere climate variability

As stated in the beginning of Chapter 1, the high correlation between Eurasian snow cover in the prior autumn and the following winter hemispheric atmospheric circulation has been shown using linear statistical methods. This gives a possible, predictive potential of pre-season snow cover on the following winter NH climate variability, although the physical mechanisms that connect between those is not yet clear, as well as the sources of variations in autumn snow cover.

Cohen and Entekhabi (1999) raise a hypothesis of a linkage of anomalous snow cover in autumn (SON) Eurasia to near-surface atmospheric circulation variations of the following winter (DJF). Anomalously extensive early-season (SON) snow cover in Eurasia cools the bottom of the atmosphere, which produces the anomalously high pressure in the region, and causes it to expand. Blocked by the high topography to the south and east, the expansion of the dense air directs north- or westward to cover the polar cap and to force the Icelandic low southwestward. When SON snow cover is sparse the Icelandic low is capable of intruding further into the north and east due to the weakened and contracted Siberian high.

The questions attempted to answer in this study are following: What is the nature of daily transition of sea-level pressure anomaly in the NH high latitudes from autumn to winter, and are there any consistent tendencies in the daily pressure changes associated with anomalous snow cover in the autumn? Is the above hypothesis supported by the observations? If so, through which route and at which time of the season does it occur? Does SON autumn snow cover have any relations with downward propagating circulation anomalies from the lower stratosphere in terms of possible source of the DJF surface-level variations. How much is the general contribution of SON Eurasian snow cover anomaly to wintertime surface pressure? What would be the specific contribution of the SON snow cover in contrast to the (semi-)hemispheric-scale DJF circulation variability in SLP, and how much?

This study is entirely based on statistical analysis of the observational data. Datasets used in this study and their quality control as well as results from preliminary analyses are described in Chapter 2. Main results are shown in Chapter 3, and discussions and

considerations on these results are also stated. Chapter 4 gives the overall summary of this study.

Chapter 2

Data

2.1 Datasets

2.1.1 Atmospheric pressure and geopotential height

The twice-daily surface pressure data in the Arctic region (poleward of 70°N) used in this study is from the International Arctic Ocean Buoy Data Products which are collected and processed at the Polar Science Center, University of Washington as part of the International Arctic Buoy Program (IABP). The spatial coverage of this dataset is the aforementioned area with grid interval of 10 degree longitude and 2 degree latitude. The temporal coverage is from 1979 to 1998 once every 12 hours.

Surface pressure were measured by a pressure sensor implemented on floating buoys, and were interpolated at the Polar Science Center onto the grid system. The pressure data were linearly interpolated to the synoptic time 0000 GMT, 0300 GMT, ..., 2100 GMT (from 1986 on, to the hourly) unless the interval of two observation exceeds two days, in which case no interpolations were made. After merging with similarly interpolated station data from about 70 high latitude weather stations, optimal interpolation (*Gandin (1965)* [23]) in space was conducted. In 1986 a routine using a polynomial fit replaced the old linear algorithm procedure. This dataset is available from either the Polar Science Center, Applied Physics Laboratory, University of Washington or the National Snow and Ice Data Center

(NSIDC), CIRES, University of Colorado. According to the description of this dataset [28], the overall unknown biases of surface pressure is expected to be on the order of 1.0hPa due to measurement error and systematic error in calibration and interpolation.

Additionally, pressure reduced to mean sea-level (MSLP), geopotential heights at 500hPa and 50hPa for the extratropic Northern Hemisphere (poleward of 20^oN) are obtained from NCEP/NCAR Reanalysis (Reanalysis-1) [31]. Grid separation of this dataset is 2.5 degree both in longitude and latitude, starting from the prime meridian and the North Pole (90.0^oN), respectively. The mean and standard deviation of these fields, i.e. MSLP, 500hPa and 50hPa geopotential height, in autumn (SON) and winter (DJF) are shown in Figures A.1 through A.6 in Appendix A, and the results are described presently.

Mean field of MSLP in autumn (SON) shows a somewhat zonally-symmetric feature, high values in the mid-latitudes, especially over the North Hemisphere Oceans and the eastern part of the North Hemisphere Continents, and slightly lower in the tropics and high latitudes (Figure A.1). Precursor of the Aleutian and the Icelandic Lows are already visible. In wintertime (DJF) seasonal high and low pressure centers become more clear. The high is in Siberia (90^o–110^oE, 40^o–55^oN), over Azores in the subtropical North Atlantic, and over Rocky in the North America, whereas the low pressure centers are found over Aleutian islands and the Icelandic Sea. The largest year-to-year fluctuations are found in the Arctic Basin in the eastern Hemisphere, in the eastern half of the NH Oceans and over the Tibetan Plateau. Their geographical positions are almost same in SON and DJF, while their magnitude is much larger in the latter season.

The SON mean 500hPa geopotential height shows annular structure with almost monotonicly decreasing from the tropics to the pole (Figure A.3). In DJF (Figure A.4) the geopotential height drops in the mid- to high latitudes, resulting in ca. 5,000 gpm over the polar cap in zonal mean, while troughs over the northeastern part of the NH Continents (i.e., Kamchatka peninsula and northeastern Canada) and ridges over their northwestern part (i.e., Alaska, and north and west Europe) develop. Largest year-to-year variations indicate interannual variation of storm tracks position, and occur almost the same location as MSLP.

The 50hPa geopotential height field (Figures A.5 and A.6) shows much more clear structure of the zonal symmetry in both seasons, except a ridge over Alaska in DJF. In this season

the polar vortex becomes strong and accordingly interannual fluctuation increases compared to that of SON.

2.1.2 Snow cover

Monthly Eurasian snow cover data from March 1972 to February 1999 used are derived from the weekly snow cover area dataset by the National Oceanic and Atmospheric Administration (NOAA) visible satellite imagery and compiled at Rutger University [55]. The original visible imagery has a spatial resolution of about 1.1 km, but the aggregated areas represented by a grid in the charts range from 16,000 km^2 to 42,000 km^2. The Rutger University routine further derives refined monthly snow-covered area in units of million km^2 by weighting the number of snow-covered days in a chart week.

2.1.3 Topography

Land surface elevation data in meters were obtained from ETOPO5, Digital relief of the Surface of the Earth, archived at the National Geophysical Data Center in Boulder, Colorado. The data are generated from several sources of databases of land and sea-floor elevations on a 5-minute longitude/latitude grid. The area of the interest in this study covers the Mountain ranges in the Northern half of Eurasia and North America, over which the horizontal resolution varies from 5-minute to 1-degree depending on the sufficiency of the available data. Elevation accuracy also varies from 1-meter to 150m.

2.2 Quality control of data

2.2.1 Sea-level pressure in the Arctic region

The reanalysis data is a merger of numerical model forecasts and observations. In regions with sparse observations, the concern is that the model bias is strongly evident in the reanalysis fields. In order to test the adequacy of the reanalysis data, a comparison is made of the MSLP across the region of overlap. While the IABP data do not suffer from any possible model biases, they are susceptible to interpolation errors in processing the measurements.

In order to facilitate check and comparison of the data quality of sea-level pressure in the Arctic region from the two datasets, i.e., IABP and Reanalysis-1, the grid-wise mean and standard deviation of the difference between the two datasets were examined on a monthly basis in the region poleward of 70^oN. Due to the unequal gridding in time and space between the two datasets, the data are resampled onto a common grid prior to the comparison. The monthly Reanalysis-1 data were interpolated linearly onto the grid-system of the IABP dataset, i.e., 10.0^o in longitude by 2.0^o in latitude, beginning from the prime meridian and 90^oN. For the IABP dataset the monthly mean is calculated over the original grid-points from its twice-daily value.

The biases, that is, mean of the difference, between the two datasets over the Arctic region, and its standard deviation, root mean square (RMS), are shown in Figure 2.1, for the autumn (September to November, SON), the winter (December to February, DJF) and the cold season (September to February, SONDJF). Maps of biases defined as median of the difference show no substantial difference (not shown).

Reanalysis MSLP data are lower relative to the IABP pressure data on the order of 1.0hPa or less over the Arctic Ocean and surrounding seas in all the three seasons examined. The value is relatively higher over the band from Greenland sea and the North Pole to the 180^o meridian. That the values of sea level pressure are lower in Reanalysis-1, where surface pressure measurements for the IABP dataset were taken by floating buoys (figure 2.2), suggests that the Reanalysis-1 tends to underestimate the mean sea-level pressure in the high-latitude, low altitude areas. Nevertheless, the two datasets can be regarded as consistent when the intrinsic error on the order of 1.0hPa in the IABP dataset.

Over Greenland, on the other hand, the biases are positive and larger with maximum values greater than 8.0hPa in each of the three periods. The RMS is on the order of the biases. The IABP dataset tends to have lower values. It is important to note that the IABP dataset incorporates no information above the sea level regardless of the surface elevation. Also this discrepancy may be partly due to the interpolation method of IABP which in 1986 changed the method from linear to polynomial procedure. Nonetheless, the MSLP over Greenland is not the primary interest in this study, and hence no correction has been made in using either dataset.

a)

1) RMS (CDAS1 - IABP)

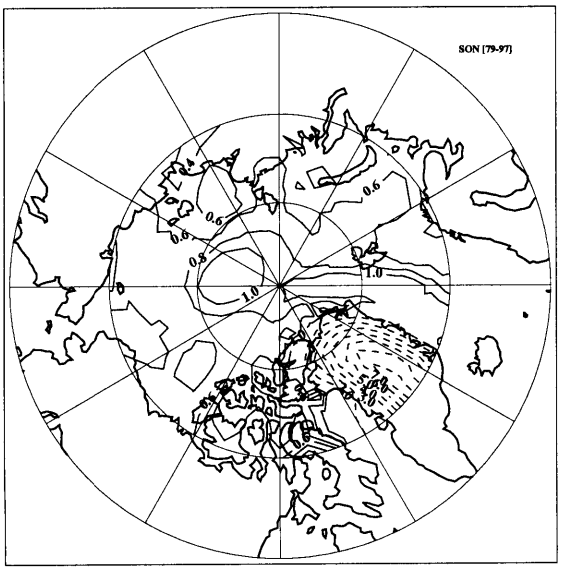

2) Bias (CDAS1 - IABP)

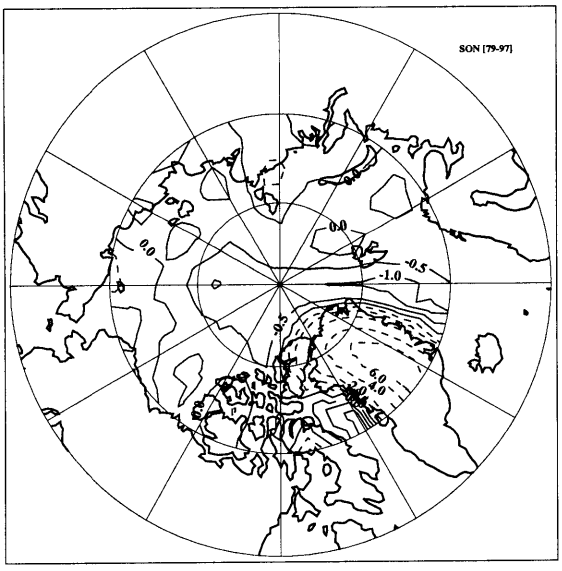

Figure 2.1: 1) Bias of sea-level pressure between IABP and Reanalysis-1, and 2) its root mean square (RMS), for a) SON (September to November), b) DJF (December to February), and c) the cold season (September to February)

b)

1) RMS (CDAS1 - IABP)

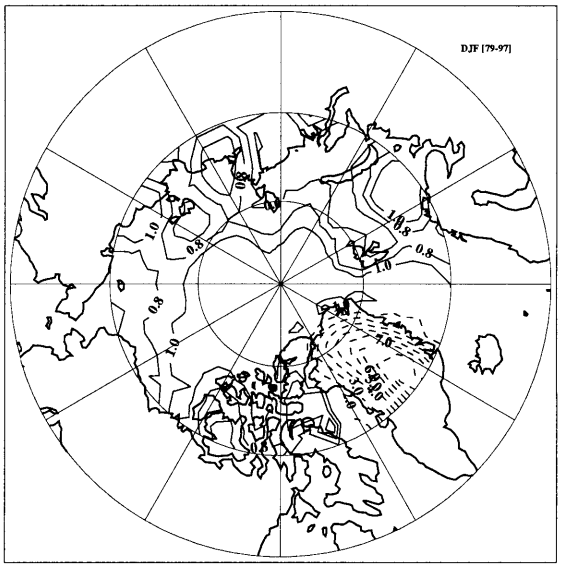

2) Bias (CDAS1 - IABP)

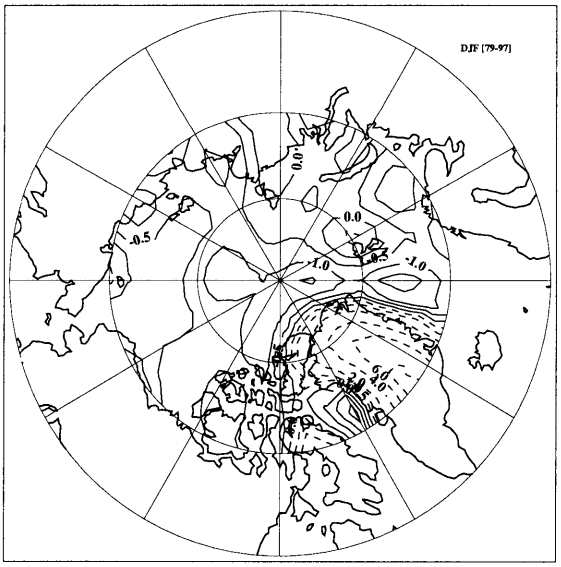

Figure 2.1 *(Continued)*

c)

1) RMS (CDAS1 - IABP)

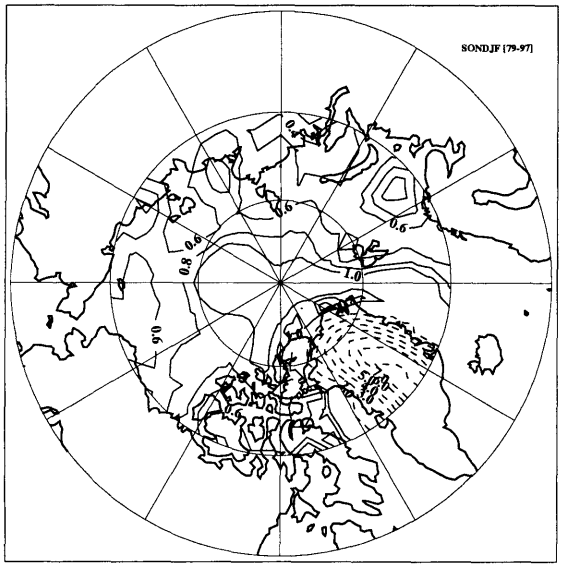

2) Bias (CDAS1 - IABP)

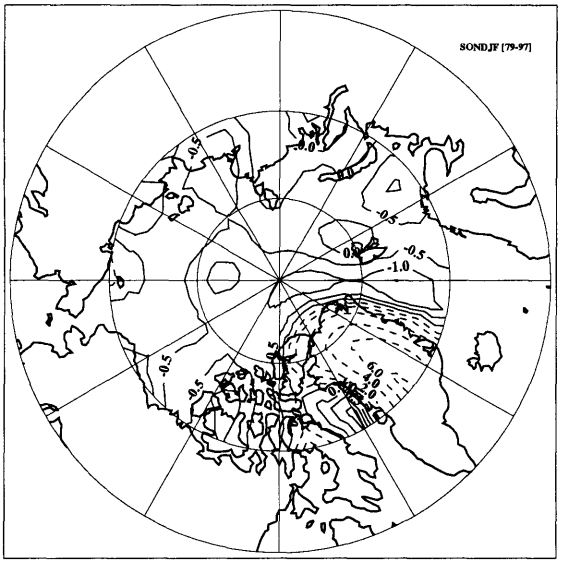

Figure 2.1 *(Continued)*

Monthly mean numbers of observation in cold season

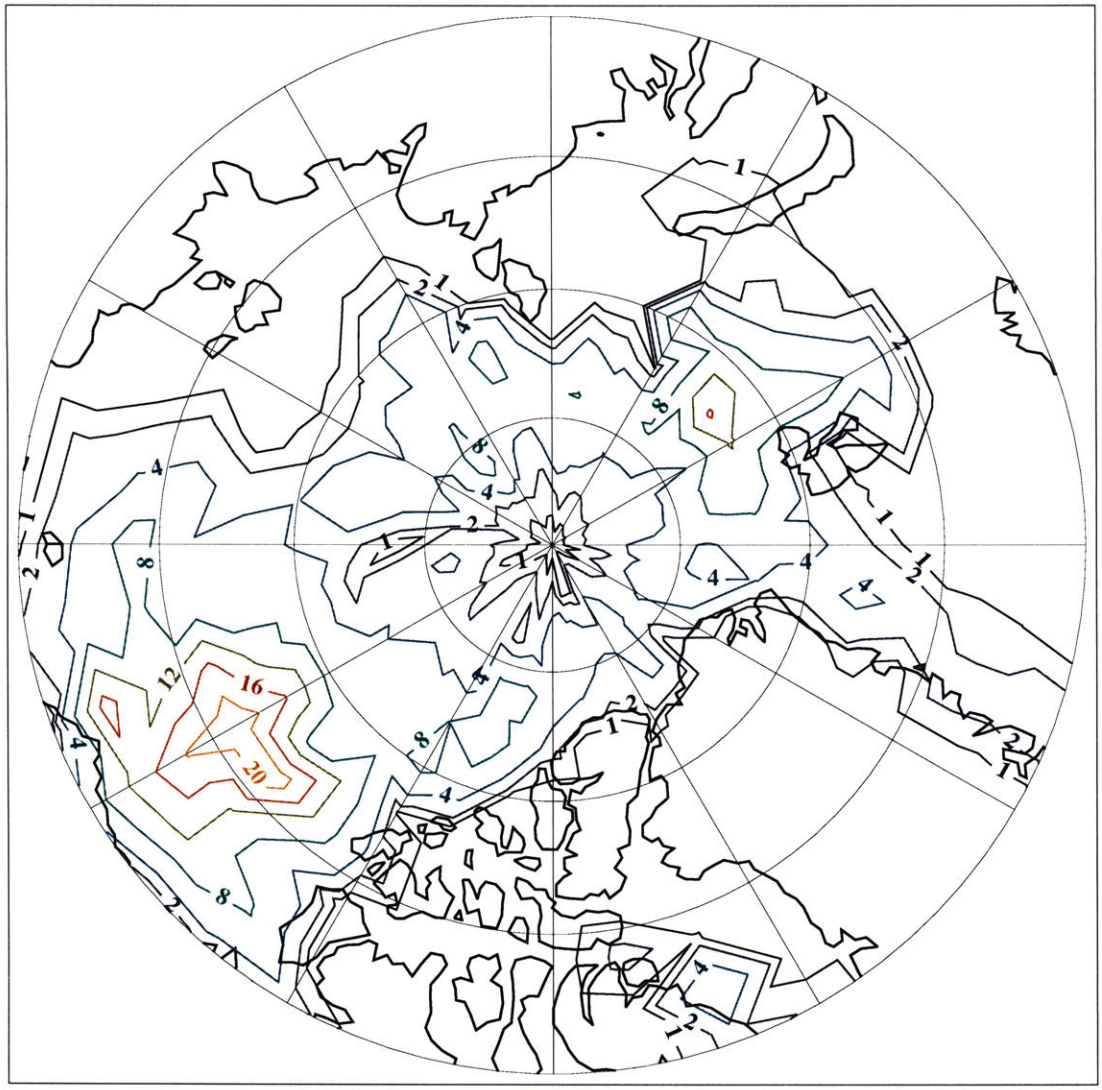

Figure 2.2: Number of monthly mean observation of IABP dataset. Contours are 1, 2, 4, 8, 12, 16, 20 and 24.

2.2.2 EOF analysis

Empirical Orthogonal Function (EOF) analysis was performed on monthly MSLP and geopotential height anomaly fields in middle troposphere to stratosphere to delineate the spatial and temporal variability in the Northern Hemisphere using the Reanalysis-1 dataset. The Reanalysis-1 dataset is used since it covers a larger domain than the IABP dataset. The IABP dataset is restricted to latitudes north of 70^{o}N. Gridding of the analyzed area is 5 by 5 degree in longitude and latitude, poleward of 20^{o}N. Monthly anomaly data from March 1972 to February 1999 are obtained after subtraction of the monthly mean computed from the original field of the period. This temporal coverage of the period is chosen to coincide snow cover observation data.

Analysis of MSLP by EOF reveals the well-known leading varying mode (Figure 2.3) that explains 18.9% of the total variance. This pattern is well-separated according to the North's criterion (*North et al. (1982)* [46]). This is the Arctic Oscillation (AO) pattern, as originally defined by Thompson and Wallace (1998). Care should be taken because the polarity is set opposite as shown in Thompson and Wallace (1998) to make the comparison with snow cover anomaly easier. The second and third EOF patterns explain 10.8% and 9.2%, respectively (not shown). Similarly, the EOF analysis is performed with the 500hPa and 50hPa geopotential height fields, to obtain similar patterns as previous studies have shown (e.g., Perlwitz and Graf (1995)). Each of the leading modes explains 14.5%, and 41.6% of the corresponding total variance, followed by the second mode with 10.4% and 14.6%, respectively (not shown). These first modes are also well-separated as well.

In order to examine the relation between the variability in the AO index (EOF1 of MSLP) and regional physiographic features, the field of MSLP is correlated with and regressed onto the index. Figure 2.4 shows the statistics together with lines marking the northern edge of 1000 meters land elevation. Since the elevation over the Greenland, including its icesheets covering over, is almost above this level except for the relatively small area along the coast line, no topography lines were drawn over this island. The choice of the altitude level of 1,000m is made so that they stand out the remarkable coincidence of the peripheral lines of significant variations over the polar cap associated with the first mode of the wintertime sea

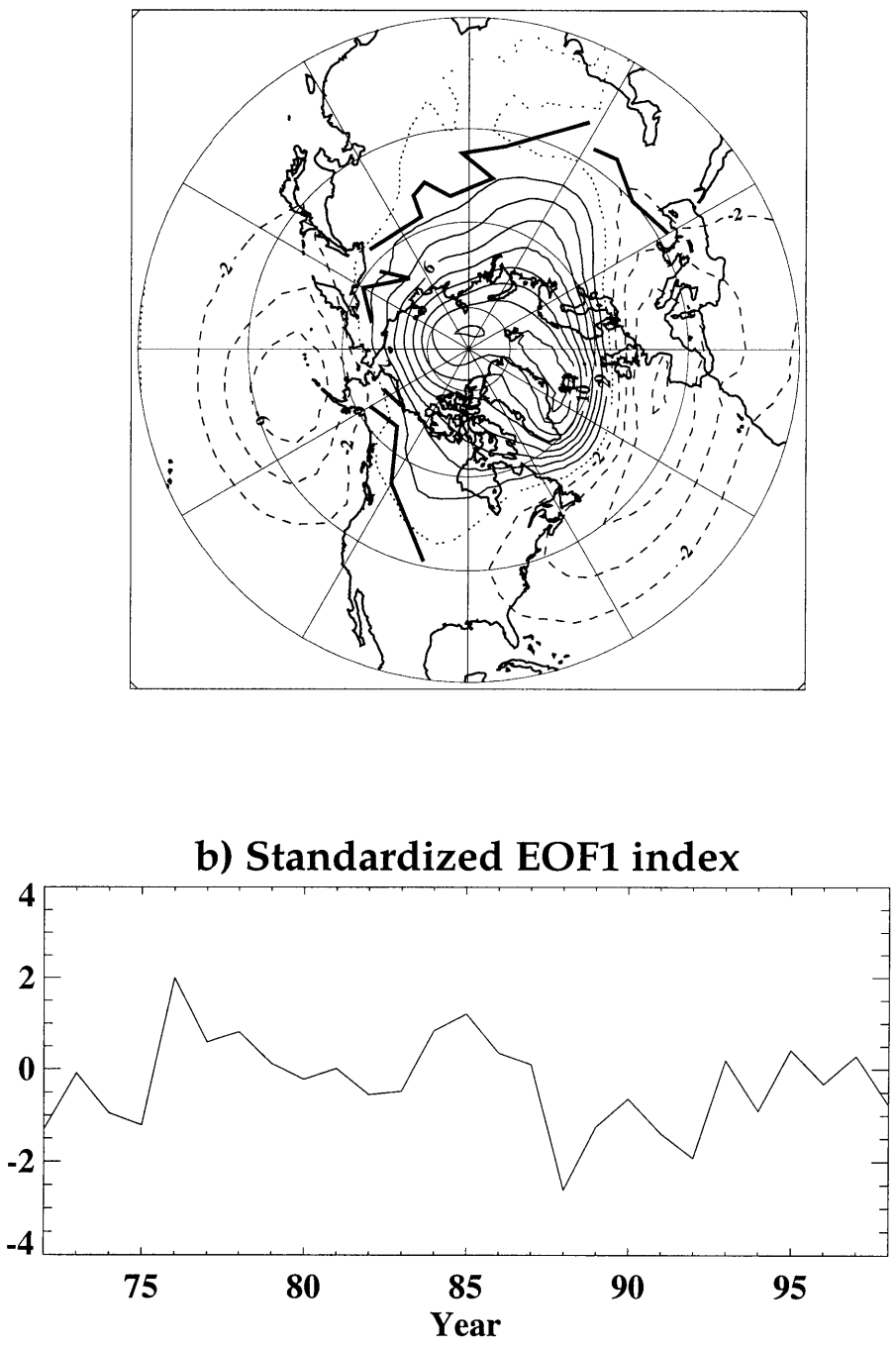

Figure 2.3: The leading mode of monthly MSLP variability (1972-1998). a) Spatial pattern of the EOF1 mode, and b) the DJF mean time series of the standardized primary component

surface-level pressure variability (Figure 2.4), with high orography, i.e., the mountainous sides extending from the Caucasus to Central Asia, to east Siberia, to west Northern Canada, and finally to the Rocky Mountains. This delineates the topographic effect of the near-surface wintertime circulation anomaly. Skewness of contours over the Greenland is also suggestive of the similar topographical effect. These lines are drawn also on the maps of geopotential height at the lower pressure levels (i.e., 500hPa and 50hPa) for a reference purpose (e.g., Figures 2.6)

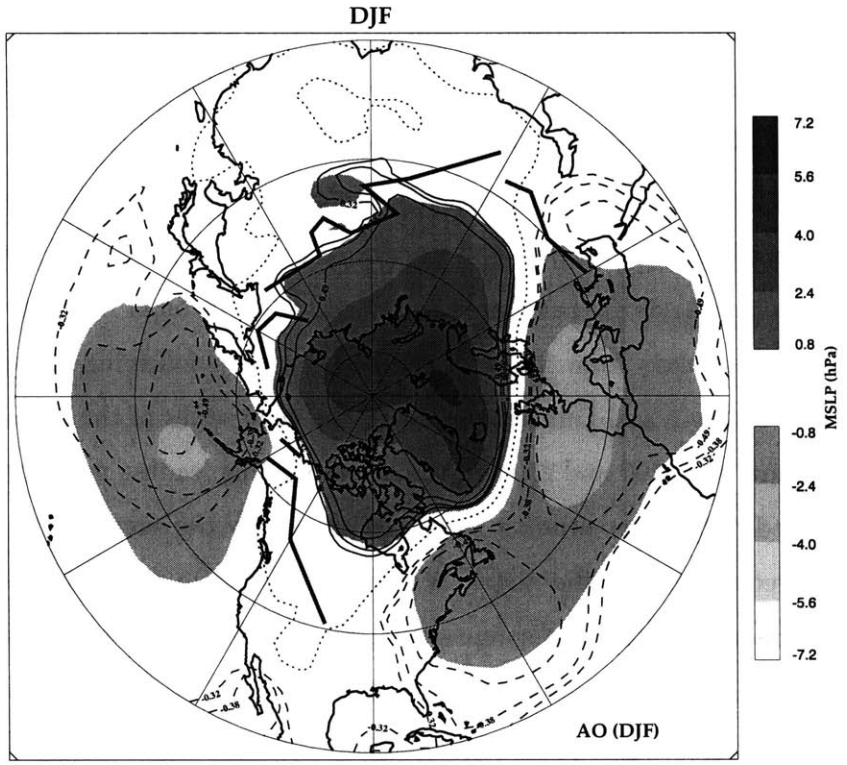

Figure 2.4: Regression map of the DJF MSLP onto the AO index (EOF1 of MSLP). The shading (the regression coefficient) corresponds to one standard deviation of the EOF1. The local correlation with the index is shown by lines which correspond to the 90%, 95% and 99% significance level. Negative correlations are dashed. Thick lines represent the northern edge of the 1000m topography lines.

EOF analysis were also conducted on combined fields in order to isolate the temporal change of the leading mode of co-varying variabilities across vertical atmospheric levels. First, a combined field of monthly 500hPa and 50hPa geopotential height anomaly is analyzed. By taking this combined field it is possible to depict the covarying variability patterns in the middle troposphere and the lower stratosphere. The first EOF mode of this combined field, denoted as (z500, z50) and not shown, which explains 20.3% of the total variance, is substantially same as the barotropic mode show in the previous studies (Figure 1 of Baldwin and Dunkerton (1999), Fig. 1. of Kodera et al. (1996), etc.). These are also shown to be associated with the Arctic Oscillation, from the surface to the middle stratosphere (10hPa). Studies have shown that this disturbance mode propagates downward from the middle stratosphere to the surface on the timescale of a few weeks (e.g., Baldwin and Dunkerton (1999), Perlwitz and Graf (1995), and Kodera and Yamazaki (1994)).

In order to extract this downward propagating mode another combined field is constructed by the following manner. First, series of 30-day period means of the 500hPa and 50hPa geopotential height anomaly fields are calculated from September through February, whereby each period is shifted by 15 days from the prior period. Secondly, following the same methodology employed by Baldwin and Dunkerton (1999), the time series of the area-weighted inner product ("signature") of z500 and z50 and the corresponding leading mode pattern obtained above is calculated. The inner product is defined as exactly the same as the ordinary inner product of two vectors except the metric is given according to the area of which the grid point of each component of the vector represents. For the next step, the lag cross-correlation of the signature time series between z500 and z50 is calculated. This lag cross-correlation (Figure 2.5) shows, on 15-day basis, that the highest correlation is observed at 1 period lead of z50, that is, the timescale of the downward propagation is about half a month. This is consistent with the result obtained by Baldwin and Dunkerton (1999), regarding the temporal resolution of this dataset.

Finally, EOF analysis is performed on the combined field of z50 and z500 where z50 leads by 1 period (15 days), which is denoted by (z500, z50(+15d)). The leading mode explains 20.3% of the total variance and well-separated by North's criterion. Its spatial pattern at the both levels and DJF time series of the primary coefficient (mean over December to February)

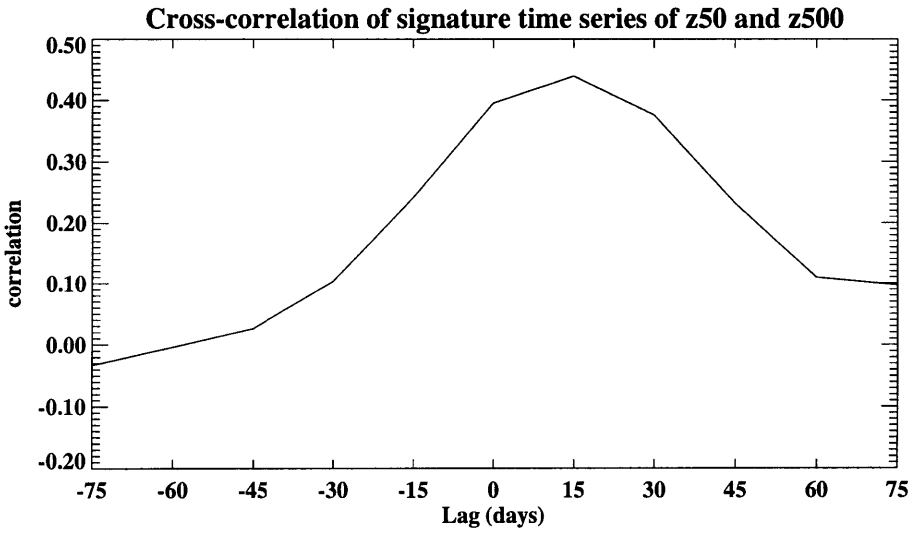

Figure 2.5: Cross-correlation between "signature" time series of 500hPa for September to February 1972-1998. Positive lags correspond to 50hPa leading 500hPa anomalies.

are shown in Figure 2.6. The remarkable difference from the similar spatial pattern of the simultaneous case is found in the 500hPa height field in which the zonally-symmetric feature is highly exaggerated. This mode is referred to as the "uAO" mode or the upper AO.

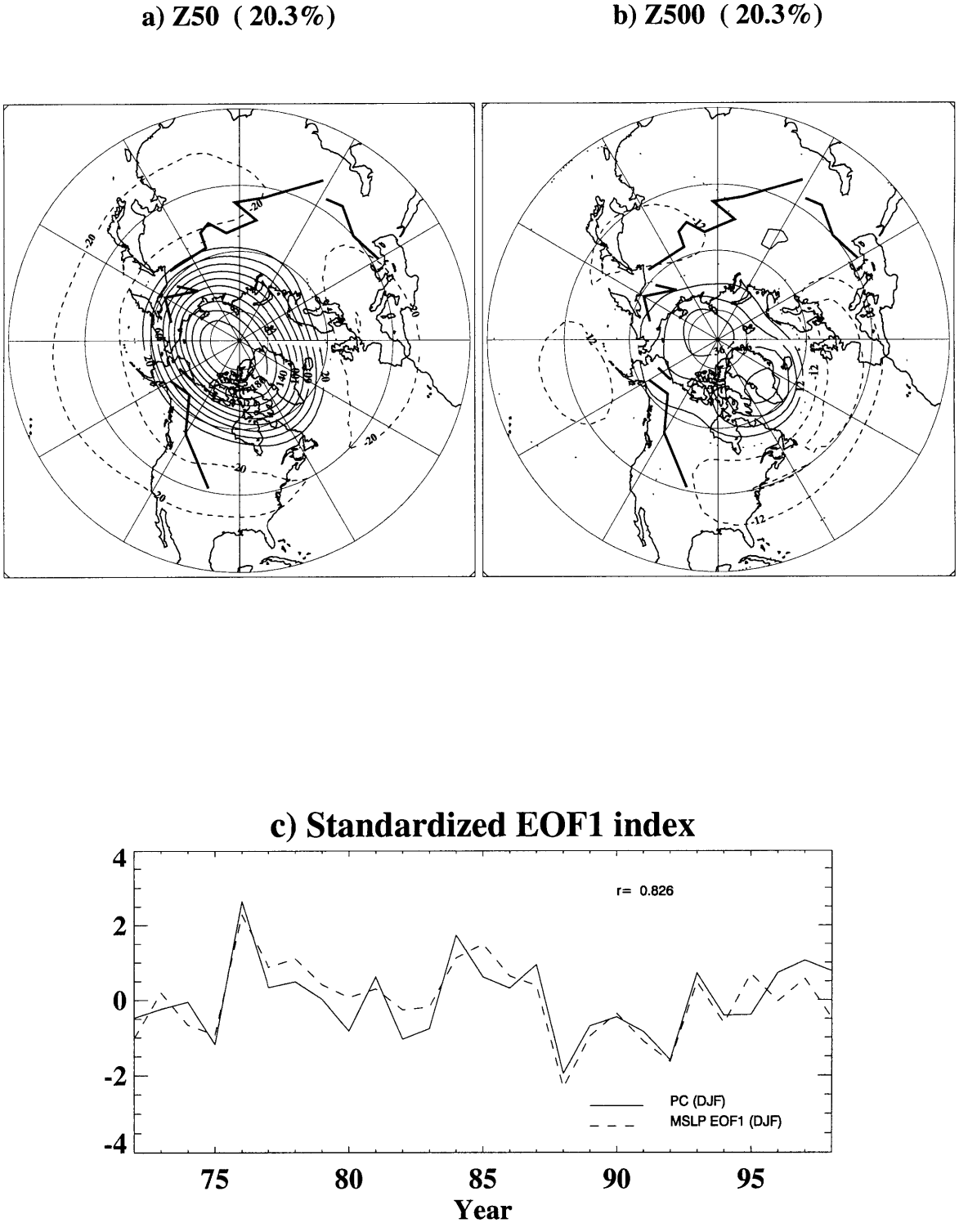

Figure 2.6: The leading mode (uAO) of a combined field of the 30-day averaged geopotential height at a) 50hPa (with 15-day lead), and b) 500hPa. Negative values are dashed, and zeros are dotted. Thick lines are the northern edges of 1000m topography. c) Standardized DJF time series of the primary component of the leading modes: the uAO (solid) and the AO (EOF1 of MSLP; dashed).

2.2.3 Correlation analysis

The correlation analysis gives another set of information concerning the linkage of Eurasian snow cover and the wintertime Northern Hemisphere climate variability.

Cohen and Entekhabi (1999) shows that Eurasian snow cover in the prior autumn and the following winter time 500hPa geopotential height has a high correlation (-0.71 for 1973-1995). In the now-available extended time span (1972-1999) there remains statistically significant correlation between the two time series.

Table 1 summaries the correlation coefficient between SON Eurasian snow cover and time series of the wintertime (DJF) primary components, indices, of the leading mode on the several fields. AO, z500, and z50 indicates the leading variability mode of the mean sea-level pressure, 500hPa and 50hPa geopotential heights, respectively. (MSLP, z500, z50) denotes the (simultaneous) monthly combined field of MSLP, z500 and z50, and (z500, z50(+15d)) denotes the uAO mode. The values in parentheses are the correlation coefficient of the time series which the two extreme years of autumn Eurasian snow cover, namely, 1976 and 1988, are removed. Statistically significant correlation with two-sided 95% and 99% confidence for 27-year (25-year) indices are given by 0.381 and 0.487 (0.396 and 0.505), respectively.

The correlation coefficient of SON Eurasian snow cover for all 27 years is 0.542, 0.504, and 0.435, with (MSLP, z500, z50), (z500, z50), and z50, respectively. This decreasing tendency of the correlation with the distance between the surface and the lowest level of the barotropic mode poses a further suspicion that the Eurasian autumn snow cover may act as a lower boundary forcing to the wintertime atmospheric circulation, especially to the leading mode of observed variability. One possible connection is that the anomalous snow cover works as extra heat sink in mid- to late autumn to modify the topographically produced tropospheric stationary Rossby wave in the high-latitude, which then may interact with the lower stratospheric circulation. It is also worth mentioning that the correlation between SON Eurasian snow cover and uAO is as large as AO. This is also true when the two years of the extreme snow cover are removed.

The above results suggest linkage between anomalous autumn Eurasian snow cover and the wintertime climate variability. However, that the extreme values of the AO and the uAO

Table 2.1: Correlation coefficients between SON Eurasian snow cover area and DJF indices of EOF modes of the fields at various levels and of various combinations.

Field Indices	Eurasian snow cover (SON)
AO	0.516 (0.405)[a]
z500	0.483 (0.326)
z50	0.435 (0.210)
(z500, z50)	0.504 (0.292)
(MSLP, z500, z50)	0.542 (0.364)
(z500, z50(+15d))	0.564 (0.372)

[a]Values in parentheses are results after removing two years of extreme ESC_{son} in 1976 and 1988.

is associated with the extreme anomalous autumn Eurasian snow cover (in 1976 in positive and in 1988 in negative), and that the result show only limited correlation when the extreme years are removed suggest that there may be a threshold for the SON Eurasian snow cover to affect the DJF NH climate variability. Nevertheless, that the DJF AO and the SON Eurasian snow cover retain statistically significant relation with more than 95% confidence when the extreme cases are removed qualifies the linear framework to continue.

The annular appearance of the leading mode of the DJF extratropical Northern Hemisphere variability of the tropospheric circulation anomaly, as stated in the Introduction, may be a linear combination of the two different modes of such variabilities in the Atlantic side and the Pacific side, which are linked neither intrinsicly nor coordinately but randomly where the influence of the Atlantic side is dominant (Deser (2000), Ting et al. (2000)). Following Deser

(2000), the leading mode variability of DJF MSLP on the Atlantic (ATL) and Pacific (PAC) sides are computed by the EOF analysis based on the corresponding semi-hemispheric fields. The division is set at the line 80°E–100°W, in contrast to the 90° line by Deser (2000), since it maximizes the sum of the explained variances of each field at 51.3%, where the leading mode of the Atlantic and the Pacific side explains 28.0% and 23.2% of the total variances of each field, respectively. The correlation between the monthly primary components of the two leading modes is 0.165. The choice of the line, within the range of 50°E–130°W to 120°E–60°W, does not change substantially the result and reproduces what Deser (2000) obtained. The correlation of AO and uAO with these (semi-)hemispheric DJF MSLP variability indices are summarized in Table 2.2. Again values in parentheses show the results after removal of the two extreme years (1976 and 1988).

Table 2.2: Correlation coefficients of the AO and the uAO with the ATL and the PAC.

	AO	ATL	PAC
AO	1.000 (1.000)[a]	0.955 (0.947)	0.648 (0.573)
uAO	0.826 (0.811)	0.800 (0.799)	0.431 (0.328)
ESC_{SON}	0.516 (0.405)	0.457 (0.363)	0.352 (0.235)

[a]Values in parentheses are results after removing two years of extreme ESC_{son} in 1976 and 1988.

The uAO and the AO indices have correlation of 0.826, that is, nearly 70% of the DJF AO variance is explained by the downward propagating signal from the stratosphere.

In turning the viewpoint to the constituents of the AO variability at the surface level, the correlation between AO and ATL is very high and exceeds 0.95, whereas, highly statistically

significant, the AO has smaller correlation with the Pacific side.

As for the connection with the downward propagating signal, the ATL shows high correlation of 0.800 with uAO, which indicates the downward propagated anomalies to the surface level predominantly affects the Atlantic side. The correlation with the PAC drops to 0.431.

Removal of the extreme snow cover years appears to affect the PAC correlation with other indices more than that of the ATL. It may be possible that extreme snow cover works to strengthen the connection between the variability on the two sides of the semi-hemisphere in the Northern Hemisphere.

Autocorrelation properties

In order to see the persistence of the Eurasian snow cover, and surface-level and upper level (middle troposphere to lower stratosphere) leading variability, i.e., AO and the (z500, z50) time series, lag 1 autocorrelation of the monthly time series (September, 1972 to February, 1999) is computed for the cold season (September to February). The uAO is not used in this analysis since the time series of it shows spurious lag-1 autocorrelation resulting from its construction, and reduction of this spurious autocorrelation causes loss of the common basis of comparison with other time series.

The lag-1 autocorrelation is computed in the following manner. The monthly mean value for each month from September to February, calculated from the 27-year series, is subtracted from the original values.Then, pairs are formed by two successive months in the same cold season; i.e., (9/1972; 10/1972), (10/1972; 11/1972), ... , (1/1973; 2/1973), (9/1973; 10/1973), ... , (1/1999; 2/1999). The correlation are obtained between the left components and the paired right components. The former leads by 1 month to the latter.

The results are 0.419 for Eurasian snow cover, 0.394 for AO, and 0.484 for (Z500, z50). The 95% (99%) confidence limit for the non-zero correlation is 0.169 (0.222), respectively. It is not unexpected that a previous month Eurasian snow cover anomaly explains, overall in the cold season, about 17.6% for that of the following month due to persistent nature of the snow cover. While the surface-level circulation anomaly shows almost same lag-1 autocorrelation with snow cover, it is astonishing that the leading upper air mode shows strong memory and explains about a quarter of the variability in the subsequent month in the same cold season.

To examine the different profile of the intraseasonal change of autocorrelation between the neighboring months, the autocorrelation coefficients between two adjacent months are calculated and shown in Figure 2.7. For these values larger than 0.377 (0.497) is statistically significant with 95% (99%) confidence,

Correlation for snow cover anomaly changes little throughout the season and always significant with more than 95% confidence (Figure 2.7a), whereas for the AO and (z500, z50) it shows abrupt increase of correlation occurring within the cold season and holds thenceafter. The period after the jump with higher correlation may be referred as "winter regime." For the upper level (Figure 2.7c), the change into the winter regime occurs in October with increase of correlation coefficient from 0.113 to 0.467 keeping its value around 0.5 afterwards. Almost same magnitude and shape of change is observed for the AO (Figure 2.7b) except for the occurrence of the shift in December (two months after the upper level). This may suggest the transition from the autumn regime to the winter regime in terms of persistence of the pattern occurs about two month earlier in the upper level than the sea surface-level.

Furthermore, the seasonal persistence, i.e. autocorrelation between SON and DJF value, is given by 0.362 for the snow cover, 0.161 for AO and 0.311 for (z500, z50). Significance level is same as the monthly results, thence none of the fields show statistical significance to seasonal lag-1 autocorrelation.

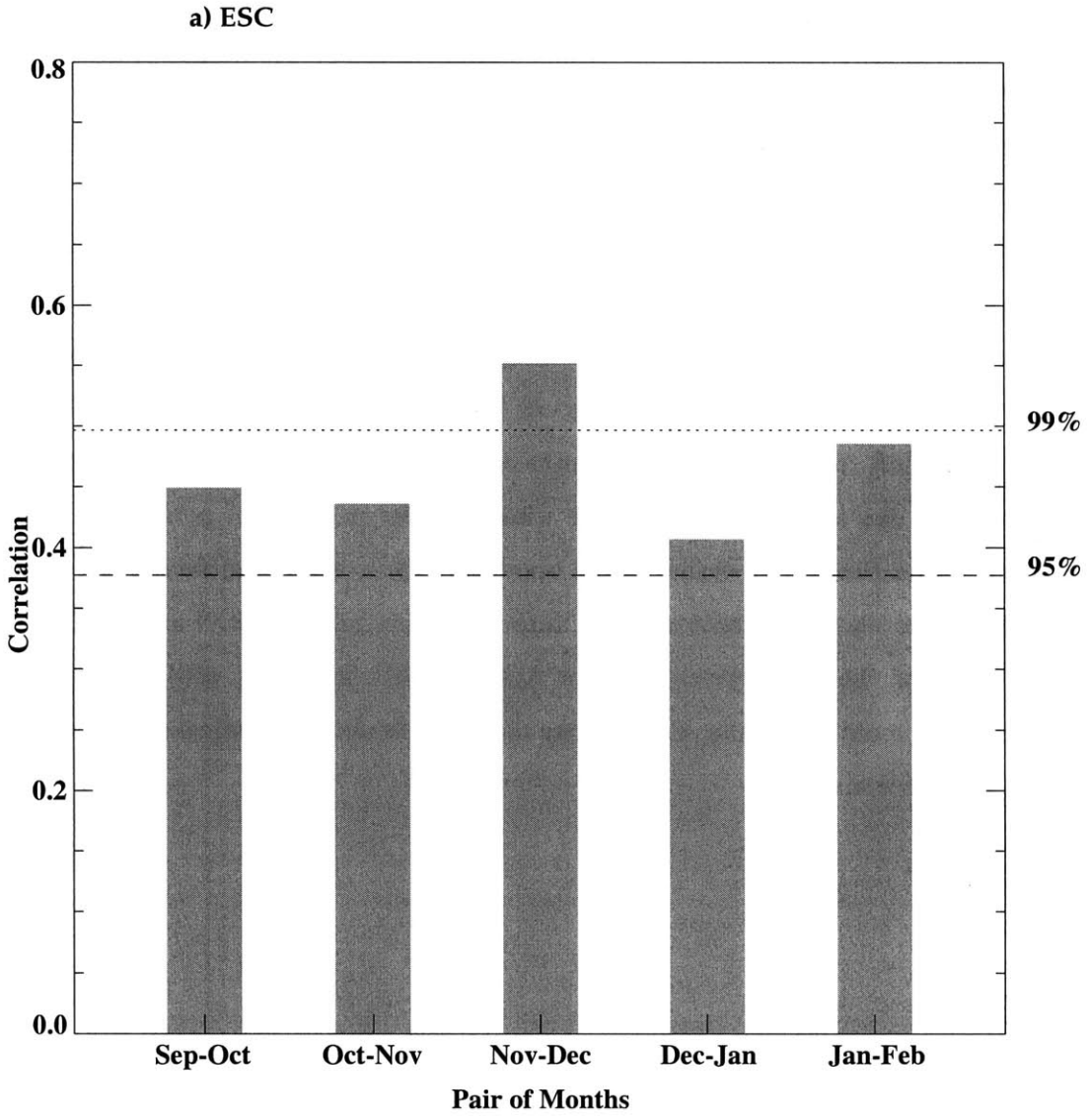

Figure 2.7: Lag-1 autocorrelation between two adjacent months for a) autumn Eurasian snow cover, b) the AO index, and c) the primary component of the leafing mode of (z50, z500), for 1972-1998.

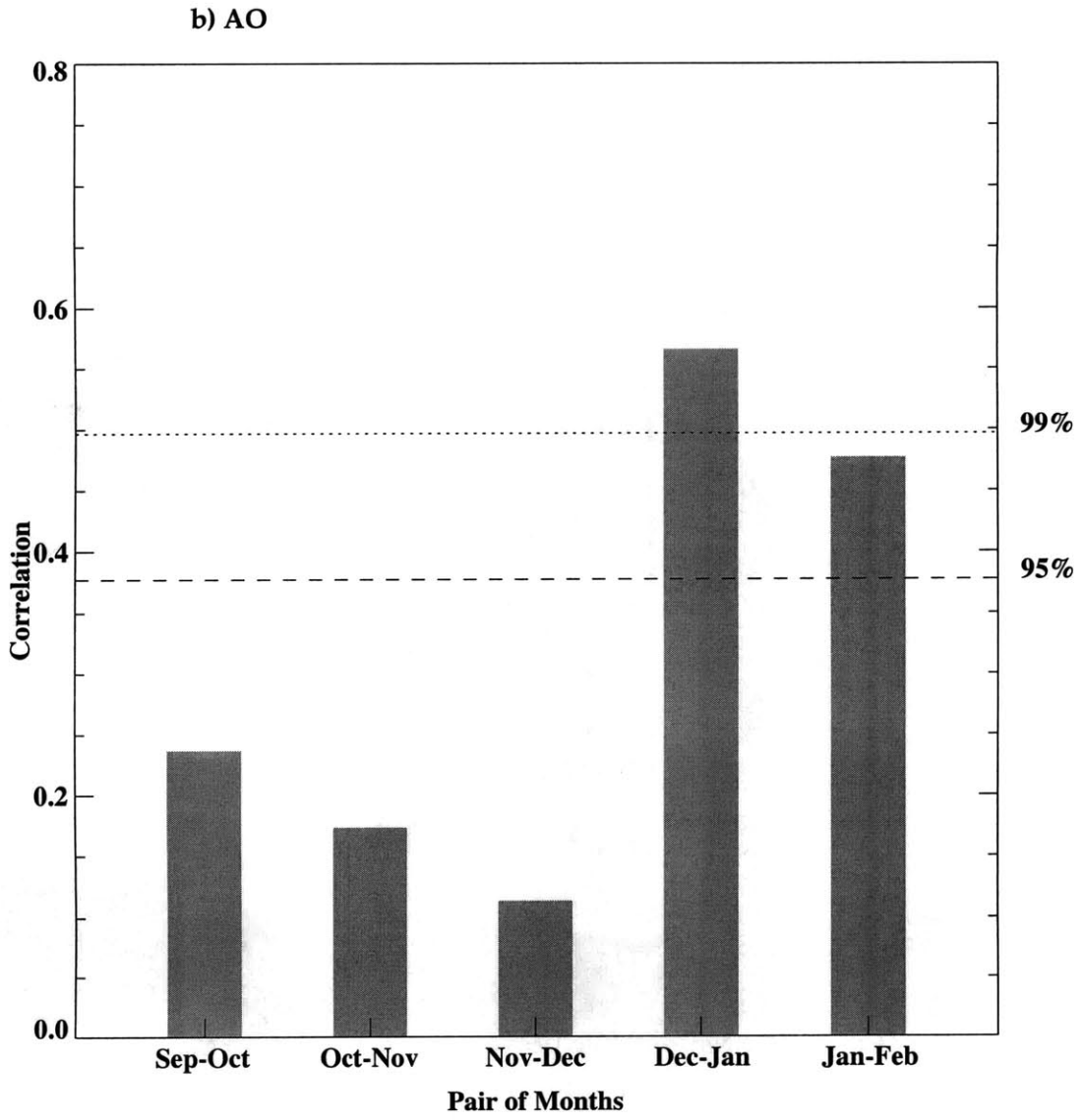

Figure 2.7 *(Continued)*

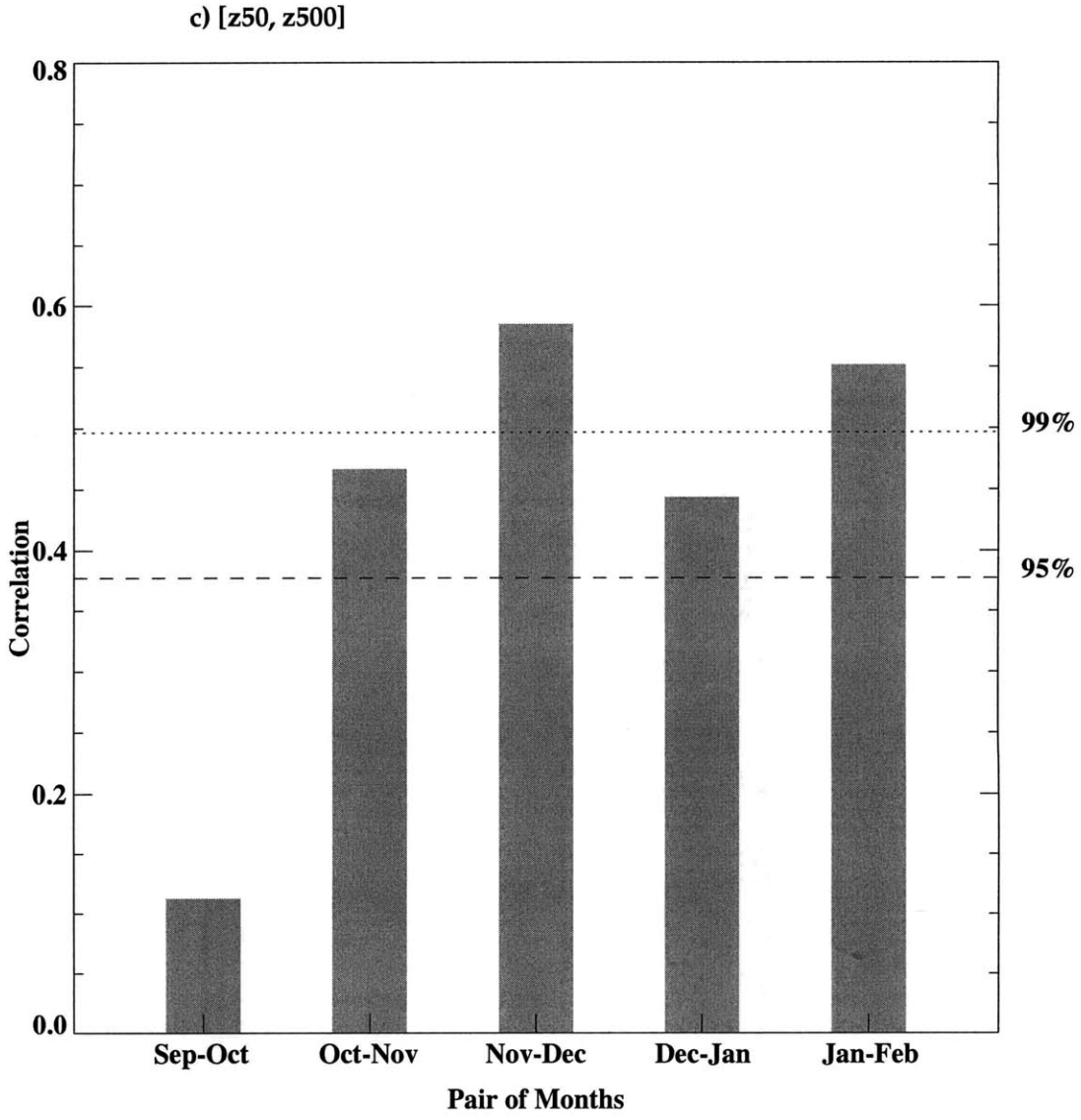

Figure 2.7 *(Continued)*

Chapter 3

Results and discussions

3.1 Daily change of MSLP

In winters following autumns in which Eurasian snow cover is above normal, anomalously high pressure systems cover the Northern Hemisphere high latitudes poleward of 70°N and the northern part of the mid-continents. One possible reason for this anomalously high pressure region is, as raised in Cohen and Entekhabi (1999), that the divergence of the cold, dense air at the lower level, which is inhibited to move south- and eastward from western Siberia due to lateral boundaries of the high topography ranging from eastern Siberia to Central Asia, expands north- and westward instead. If this is the case, the mass of the dense air is considered to spread out into the low topography area as density currents (gravity currents) with its moving direction affected by coriolis force. Passages of these gravity currents can be captured by surveying the daily change of the anomalous pressure along possible paths of the expansion. Further, the result of month-wise autocorrelation in the previous Section suggests that the expansion is expected to start in December.

The following Hovmoeller diagrams are drawn to study the daily change of mean sea-level pressure anomaly from the climatology, in the domain of October through February and along the following three routes (Figure 3.1):

A (110^oE, 60^oN)– (110^oW, 60^oN)

B (30^oW, 40^oN)– (110^oE, 60^oN)

C (60^oE, 80^oN)–(60^oE, 40^oN)

The first path is chosen in prospect of capturing the passage of the gravity current along the lateral boundaries of the high orography from eastern Siberia to the North America, namely, the Brook Range and Rocky Mountains. The second one is chosen, reversely, to see the intrusion of the Icelandic low pressure systems which would be blocked by the expanding high anomalies. The third path runs through the area in which Eurasian SON snow cover turns out to have specific contribution, as will be shown in Section 3.2.2 to the DJF MSLP variability, and not linearly associated with the leading mode of MSLP anomaly, i.e., the AO.

For the cross-section A, in winter of 1976 to 1977, after the most extensive snow cover in Eurasia since the NOAA satellite data has been made available, high pressure anomaly is observed over the western Hemisphere in early December and in the eastern Hemisphere from the end of December to mid February (see Figure 3.2). The direction of expansion appears from the North American side to Eurasia. In opposition, in winter of 1988 to 1989, the winter after the least snow cover in the Eurasian autumn since 1972, the high pressure anomaly is scarcely observed in the Eurasian side, and the date line (180^o) is mostly covered by low pressure anomalies.

However, in the winters after the second and third extensive snow cover in autumn, namely, 1972–73 and 1993–94, passage of high pressure anomaly is somewhat observed, it is difficult to tell the difference from those of 1990–91 and 1979–80 in which the autumn snow cover was the second and third least since 1972. As far as the pathway along the orography from east Siberia to the northwestern North America, evidence of high pressure anomaly expansion due to the extensive snow cover is not found.

Along the path from the mid-latitude central North Atlantic to Siberia (cross-section B), consistent slope towards Siberia in the anomaly fields is the synoptic advection by the background southwesterly. In the winter of 1976–77 a group of anomalous high is observed in December and January over the Norwegian Sea and the Barents Sea, and move southwestward

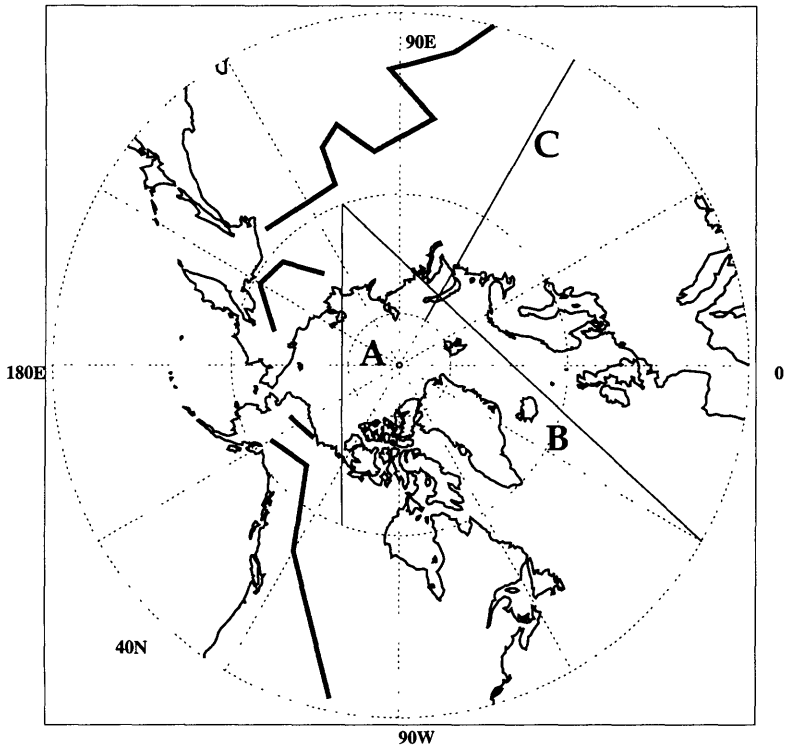

Figure 3.1: The cross-sections for Hovmoeller diagram of MSLP anomaly as shown in Figures 3.2 to 3.4

relative to the synoptic background flow. Of these anomalies, those found in December expand southwestward but appear originated around 10°E, 70°N, not in Siberia. Another group of high anomalies, from the end of December to mid February, occupies large area near Kara Sea (60–70°E and 70–80°N). In opposition, in the winter of 1988–89 intrusion of low systems are apparent over the entire high latitude portion and reach deep into Siberia.

Except these two extreme winters the patterns of daily change of pressure anomaly along this pathway does not vary in association with the anomalous Eurasian snow cover in the previous season, and therefore does not clearly provide evidences to illustrate the view of the gravity current.

Finally, the cross-section C shows some episodic passages of high pressure anomalies *from Kara Sea to into Central Asia* from late autumn to early winter of 1976–77, and stationary high anomaly in Siberia after the end of year. In 1988-89, in opposition, none of these transient nor stationary high pressure anomalies are observed, and covered by low anomalies. However again, except these two extremes consistent evidence of connecting the two opposite ends monotonically is not found.

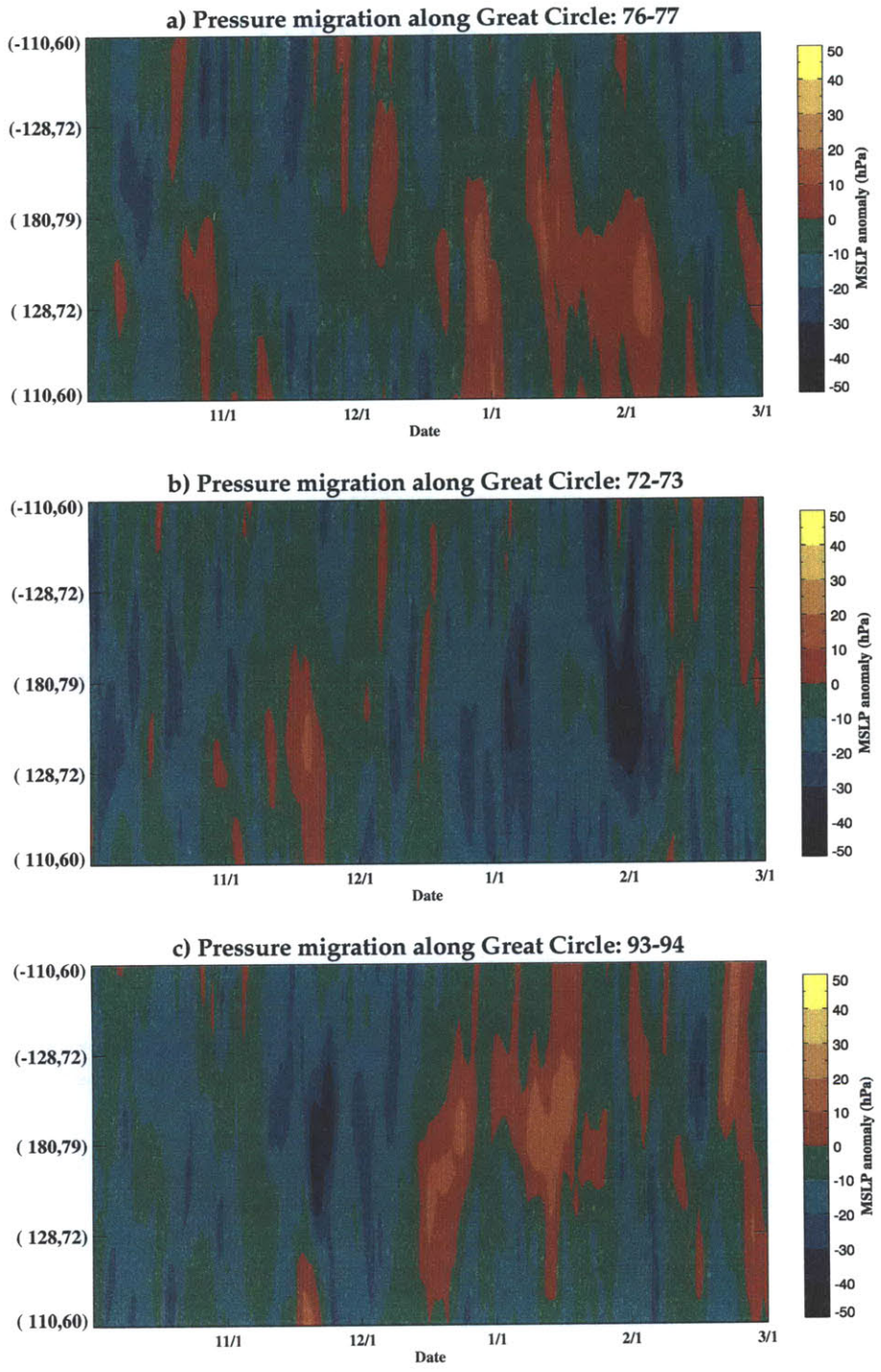

Figure 3.2: Hovmoeller diagram of MSLP anomaly from October to February along the cross-section A: (110°E, 60°N)– (110°W, 60°N) for three years of the largest snow cover in Eurasian SON after 1972, a) 1976-77, b) 1972-73, and c) 1993-94, and for three years of the least snow cover, d) 1988-89, e) 1990-91, and f) 1979-80. Longitude in the negative number indicates the western Hemisphere.

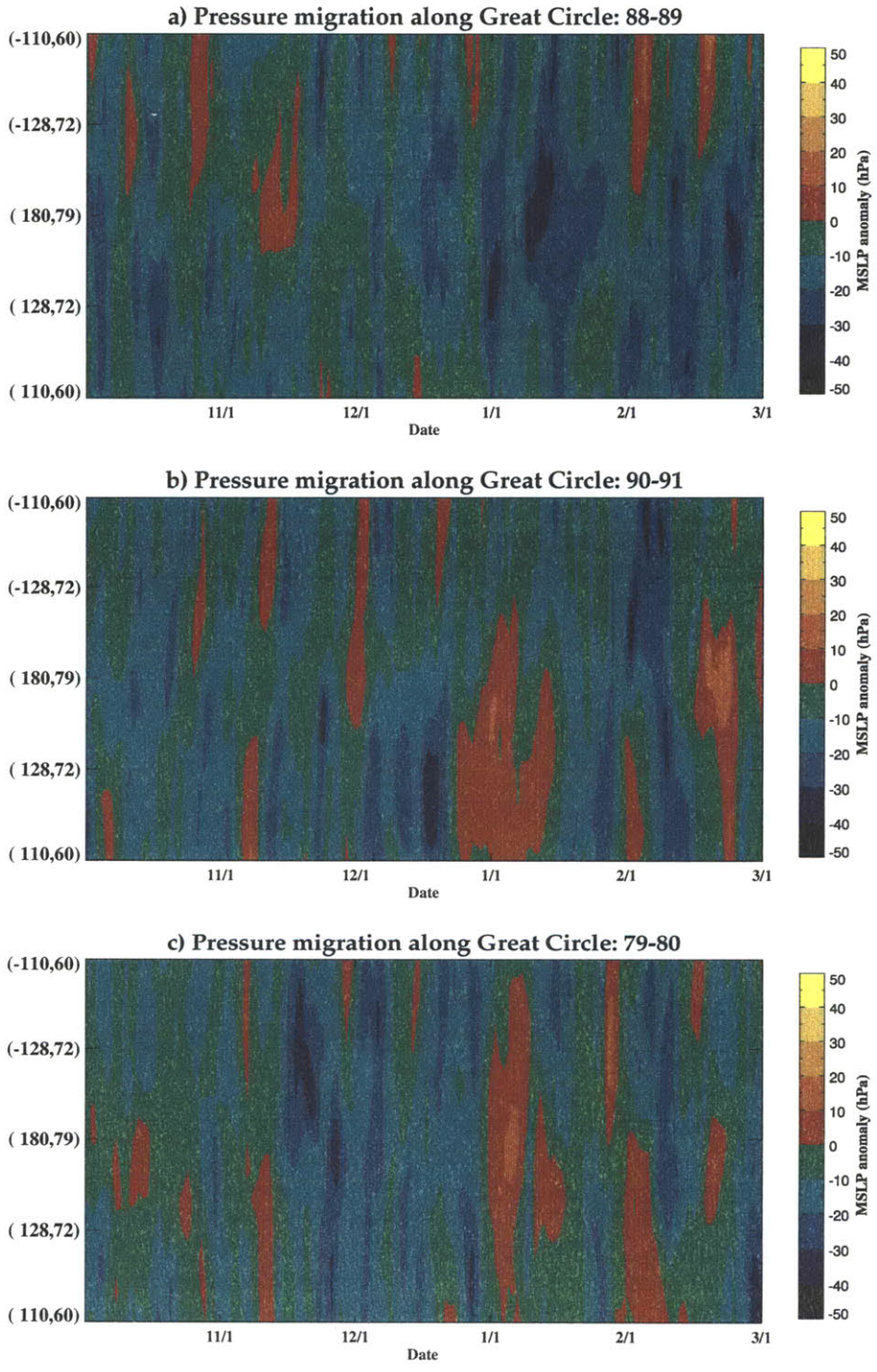

Figure 3.2 *(Continued)*

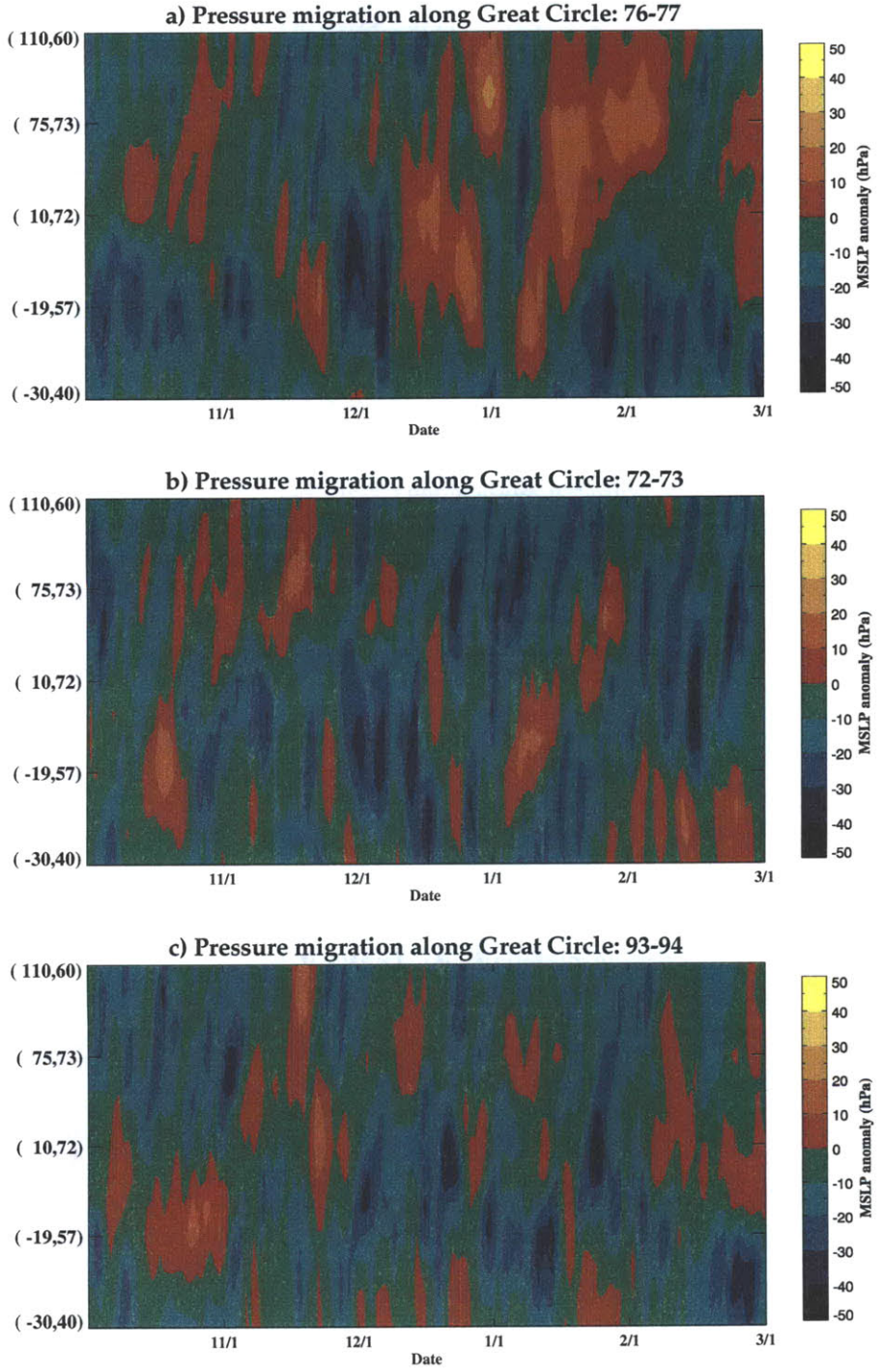

Figure 3.3: Same as Figure 3.2 except for the cross-section B: (30°W, 40°N)– (110°E, 60°N).

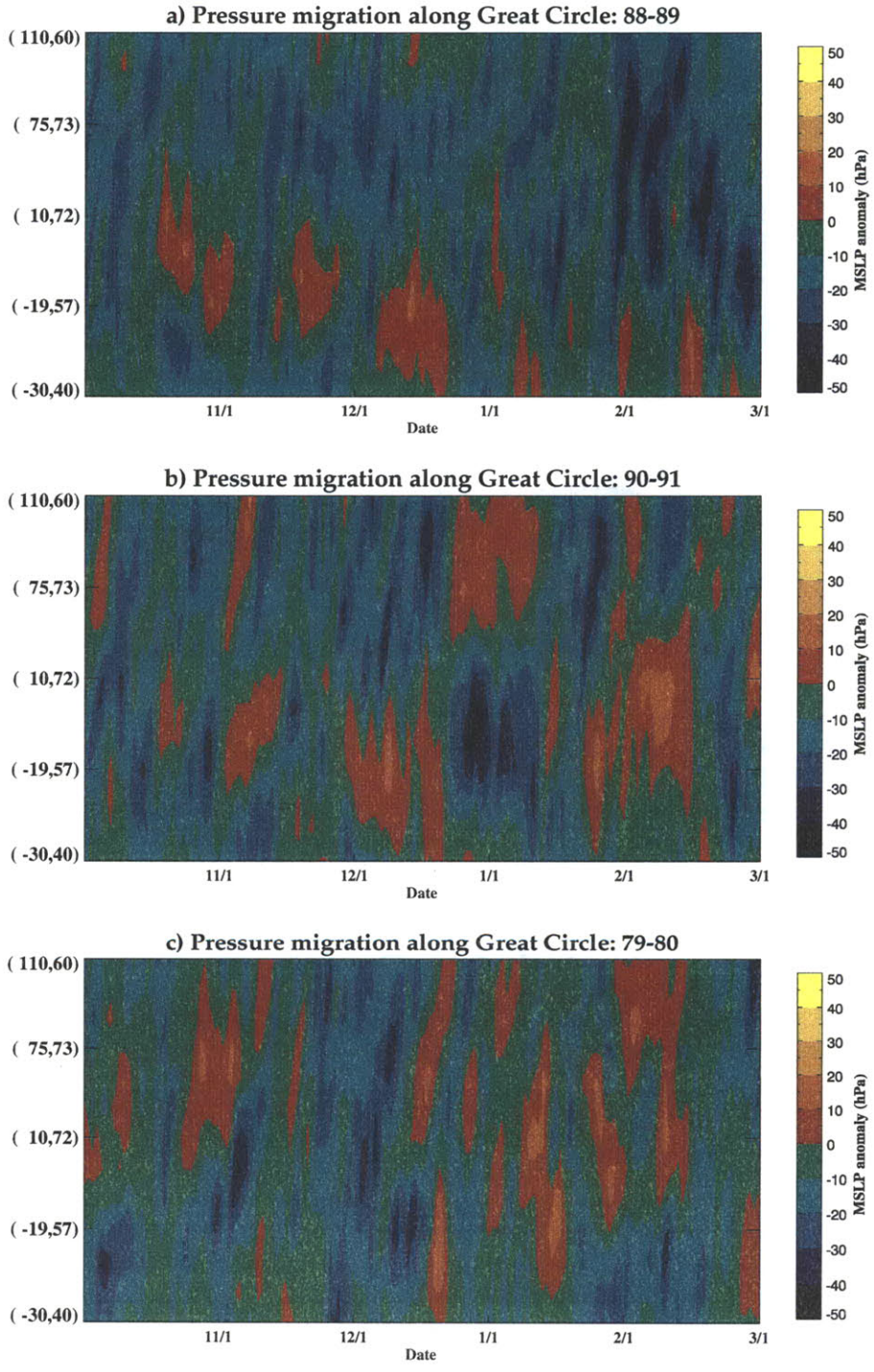

Figure 3.3 *(Continued)*

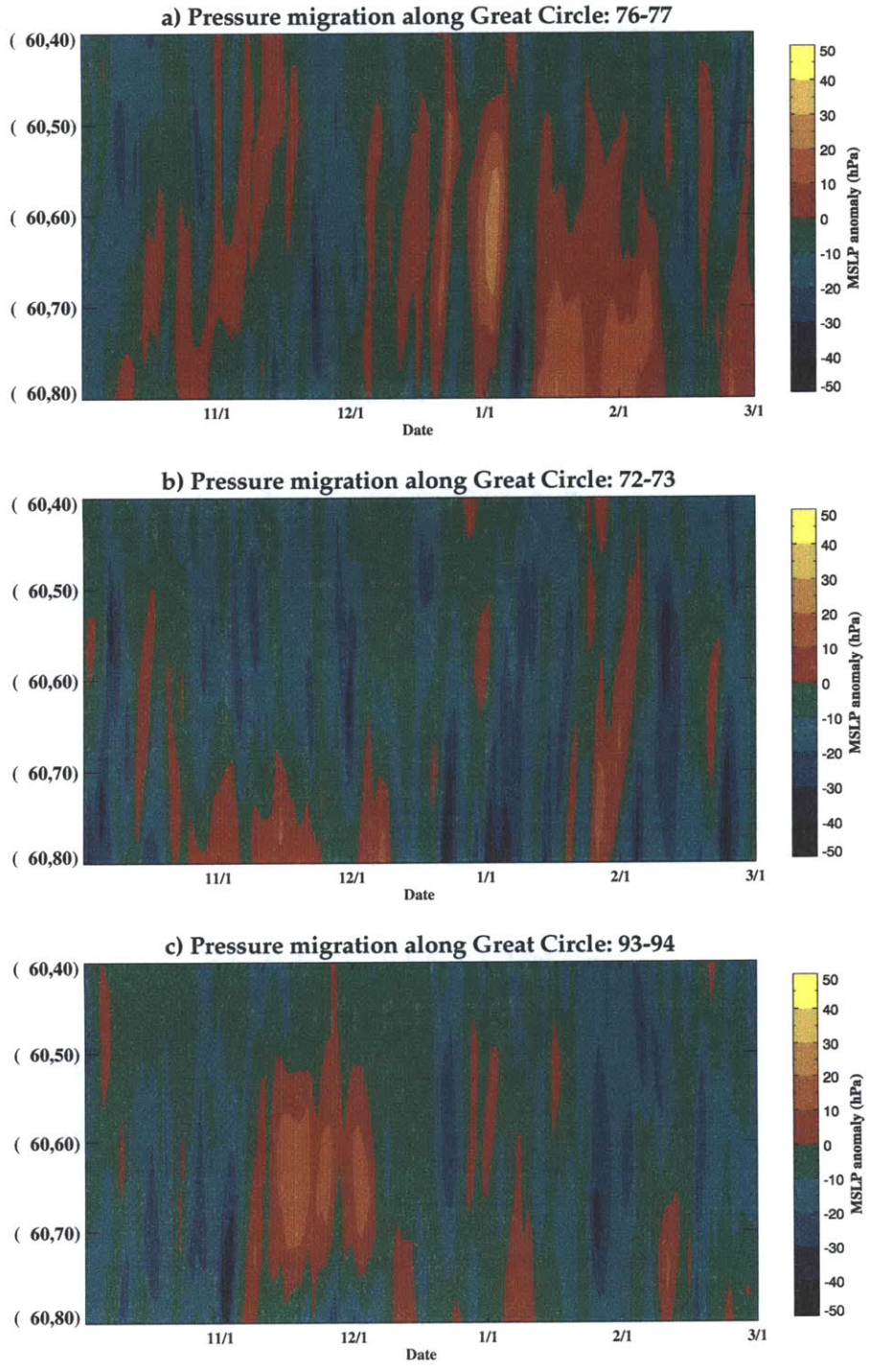

Figure 3.4: Same as Figure 3.2 except for the cross-section C: (80°E, 60°N)–(40°E, 60°N).

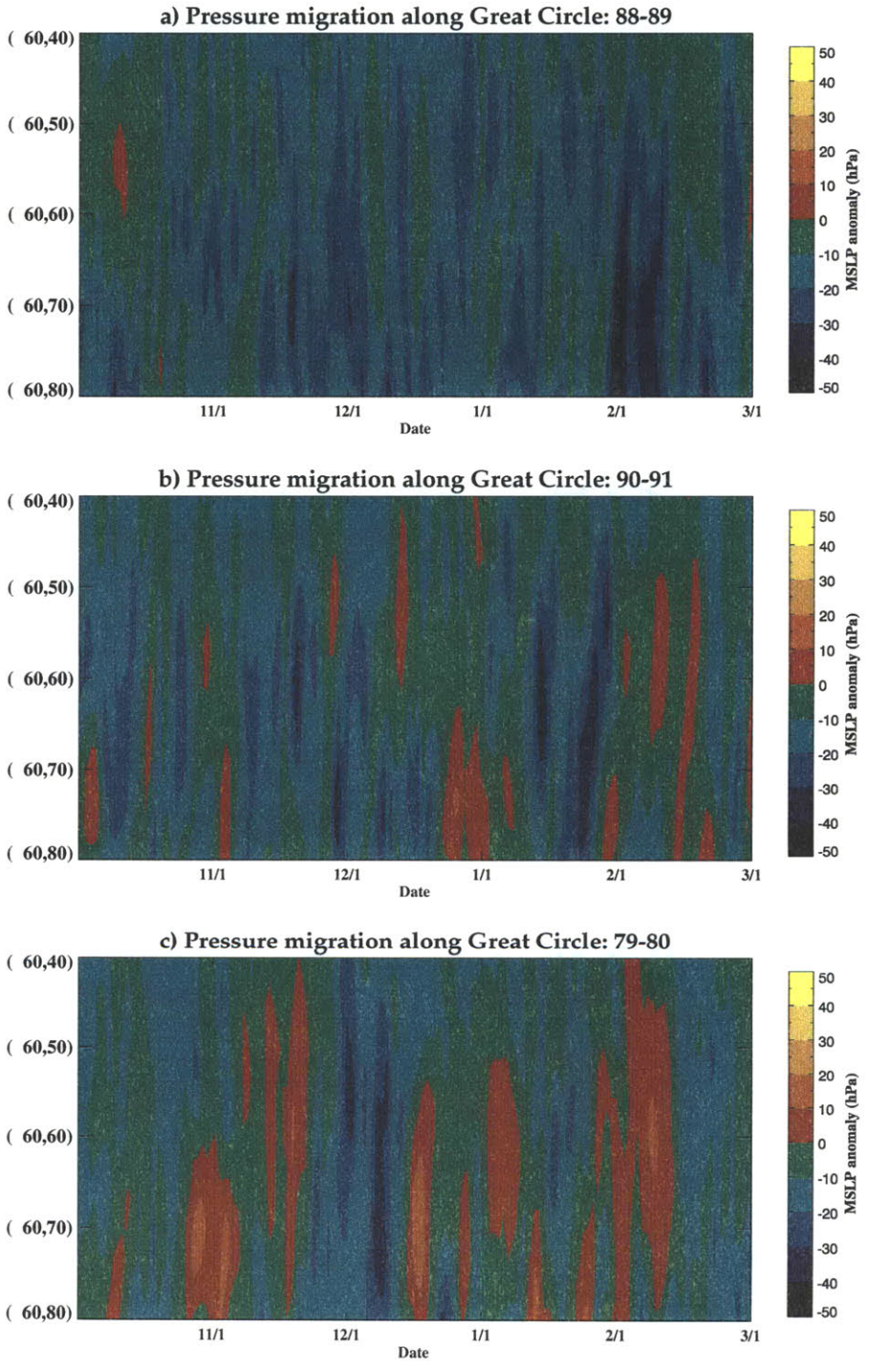

Figure 3.4 *(Continued)*

3.2 Regression analyses between wintertime NH climate variability and autumn Eurasian snow cover

3.2.1 Seasonal change of atmospheric circulation

Mean sea-level

A series of regression/correlation maps onto 27-year autumn Eurasian snow cover, of each 30-day period mean MSLP field with 15-day shift is shown in Figure B.1 in Appendix B from October to February. Local regression coefficient is derived as result of simple linear regression of grid point's time series to the snow cover time series, and is identical to the departure of the local MSLP corresponding to the unit standard deviation of the snow cover. The correlation coefficient is computed according to Pearson's definition. The regression coefficients are shown by shades, and the correlation coefficient by lined contours. The contours of correlation coefficient 0.323, 0.381 and 0.487 coincide with the statistically critical value of 90, 95 and 99% probability, respectively, for rejecting the null hypothesis of white-noise, zero correlation coefficient, and hence zero regression coefficient. This set of maps delineates the intraseasonal placement and transition of such interannual variability in the MSLP residuals that are linearly related to the autumn Eurasian snow cover fluctuation.

Starting around the end of November (Figure B.1d in Appendix B) an area of positive regression (and correlation) emerges over the polar cap extending from west Siberia to Northwestern Canada. There are two centers of statistical significance, one over Kara Sea (60–70^{o}E and 70–80^{o}N) and the other in Central Asia between Caspian Sea and Aral Sea. These two centers become more prominent in December. Then the center over Kara sea, moving slightly westward, eventually merges with the other center which has expanded from Central Asia. By the end of year (B.1f) the positive area covers the almost entire polar cap, surrounded by the northern edge of the 1000m topography lines which are depicted by a group of thick lines in the figures, and Greenland, with exception of the southern part of central Siberian uplands (90^o–120^{o}E, 55^o–65^{o}N), the climatological center of the Siberian High (e.g., Sahsamanoglou et al., (1991)). Watanabe and Nitta (1999) show, according to their division of the Eurasian Continent, the autumn snow cover fluctuation in "eastern Eurasia" area has distinct re-

lationship with atmospheric circulation in the following winter. This area, approximately surrounded by 75^o–140^oE and 40^o–65^oN, almost coincides with the climatological position of the strongest Siberian High as stated above. The previously mentioned two positive centers of action found in the early winter regression map are located somewhat on the edge of this area. This may imply that pressure anomaly in the winter due to anomalous snow cover manifest itself not by deepening at the location of cooling but by expansion to the adjacent areas. However, it should be noted that this analysis does not serve to confirm the causal effect of the anomalous snow cover since these linear statistical methods gives no proof of causality.

In the meantime a negative center with more than 95% significance appears over the Atlantic coast of Europe and is maintained until the end of winter with slow eastward movement of the center and zonal expansion. There is another negative area in North Pacific with minor magnitude in regression. This spatial pattern, one center over the polar cap and two centers of the other polarity over the North Atlantic and North Pacific, is quite similar to the leading mode of the wintertime MSLP variability. This is, in fact, to be expected considering the moderate correlation between the two time series ($r = .516$. Table 2.1).

The transition of the centers in regression maps from late autumn to mid-winter (B.1c-g) appears to support the hypothesis raised in Cohen and Entekhabi (1999) that cold, dense near-surface air induced by anomalous snow cover in Eurasia, with its south- and eastward expansion blocked by the topographical barrier, expands over the Arctic to the western Hemisphere, whereby pushing the climatological, Icelandic Low equatorward which then brings anomalous low over mid-latitude North Atlantic.

Focusing on predictability of wintertime climate in Europe, the negative area appearing over Europe in the winter is a statistical suggestion that an autumn of extensive (deficient) snow cover over the Eurasian continent would be followed during winter by negative (positive) sea-level pressure anomalies over Europe, and the storm track shifted southward (northward) (e.g., Hurrell (1995)).

Following the mid-winter the positive area retreats from the mid-latitude to the high-latitude in both Eurasia and North America, and the positive center moves poleward to Kara Sea and then to Greenland. The retreat of the positive area corresponds to the resumption

of the solar radiation in the Northern Hemisphere high latitude. The sun illuminates the area southward of ca. 72°N by the end of January, that of ca. 83°N by the end of February (*Wallace and Hobbs (1977)* [70]). In February the positive area over the polar cap is contained to poleward of 60°N.

As introduced in Section 2.2.2, the uAO index is defined as the primary component time series of the first EOF mode of the lagged combined field of 30-day mean 500hPa and 50hPa geopotential height where the latter leads by 15 days, and represents the leading, downward propagating mode of the circulation variability from the lower stratosphere to the middle troposphere. Care must be taken since the polarity is set opposite to the conventional direction so that it has positive correlation with the Eurasian snow cover. The transition of patterns in course of season shows progress of MSLP variability linearly associated with interannual fluctuation of downward propagating upper air circulation anomaly.

As is expected by moderate correlation ($r = .564$) between the uAO index and autumn Eurasian snow cover, placement and transition of the patterns in winter are similar between the two (*Cf.* Figure B.1). However, some different features are observed, of which some points of physical interests will be described in the following.

The center of the positive area resides always near the northern coast of Siberia from early October (B.3a) and this center keeps continuity for the most of the season, opposite to two separated centers in the case of the snow cover. The positive area expands from western Siberia to Central Asia, Arctic Ocean, to Greenland and then to eastern Siberia as the winter progresses, whereas two negative areas grow in the both sides of Atlantic coasts and in the Pacific, to form at the end of year a pattern almost congruent to the AO pattern (B.3f. *Cf.* Figure 2.4). The spatial pattern maintains its basic form thenceafter with decrease in size and magnitude in late winter parallel to that of the snow cover, except the negative area in the Atlantic which continues to place its center over the North Atlantic. In contrast to snow cover, no significant positive area is found over subtropical central Pacific.

Middle troposphere

In late autumn to mid-winter the pattern of the regression map of 500hPa geopotential height onto autumn Eurasian snow cover (Figure B.2c–f) appears to be a superposition of several

planetary-scale circulation anomalies. The dominant feature is the annular pattern with positive area over the polar cap and negative band in the mid-latitude with more weight on the Atlantic side. The pattern on the Pacific side is reminiscent of Pacific-North American pattern (e.g., Wallace and Gutzler (1981)) but somewhat distorted. These regression maps, especially in winter, are similar to the leading mode of 500hPa geopotential height as shown by the previous studies.

In year of extensive autumn snow cover in Eurasia, two centers of positive anomaly, one over Kara Sea and the other over Alaska and Northwest Canada, start to form in November and they eventually merge over the Arctic Ocean (B.2c–d). Surrounding this positive area over the Arctic basin there is a zonal band of negative area between 40^oN and 60^oN, whose four centers are located above the both sides of the Atlantic, eastern Siberia, and North Pacific (B.2c). This zonal band of negative anomaly persists through the winter, though with some distortion and modulation. Another area of positive regression appears over the Caucasus in December and gradually moves poleward until it eventually merges to the center in the Arctic in January (B.2e–h).

In late winter the overall pattern shifts in such direction that its center moves to the south of Greenland, whereby statistically significant, positive coefficients are found in three distinct areas, that is, Labrador Sea, Gulf of Suez, and subtropical Central Pacific, and negative areas are found in another three ares, namely, Central Europe, Gulf of Alaska, and southeast North America. As mentioned in the previous subsection, a wave-like pattern extending from subtropical Pacific over the Arctic to Europe has barotropic structure, which is confined to the troposphere since correspondence is not found in the 50hPa geopotential height regression map (not shown).

Field significance

In the previous correlation maps and analysis statistical significance is tested locally at each grid point. Due to spatial correlation of underlying data between adjacent grid points and multiplicity problem of conducting independent tests, however, a question still remains if they are collectively significant. In order to investigate the global significance the following field significance test was performed.

The results of the field significance test is summarized in the Table 3.1. The figures in Table 3.1 are the percentage area in the extratropical NH (northward of 40°N) in which the correlation between the mean field (e.g., MSLP) in the corresponding period and the index time series (e.g., SON Eurasian snow cover) is significant at 95% level. The test was done by comparing these values with the null distribution of the percentage area which is produced by the Monte-Carlo method, following the method of *Wilks (1995)* [77]. The test time series is produced to have same AR(1) (first-order autoregression) structure with the index being tested.

At mean sea-level, the patterns of the correlation between MSLP and all three indices, that is, SON Eurasian snow cover (ESC_{SON}), the AO, and the upper AO (uAO), start to fall into upper 5% region, suggesting field significance at 95% critical level, from December (the period f, 12/1–12/31), and continue to show significance for the subsequent period. In opposition, with extratropical NH 500hPa geopotential height field the SON Eurasian snow cover starts to correlate globally significantly one period earlier than it does with the MSLP field, and than the AO does with 500hPa height field. This appears to suggest the view that the Eurasian snow cover affects the tropospheric circulation earlier than the MSLP variations which is directly or indirectly associated to the snow cover, emerge. However, as for the way that the snow cover associates itself to the tropospheric circulation variability, the results of this study is not indicative of an initiation but rather a modulation, for two reasons. One is that the result of the autocorrelation analysis in Section 2.2.3 shows the abrupt increase of the autocorrelation in the combined field of the middle troposphere and stratosphere geopotential height occurs between October and November (Figure 2.7c). And the other is from the field significance test (Table 3.1) that the significant correlation pattern between the DJF uAO and 500hPa geopotential field appears to start earlier in November. These results suggest that in the middle troposphere it may be in October to November that the "winter regime" is initiated.

Table 3.1: Field significance test of correlation of SON Eurasian snow cover area and DJF indices of EOF modes with circulation fields from October to February.

		MSLP			z500		
	Period	ESC_{SON}	AO	uAO	ESC_{SON}	AO	uAO
	9/1–9/30	9.0	4.6	9.2	13.8*	8.2	10.5
	9/15–10/15	7.0	8.7	4.0	15.6*	10.8	1.9
a	10/1–10/31	1.6	9.4	9.5	2.3	14.8*	10.5
b	10/15–11/15	2.0	4.8	10.0	0.4	2.9	7.9
c	11/1–11/30	1.5	5.3	13.2	9.2	7.1	14.1*
d	11/15–12/15	6.9	3.8	11.6	15.1*	3.9	13.0
e	12/1–12/31	16.3*	23.0*	25.3*	16.2*	19.1*	21.6*
f	12/15–1/15	15.6*	44.6*	38.4*	13.1	42.5*	34.1*
g	1/1–1/31	11.3	54.3*	47.9*	6.8	51.3*	40.6*
h	1/15–2/15	10.0	48.0*	32.6*	5.3	41.9*	30.8*
i	2/1–2/28	18.3*	40.8*	25.4*	7.6	24.9*	15.5*
	DJF	28.6*	60.7*	48.0*	27.9*	56.4*	42.4*

*: Within upper 5%.

3.2.2 Multiple linear regression analysis

In the previous section intraseasonal transition of the relation between the SON Eurasia snow cover and circulation variability at the surface and the middle troposphere was shown. In this section it is surveyed what is the specific contribution of the ESC_{SON} to the DJF MSLP variability, in comparison to the linear trend, and the Atlantic and the Pacific side of the leading MSLP variability. To this end, multiple linear regression was performed. In each of the multiple linear regression, only two predictors were used. One predictor is always ESC_{SON}, and the other is either the linear trend, the PAC or the ATL index. The latter two indices are defined in the Section 2.2.3. By using these predictors the statistical analysis technique allows to isolate the specific contribution of ESC_{SON} when the effect of each of the three variabilities is removed.

In the following figures from 3.5 to 3.7 local value of the partial regression coefficients are shown in shades, whereas the contribution (square of the partial correlation) of the predictor to local variability is line-contoured every 10%, beginning from 10% with alternating thin and thick lines. The regression coefficient denotes the deviation of the local field value corresponding to the one standard deviation change of the predictor when the effect of the other predictor is removed. Only in the linear trend cases, the regression coefficient is expressed in terms of annual change in the 27 years from 1972 through 1998.

Linear trend The simple regression analysis showed large areas of significant increasing trend of 1.2hPa/year or more over Tibetan Plateau and the Caucasus. In contrast, no statistically significant decadal decrease with more than 95% confidence was found (not shown). These results are also visible in the multiple regression analysis (Figure 3.5b). The ESC_{SON} partial regression retains the almost same shape and intensity as the single regression (e.g., Figure B.1e-i). This suggests that the ESC_{SON} contribution to the DJF MSLP variability does not show strong linear trend, despite the results of *Thompson et al. (2000)* [65] that notes decadal trend from a longer dataset.

The PAC index Figure 3.6a shows the partial regression of the DJF MSLP onto the PAC index. Although the response over the north and west North America is weak, the spatial

pattern is reminiscent of the PNA pattern. Indeed, the regression map of 500hPa geopotential height reproduces well the three centers of action of the PNA pattern (not shown). As for ESC_{SON}, although the shape and extent of the response are somewhat weaker than the single regression (*Cf.* Figure 3.5b), it retains the basic characteristic of the response, and contributions over the polar cap, Central Asia and western Europe.

The ATL index The ATL mode, the NAO-like pattern on the semi-hemispheric scale (Figure 3.7a), depicts the seesaw pattern of the high-latitudes and the mid-latitudes, with the centers of action somewhat shifted eastward. The ESC_{SON} partial regression is almost statistical residual (3.7b). Together with the results of the correlation analysis in the Section 2.2.3 and the above multiple regression with the PAC, it is suggested that the wintertime MSLP variability associated with the ESC_{SON} variability is largely confined to the Atlantic side of the Northern Hemisphere, and that such specific contribution of ESC_{SON} that is linearly-independent from the hemispheric-scale variability mode (i.e., the PAC, the ATL and the AO), is found in Central Asia.

Field significance Field significance test is conducted similarly to the case in Section 3.2 with necessary adjustment to the loss of one degree of freedom due to estimation of the partial correlation (*Anderson (1958)* [1]). The result is summarized in Table 3.2. When the linear trend is removed from DJF MSLP variability, the field significance of SON Eurasian snow cover with the DJF MSLP field is greater than the 5% level. Removal of the Pacific side variability decreases the field significance to 10% level. Finally, when the Atlantic side variability is removed, the percentage area becomes extremely small that less than 2% of the area northward of 40^{o}N shows significant correlation. This supports the results from visual inspection of the multiple regression map that the association of SON Eurasian snow cover association to the DJF MSLP variability is largely confined to the Atlantic side.

Table 3.2: Field significance test of the partial correlation of SON Eurasian snow cover area in the DJF circulation fields with the (semi-)hemispheric effects are removed.

Effect removed	Linear	The Pacific side	The Atlantic side
	25.2*	15.3+	1.7

+: Within upper 10%.

*: Within upper 5%.

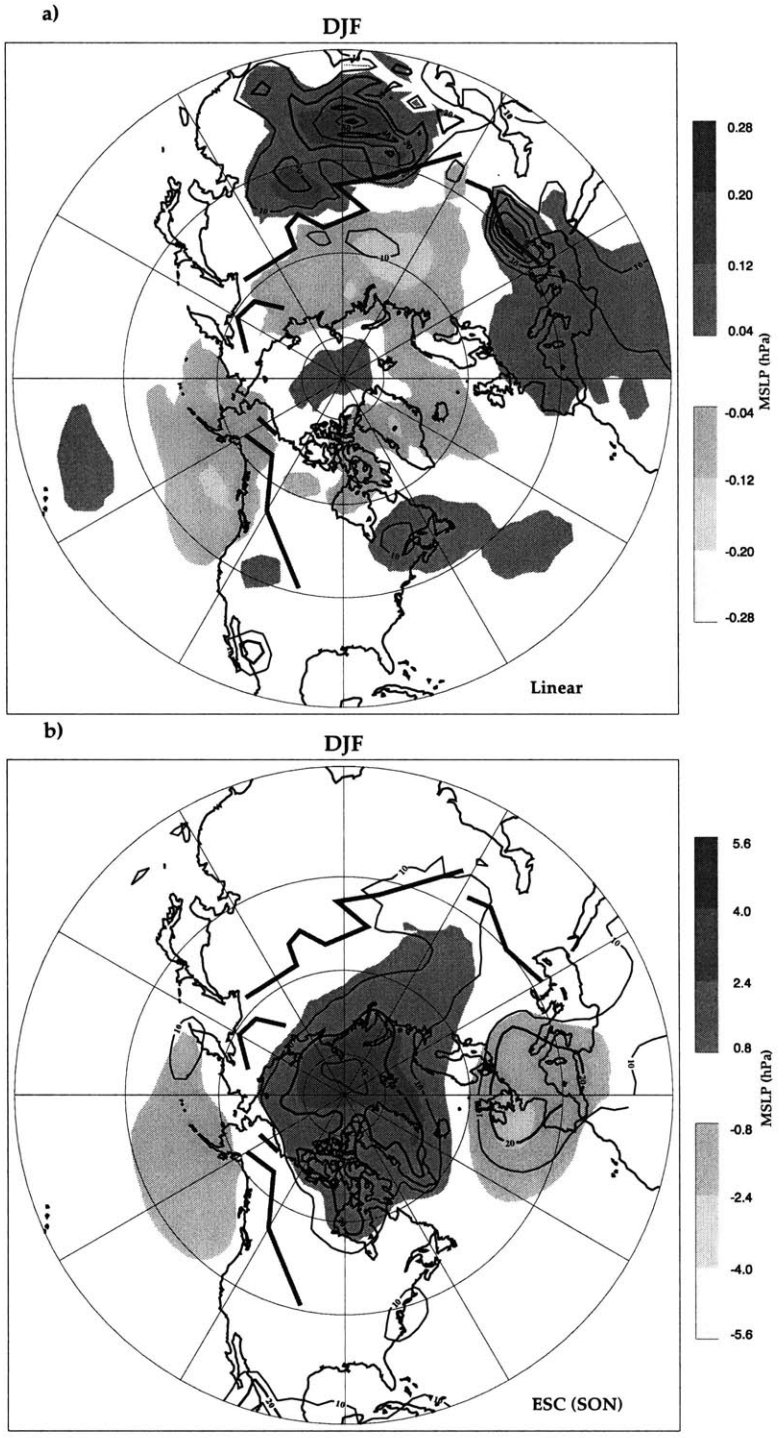

Figure 3.5: Partial regression correlation (shaded) and contribution (line-contoured) in multiple linear regression of DJF MSLP onto ESC_{SON} and liner trend, a) for linear trend and b) for ESC_{SON} . In a) regression coefficient shows linear trend of DJF MSLP per year in 27 years (1972-1998), while in b) it indicates MSLP deviation corresponfing to one standard deviation change of ESC_{SON} when effect of linear trend is removed. Contribution is lined every 10% from 10% by alternating thin and thick lines.

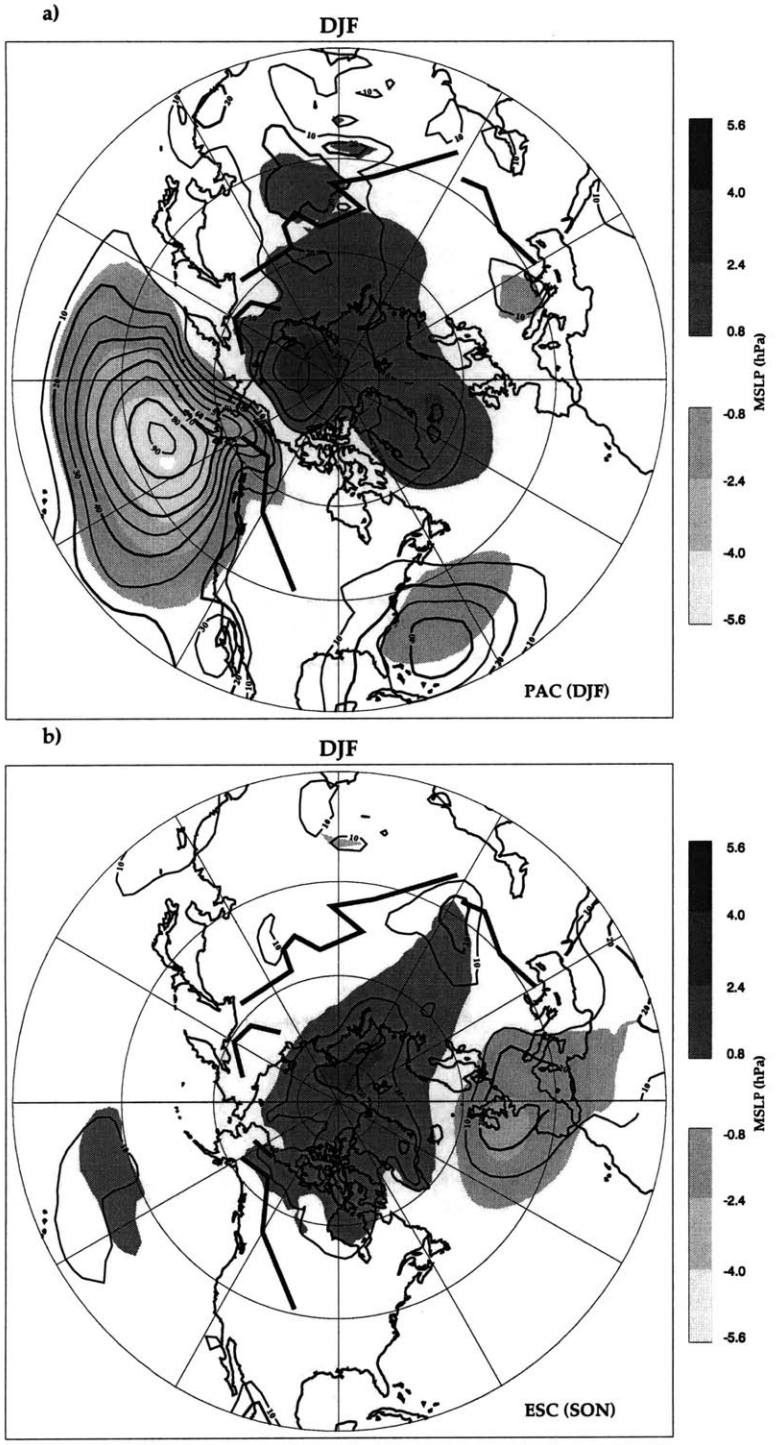

Figure 3.6: Same as Figure 3.5 except for ESC_{SON} and the PAC.

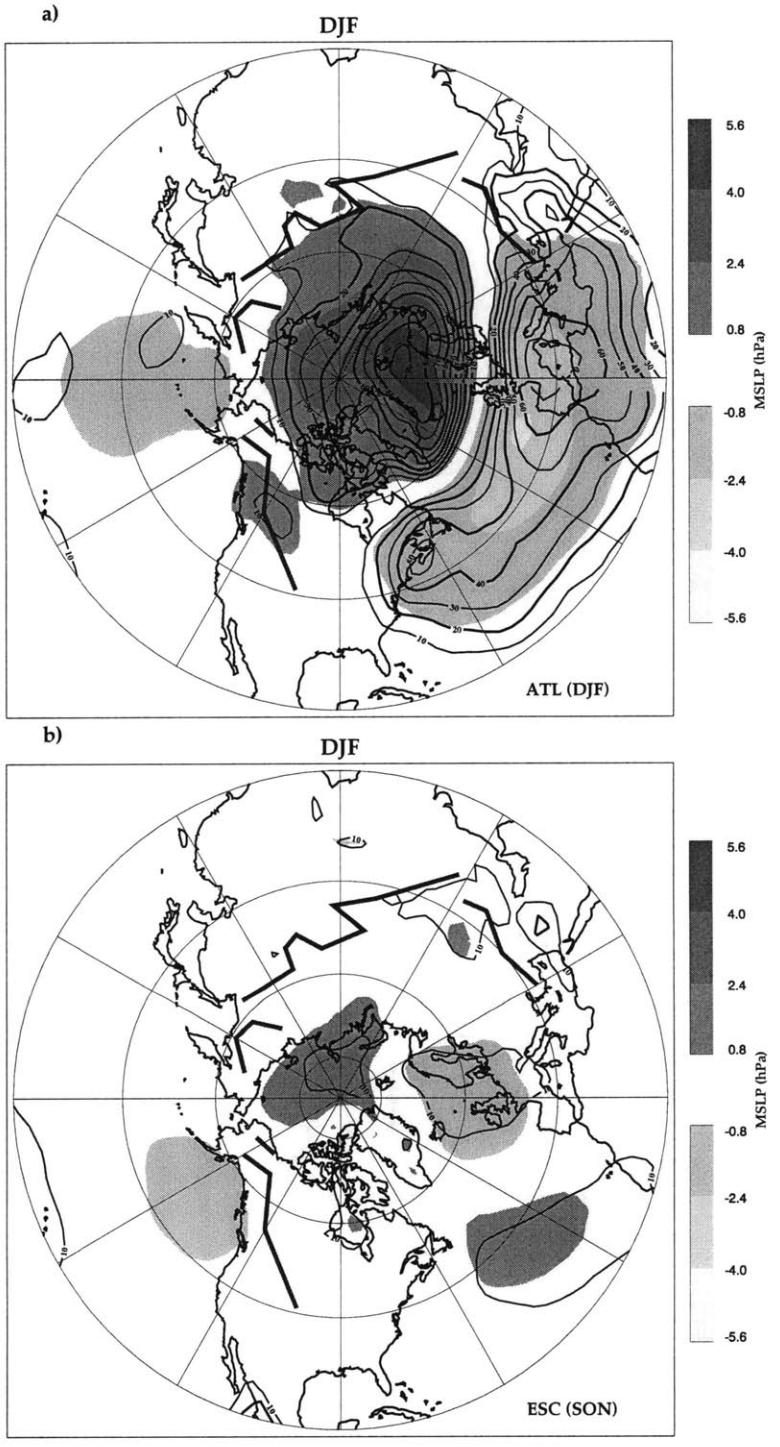

Figure 3.7: Same as Figure 3.5 except for ESC_{SON} and the ATL.

Chapter 4

Conclusions

In this research, the following things are shown:

- The autumn (SON) Eurasian snow cover ESC_{SON} of 1972 – 1998 shows statistically significant correlation with the leading variability mode of the wintertime (DJF) atmospheric circulation with barotropic characteristics in the Northern Hemisphere extratropics. The correlation coefficient decreases as the distance between the snow cover (i.e. surface) and the pressure level of the circulation considered, implying the snow cover may act as a lower boundary forcing to the atmospheric circulation in the troposphere.

- The mechanism that is built on the connection between the anomalous snow cover in autumn Eurasia and wintertime sea-level pressure variability through gravity current of the divergent cold, dense air (high pressure anomaly) from inner Eurasia, whereby the expansion is only allowed north- and westward due to lateral boundaries of high orography is only one among several possible mechanisms forcing the leading mode of the winter NH climate variability.

- Constructed downward propagating circulation anomaly from the lower stratosphere to the middle troposphere (uAO) is shown to also have high correlation with ESC_{SON} as the AO mode does. The upper air mechanism may also be active.

- From the correlation analysis, the Atlantic side of the DJF MSLP variability (ATL) is suggested to have stronger relationship with the ESC_{SON} variability than the Pacific

side (PAC) does, reflecting the dominance of the ATL in the AO mode. The uAO also shows stronger connection with the ATL than with the PAC.

- The correlation between the ESC_{SON} and the AO, and that between the former and the uAO diminished when the two extreme years of snow cover (1976 for the largest and 1988 for the least snow cover since 1972) are removed, but ESC_{SON} retains statistical significance of more than 95% confidence only with the AO mode. This suggests there may be threshold values for the autumn snow cover extent to activate a certain mechanism, if any, to affect the atmospheric circulation at the upper level. Also, the connection between the Atlantic and the Pacific sides of wintertime variability in MSLP may be intensified when the ESC_{SON} exceeds, or fall short of, certain threshold values.

- The ESC_{SON} relationship with wintertime MSLP variability is mostly confined to the wintertime variability of the Atlantic side. It has only a little association with the linear trend and the Pacific side variability.

Future work may include:

- Reexamination of the results using the longer data of the observation, which are being done by several efforts (e.g., Frei et al. (1999)) and extension of variables such as snow depth (equivalent water) data. Especially the data of years with extreme snow cover extent in autumn Eurasia, in both directions, will be essential to the research on the role of ESC_{SON} on the wintertime NH climate.

- Further research to seek for the mechanism to connect the ESC_{SON} anomaly and the upper level circulation anomaly. One possible approach is analysis of the wave activity and energy propagation in the troposphere and stratosphere.

- Another approach to broaden our understanding on the role and effect of ESC_{SON} on the hemispheric climate will be the numerical experiment using the GCMs.

Appendix A

Statistics of the cold season NH climate fields

The Mean and standard deviation of the various fields in autumn (SON) and winter (DJF) are shown here. The analyzed fields are obtained from NCEP/NCAR Reanalysis project, and are mean sea-level pressure, 500hPa and 50hPa geopotential height, temperature at 850hPa, and precipitable water. The description and discussion of these results are in Section 2.1.1. shown here.

a) Mean of Mean Sea-Level Pressure [SON]

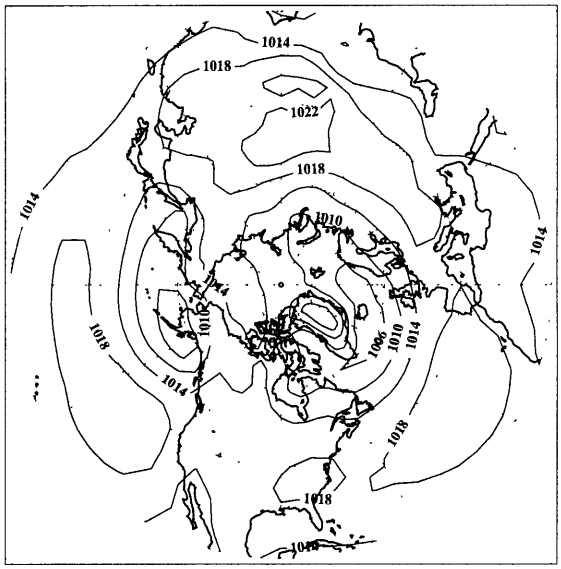

b) Standard deviation of Mean Sea-Level Pressure [SON]

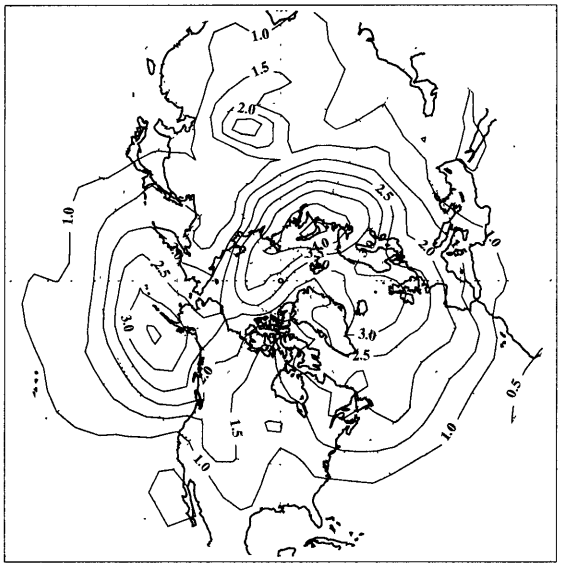

Figure A.1: a) Mean, and b) standard deviation, of mean sea-level pressure (MSLP) (hPa) in SON (1972-1998) from Reanalysis-1.

a) Mean of Mean Sea-Level Pressure [DJF]

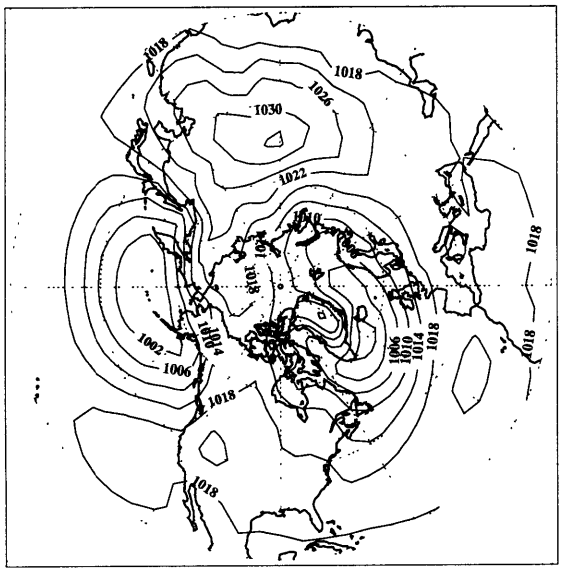

b) Standard deviation of Mean Sea-Level Pressure [DJF]

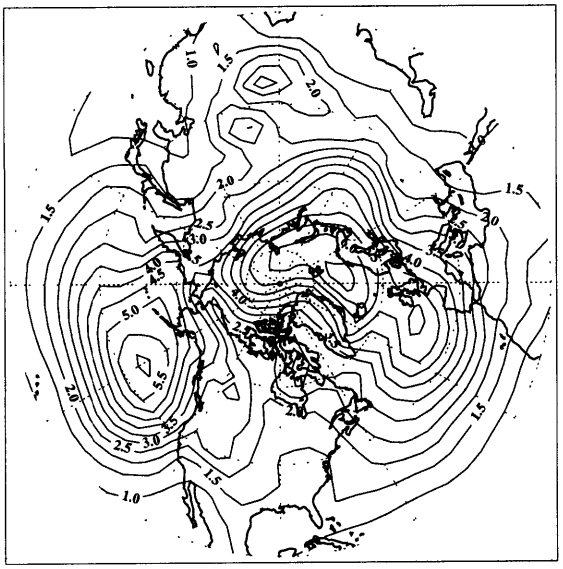

Figure A.2: Same as Figure A.1 except for DJF.

a) Mean of 500hPa Geopotential Height [SON]

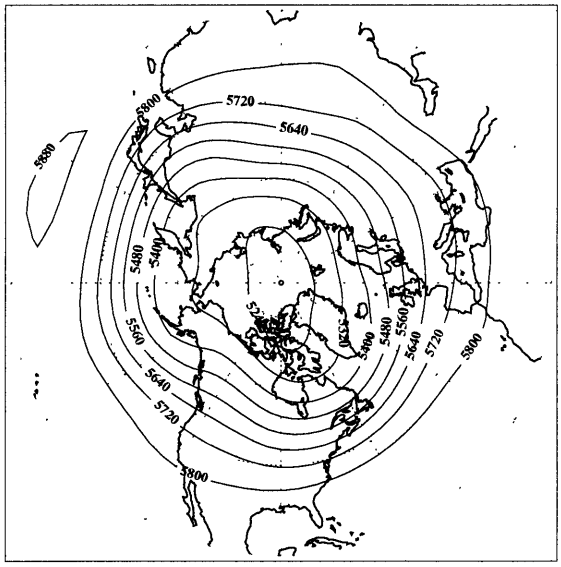

b) Standard deviation of 500hPa Geopotential Height [SON]

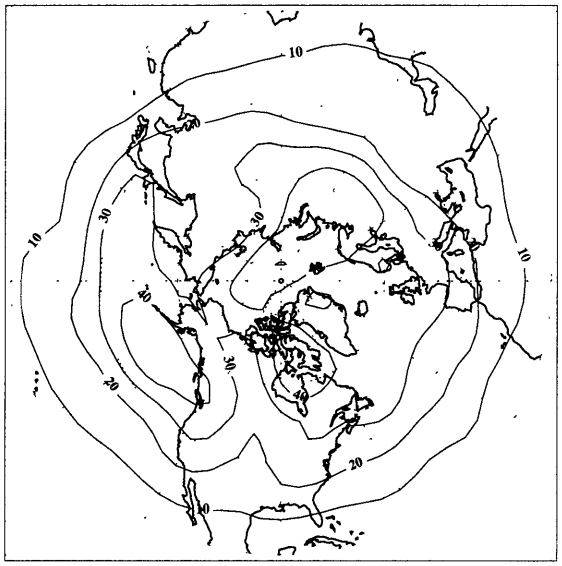

Figure A.3: Same as Figure A.1 except for 500hPa geopotential height (gpm).

a) Mean of 500hPa Geopotential Height [DJF]

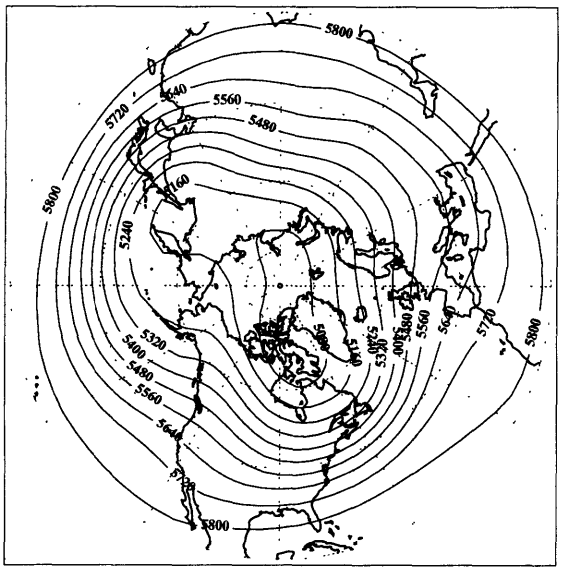

b) Standard deviation of 500hPa Geopotential Height [DJF]

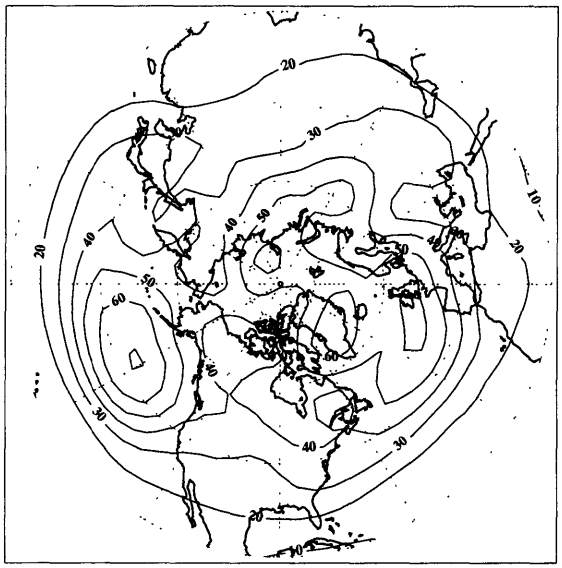

Figure A.4: Same as Figure A.3 except for DJF.

a) Mean of 50hPa Geopotential Height [SON]

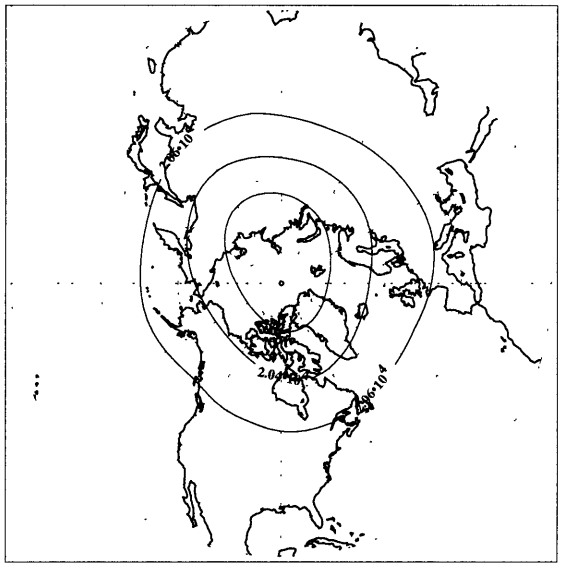

b) Standard deviation of 50hPa Geopotential Height [SON]

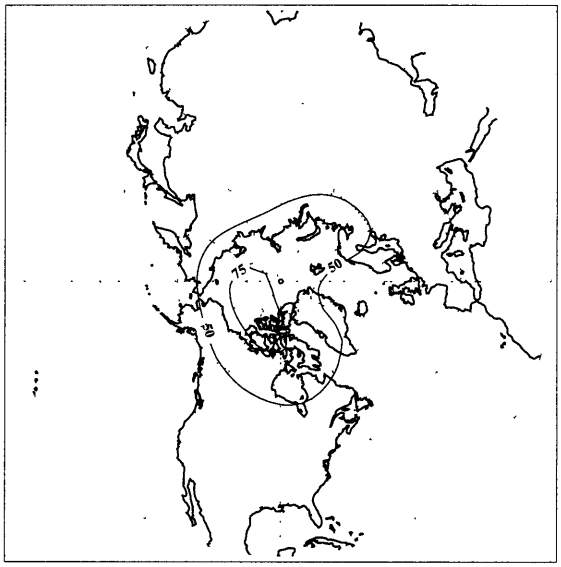

Figure A.5: Same as Figure A.1 except for 50hPa geopotential height (gpm).

a) Mean of 50hPa Geopotential Height [DJF]

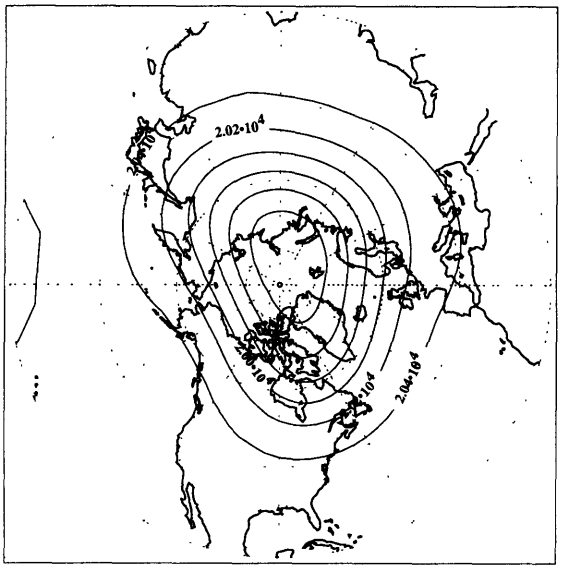

b) Standard deviation of 50hPa Geopotential Height [DJF]

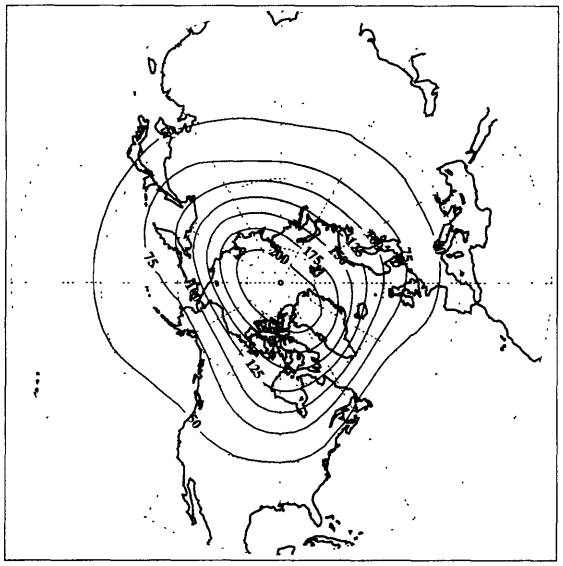

Figure A.6: Same as Figure A.5 except for DJF.

Appendix B

Series of regression/correlation maps

The series of regression/correlation map which are referred and discussed in sections 3.2 are shown here.

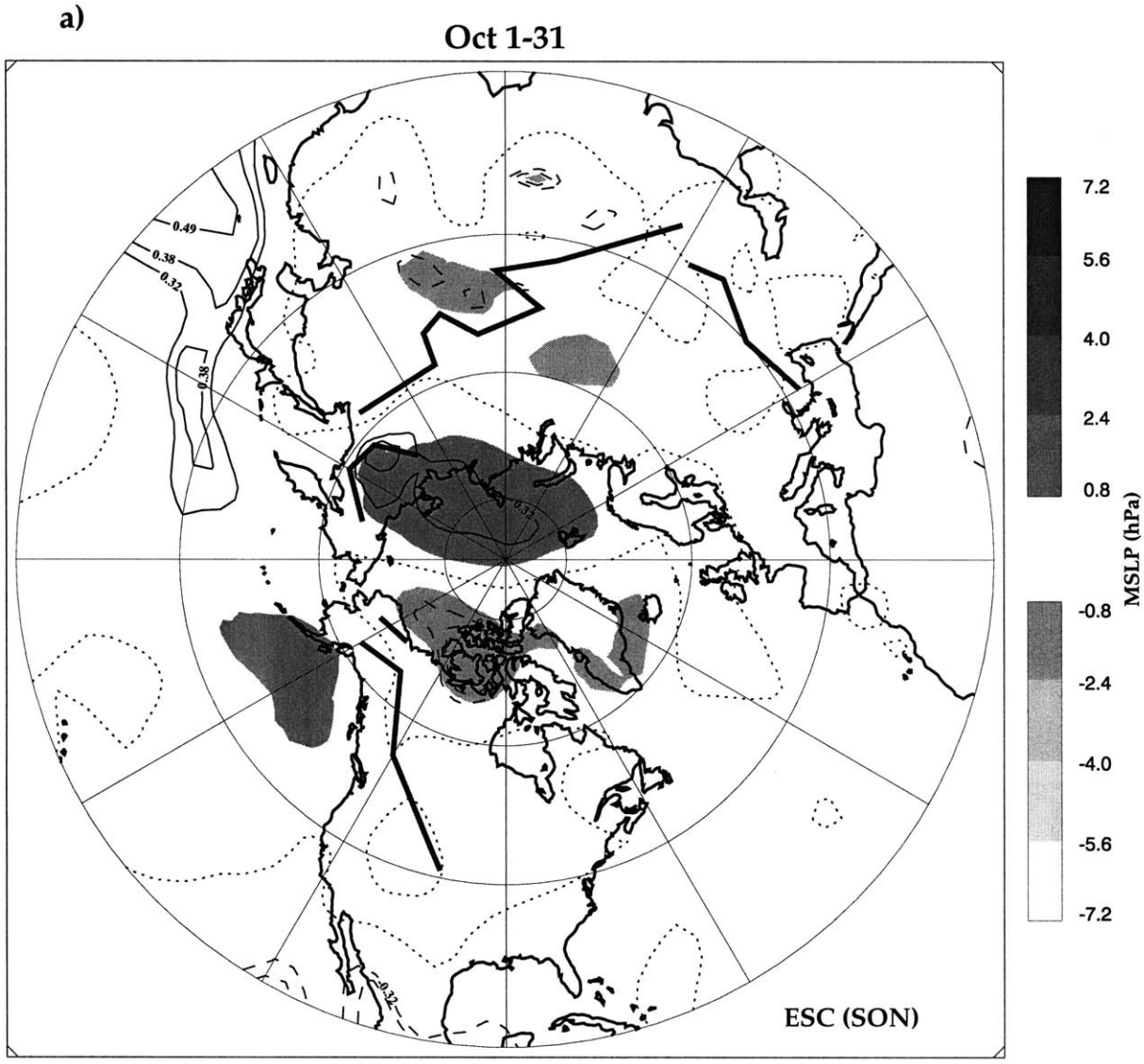

Figure B.1: Regression/Correlation map to autumn Eurasian snow cover of MSLP for a) October 1-31, b) October 15-November 15, c) November 1-30, d) November 15-December 15, e) December 1-31, f) December 15-January 15, g) January 1-31, h) January 15-February 15, and i) February 1-28. Shaded are Regression coefficients. Line contours are correlation coefficient and correspond to 90%, 95% and 99% confidence level. Thick lines depict northern edge of 1000m topography line.

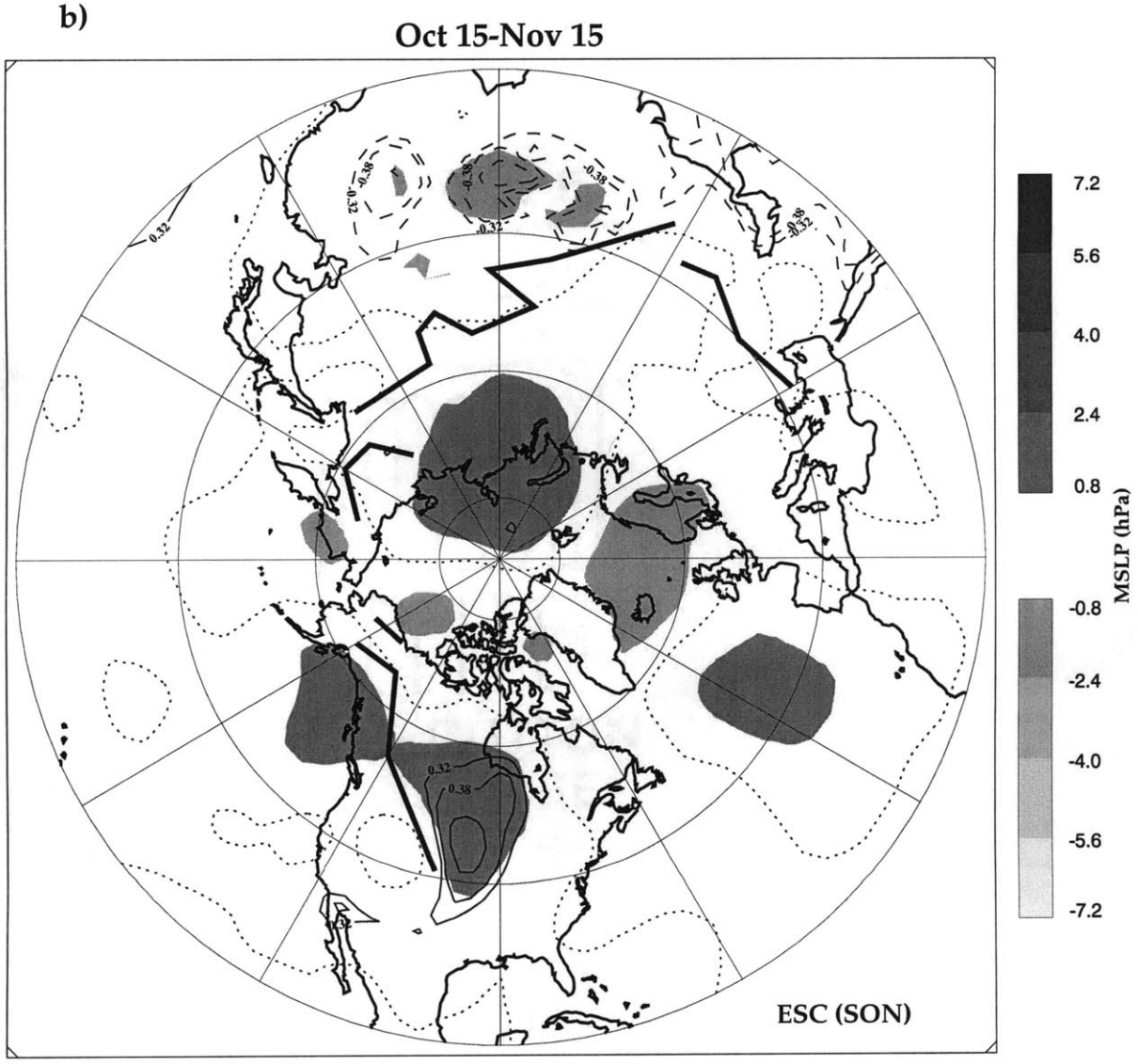

Figure B.1: *(Continued)*

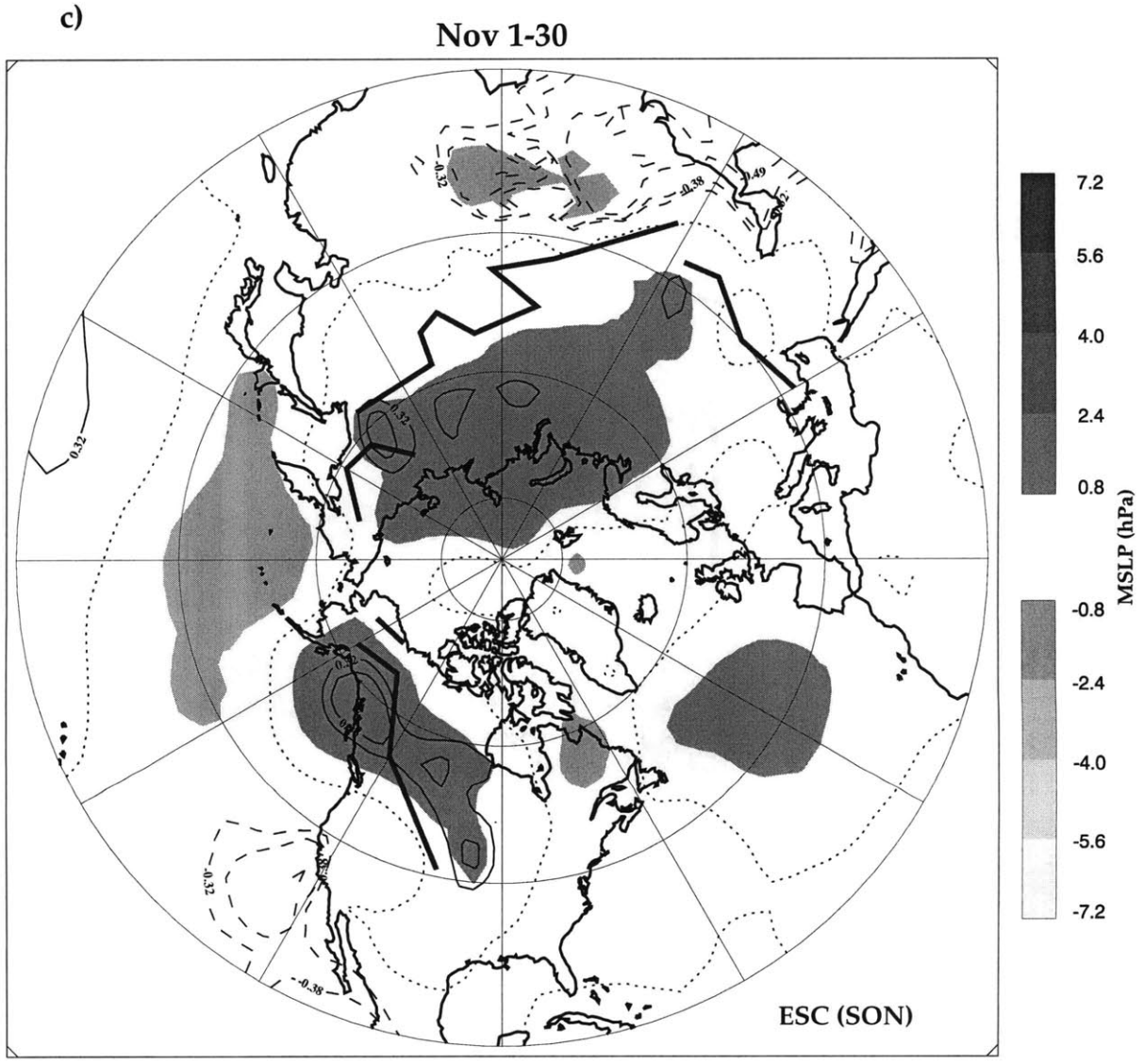

Figure B.1: *(Continued)*

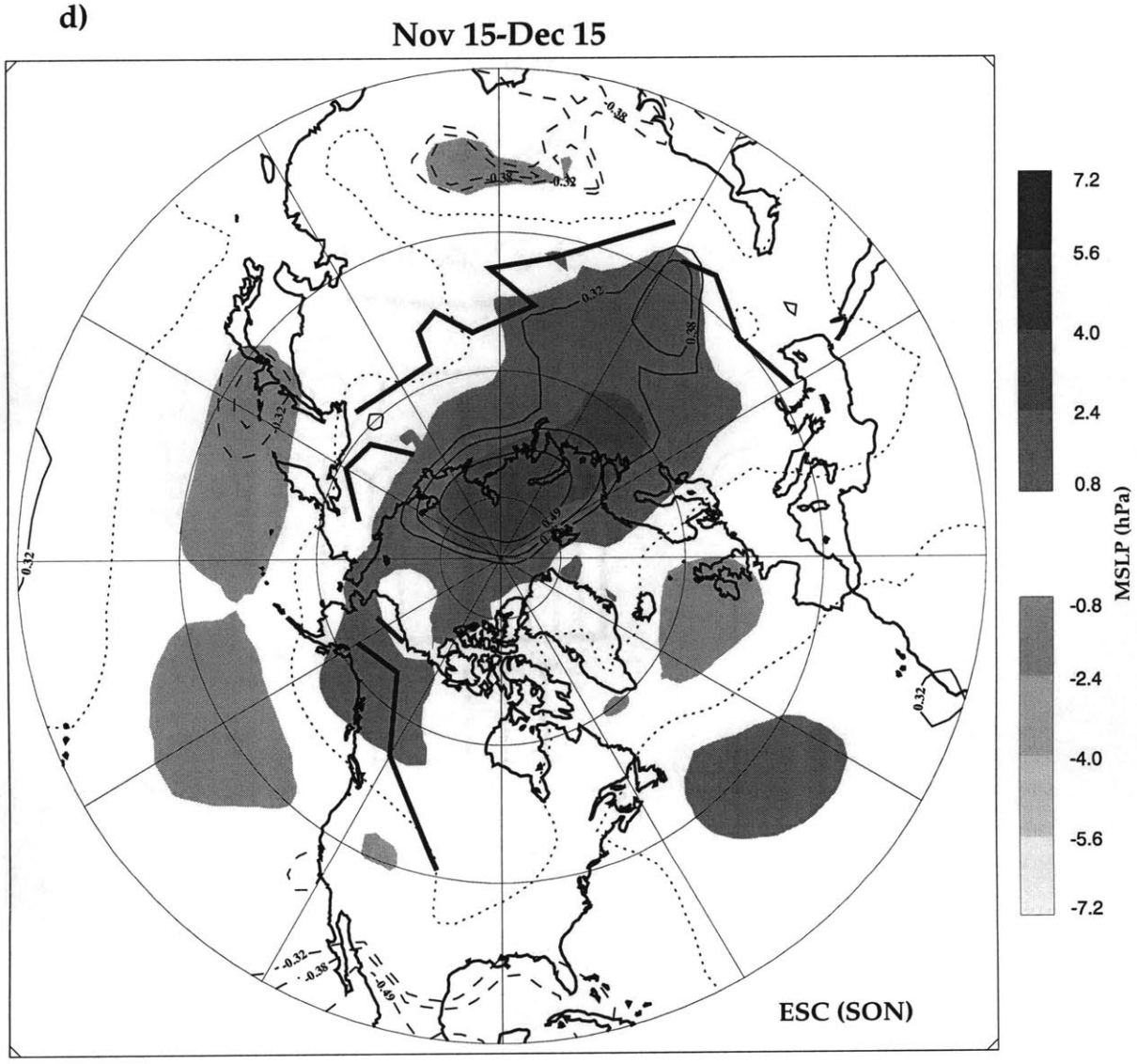

Figure B.1: *(Continued)*

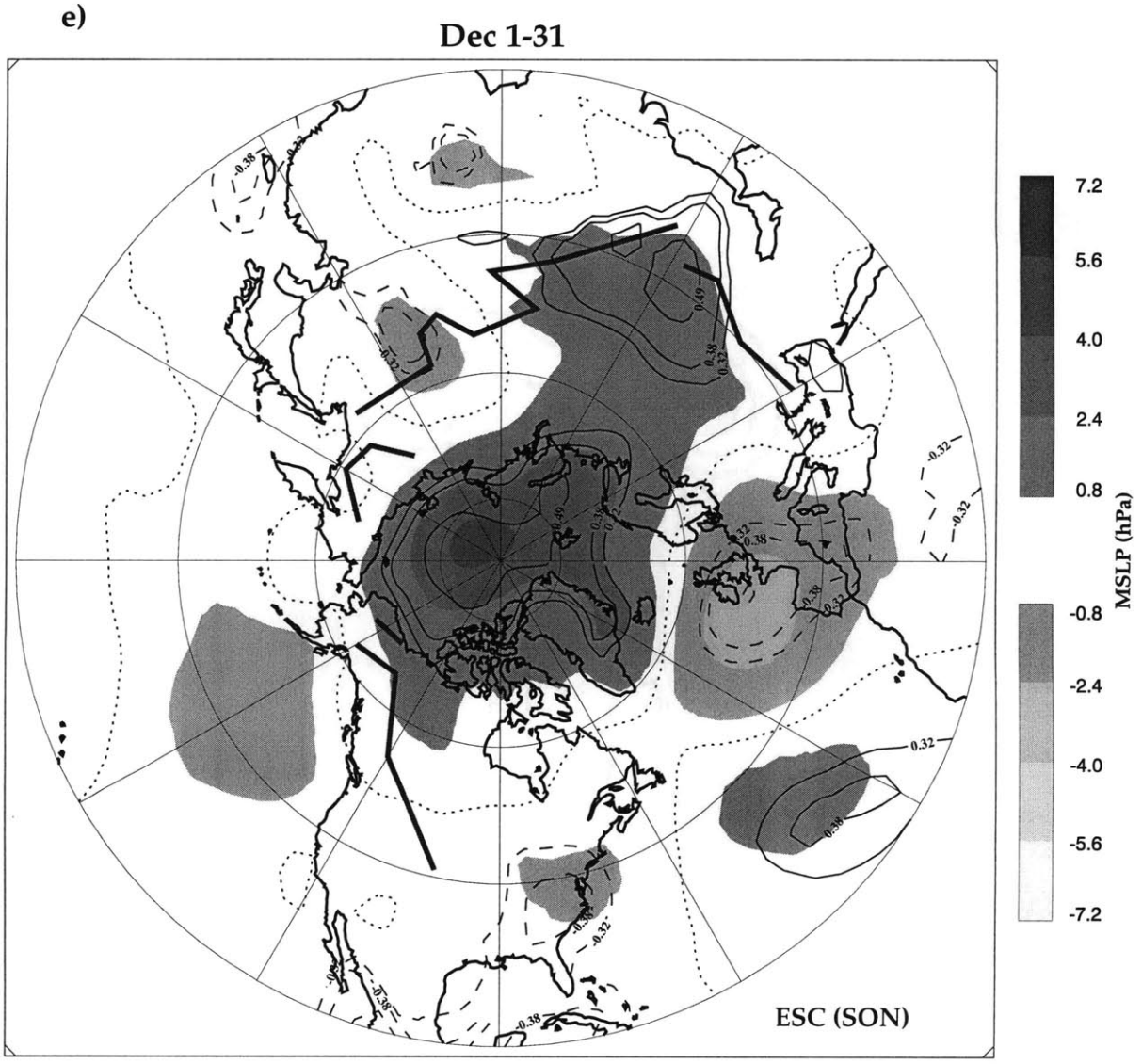

Figure B.1: *(Continued)*

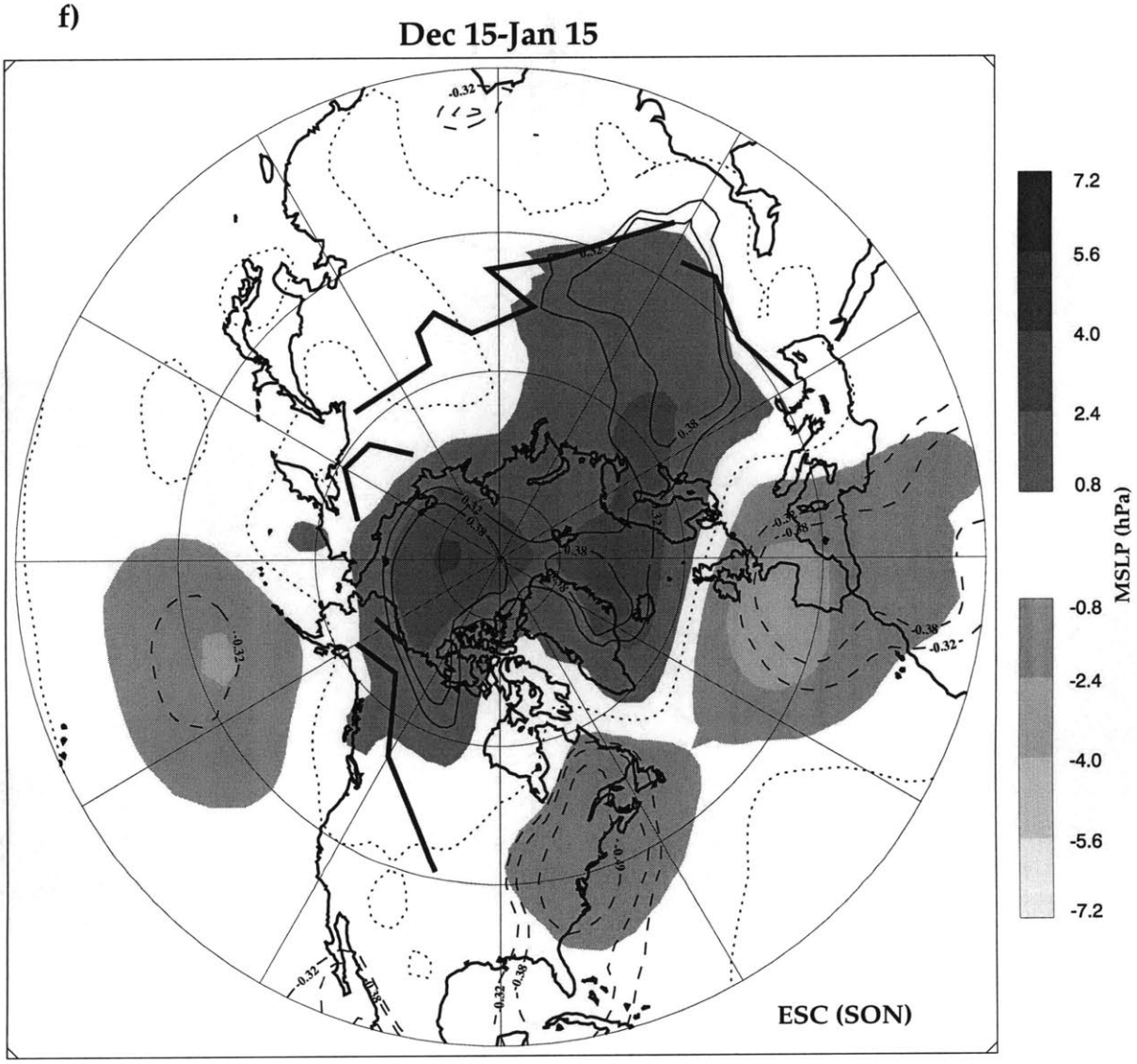

Figure B.1: *(Continued)*

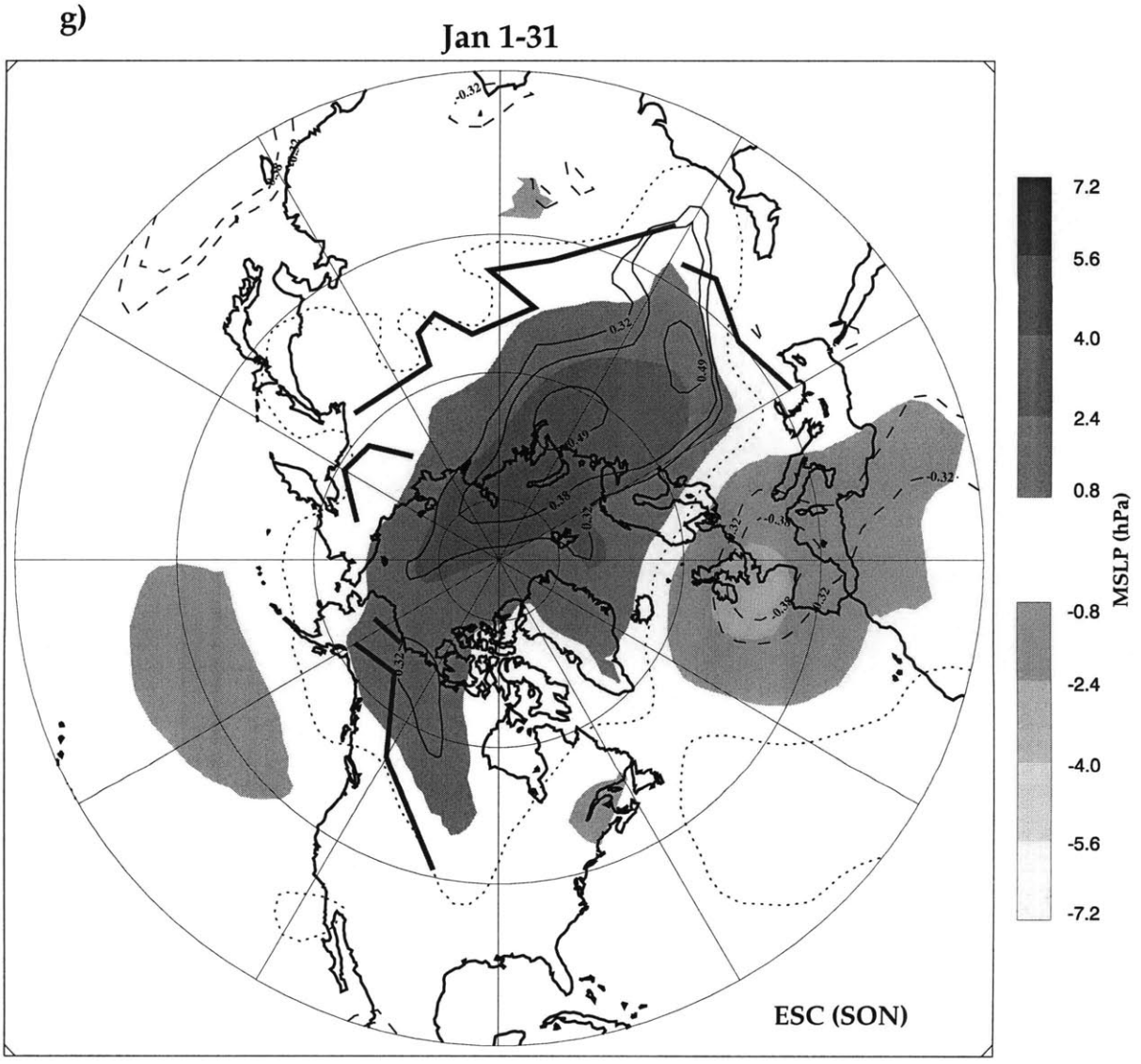

Figure B.1: *(Continued)*

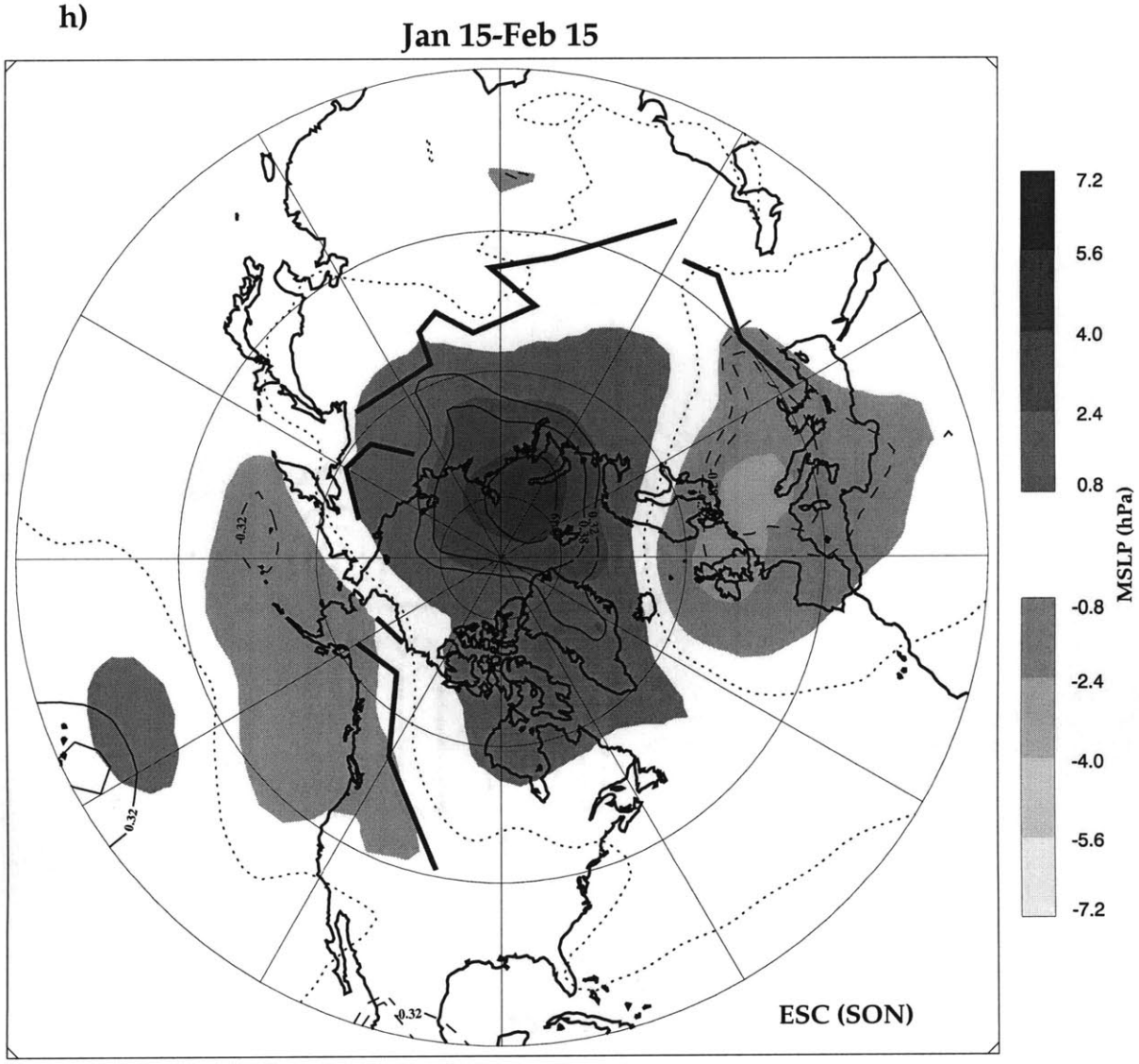

Figure B.1: *(Continued)*

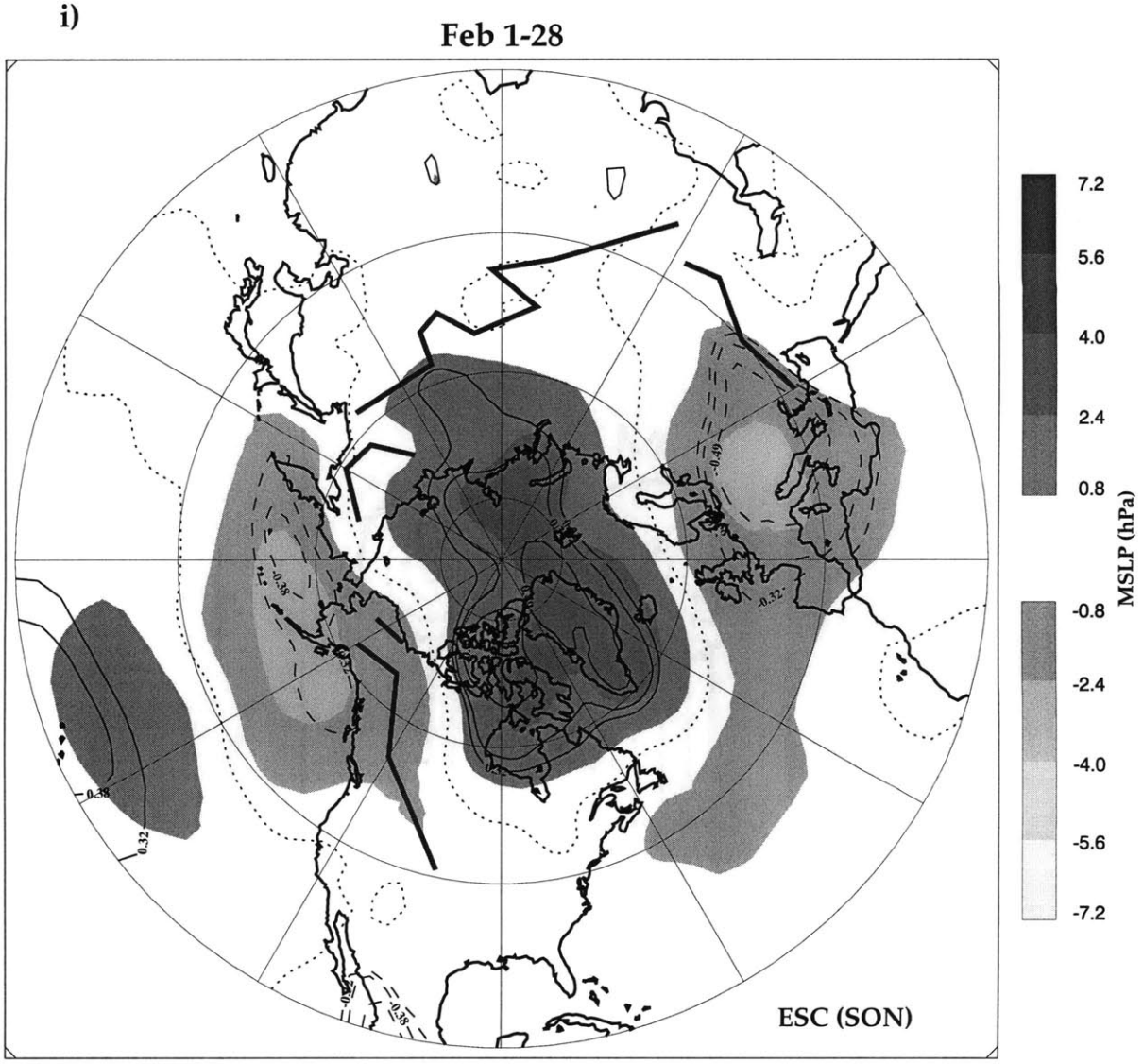

Figure B.1: *(Continued)*

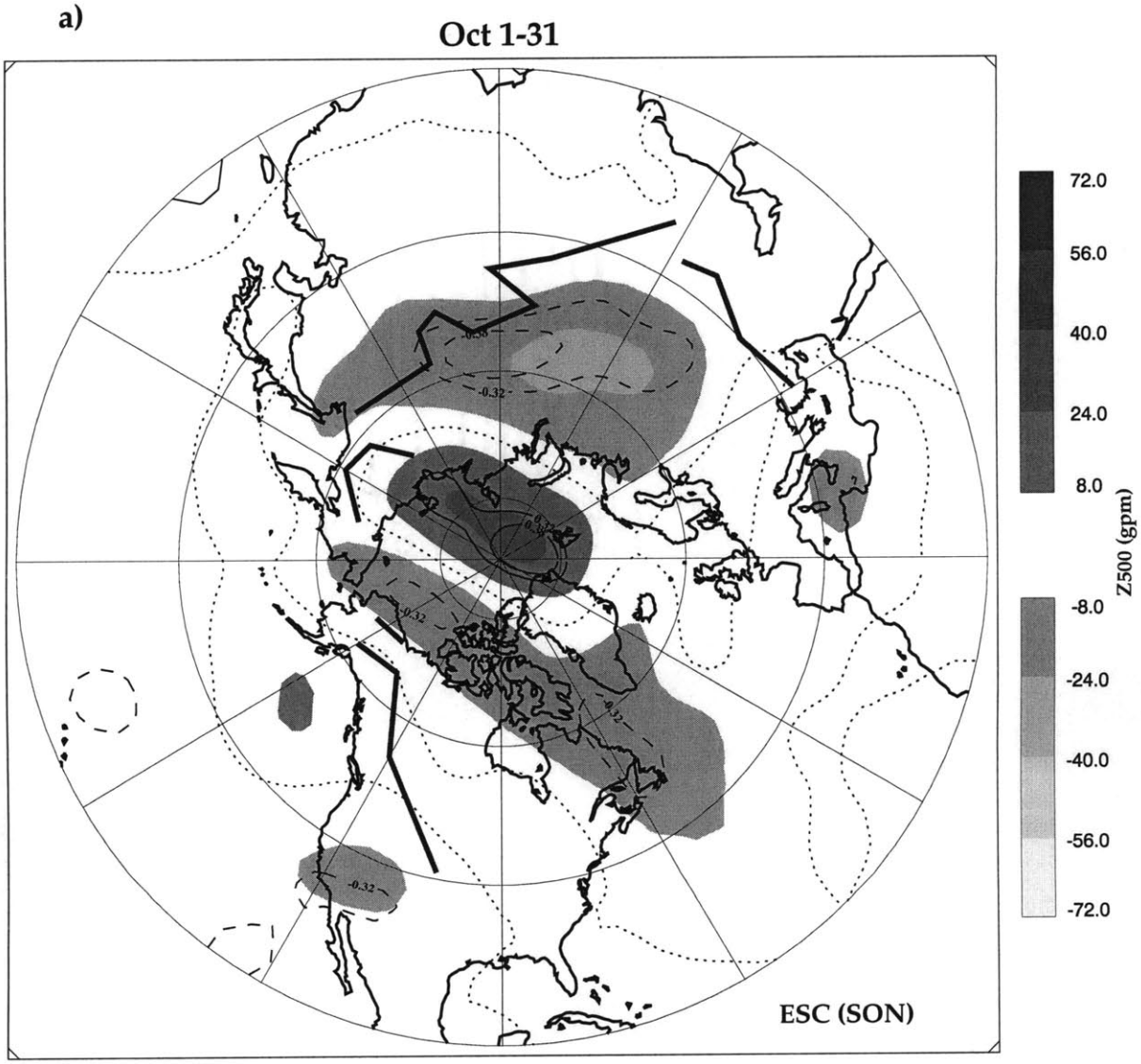

Figure B.2: Same as figure B.1 except for 500hPa geopotential height

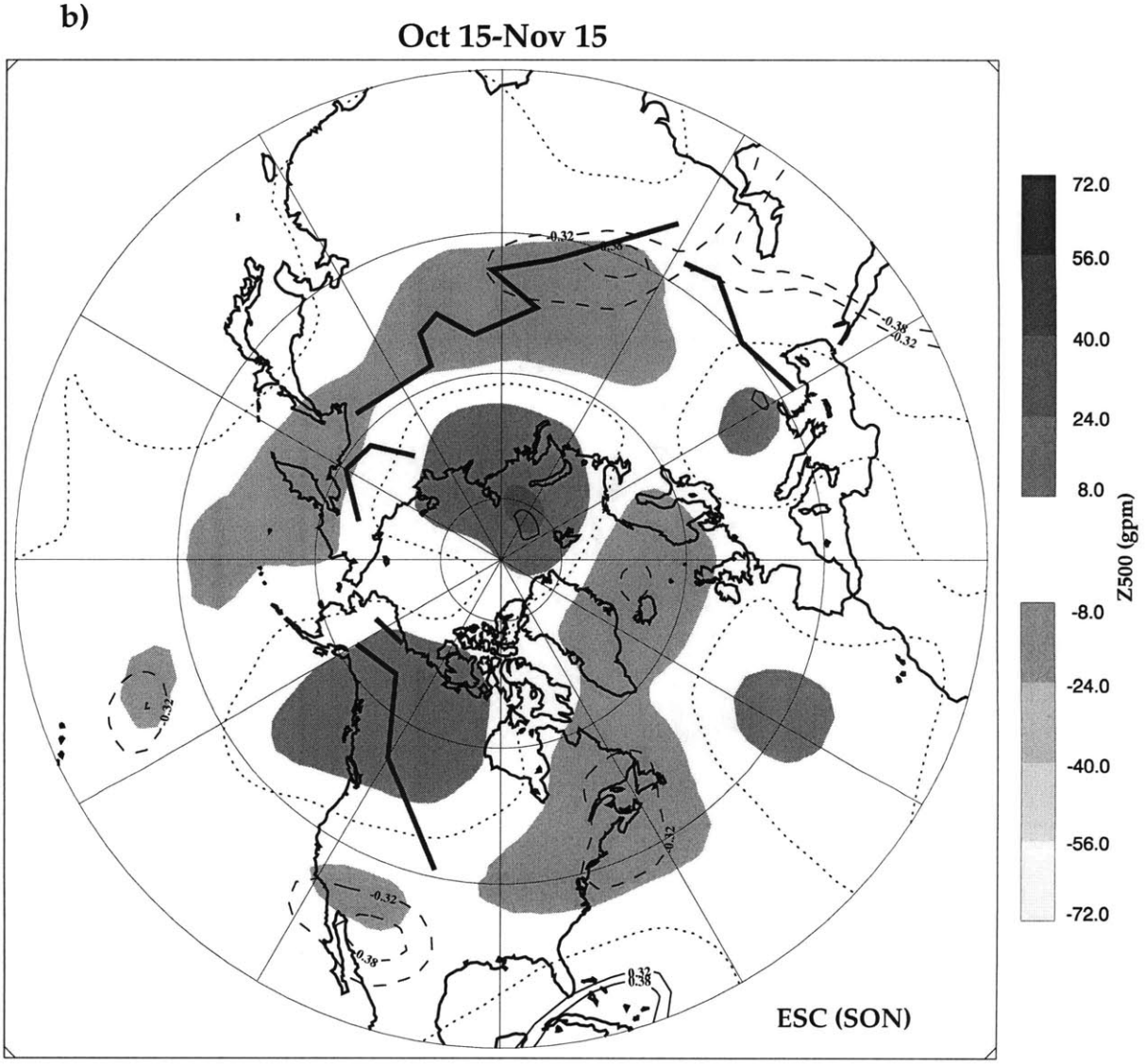

Figure B.2: *(Continued)*

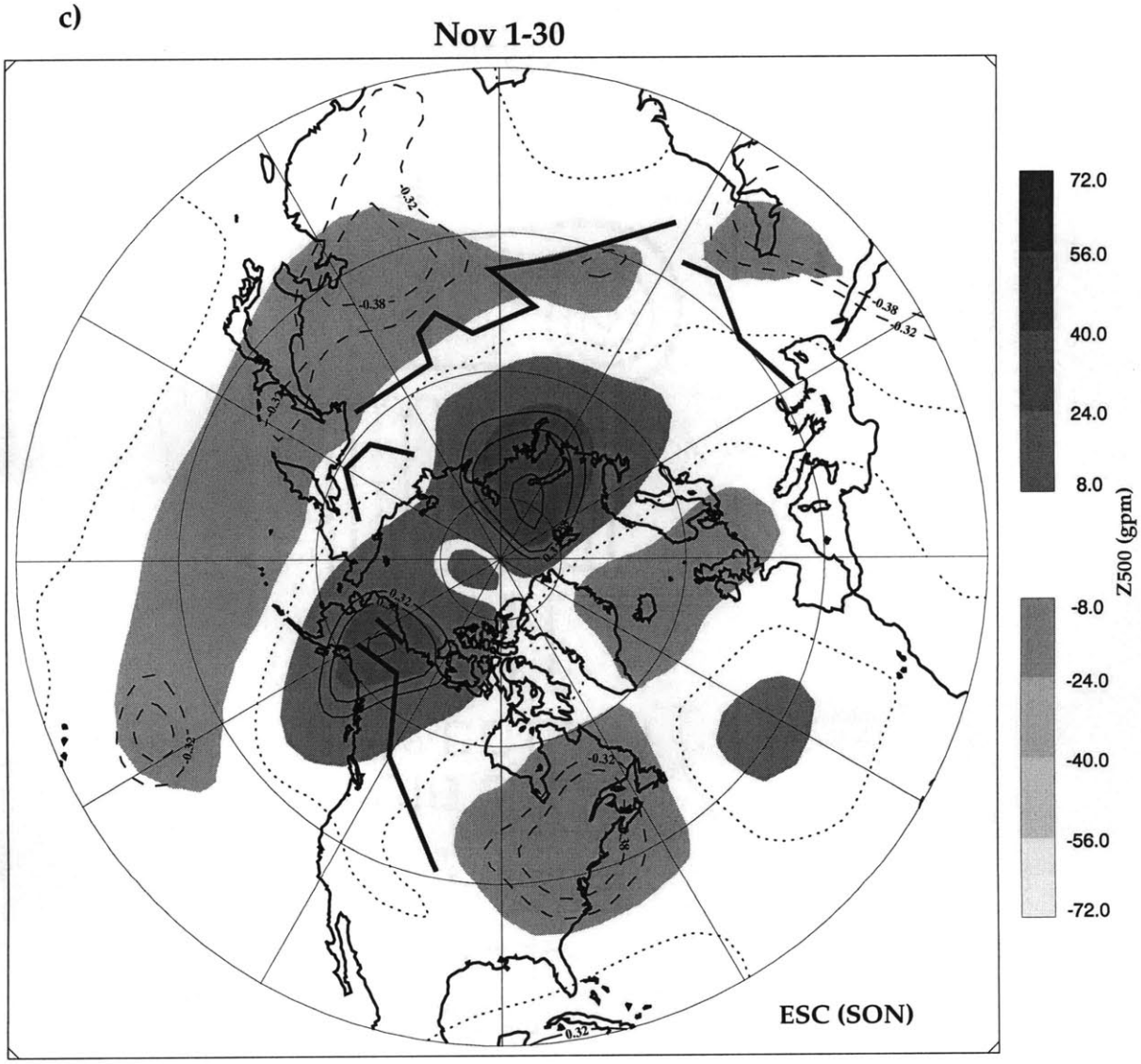

Figure B.2: *(Continued)*

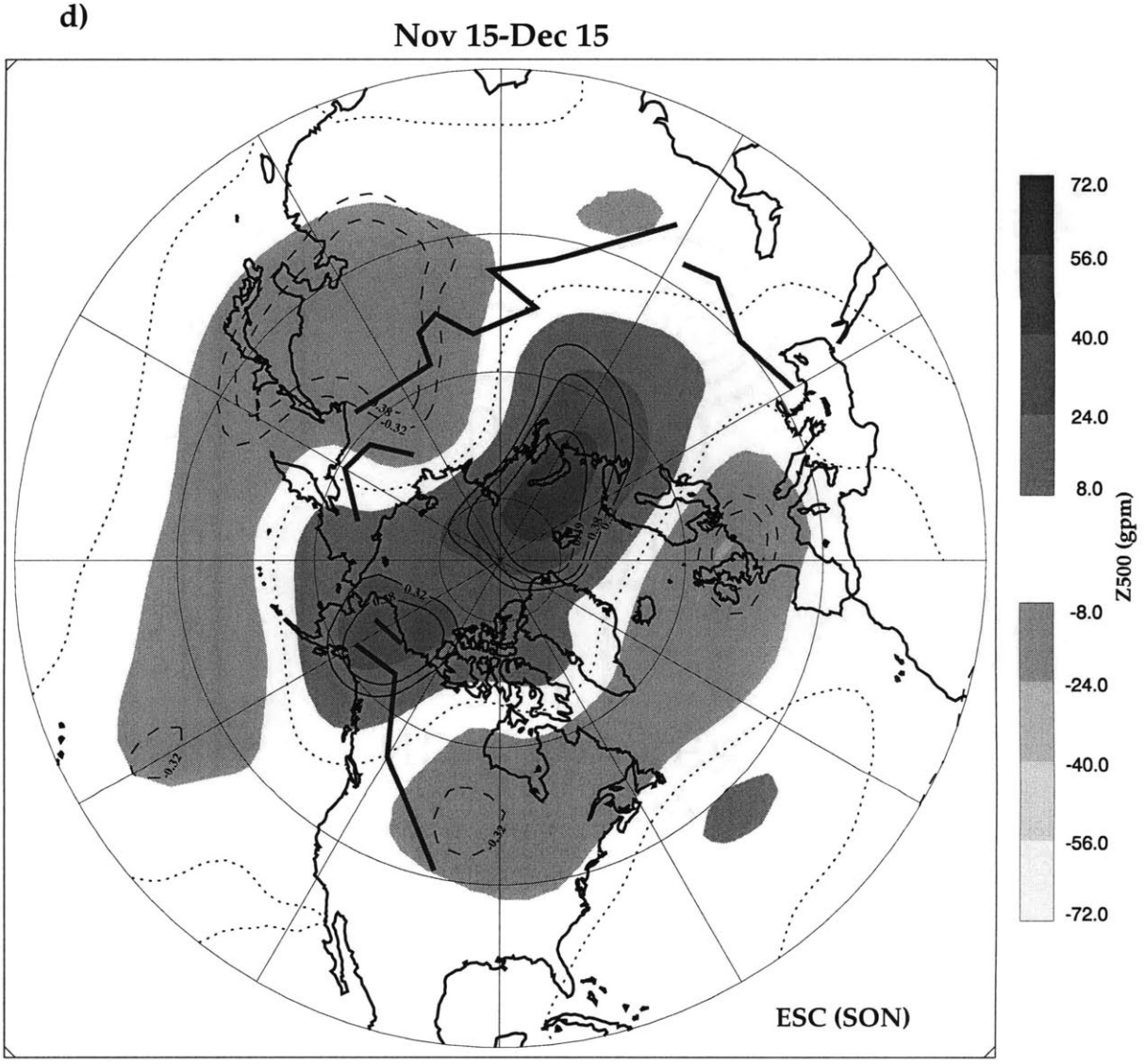

Figure B.2: *(Continued)*

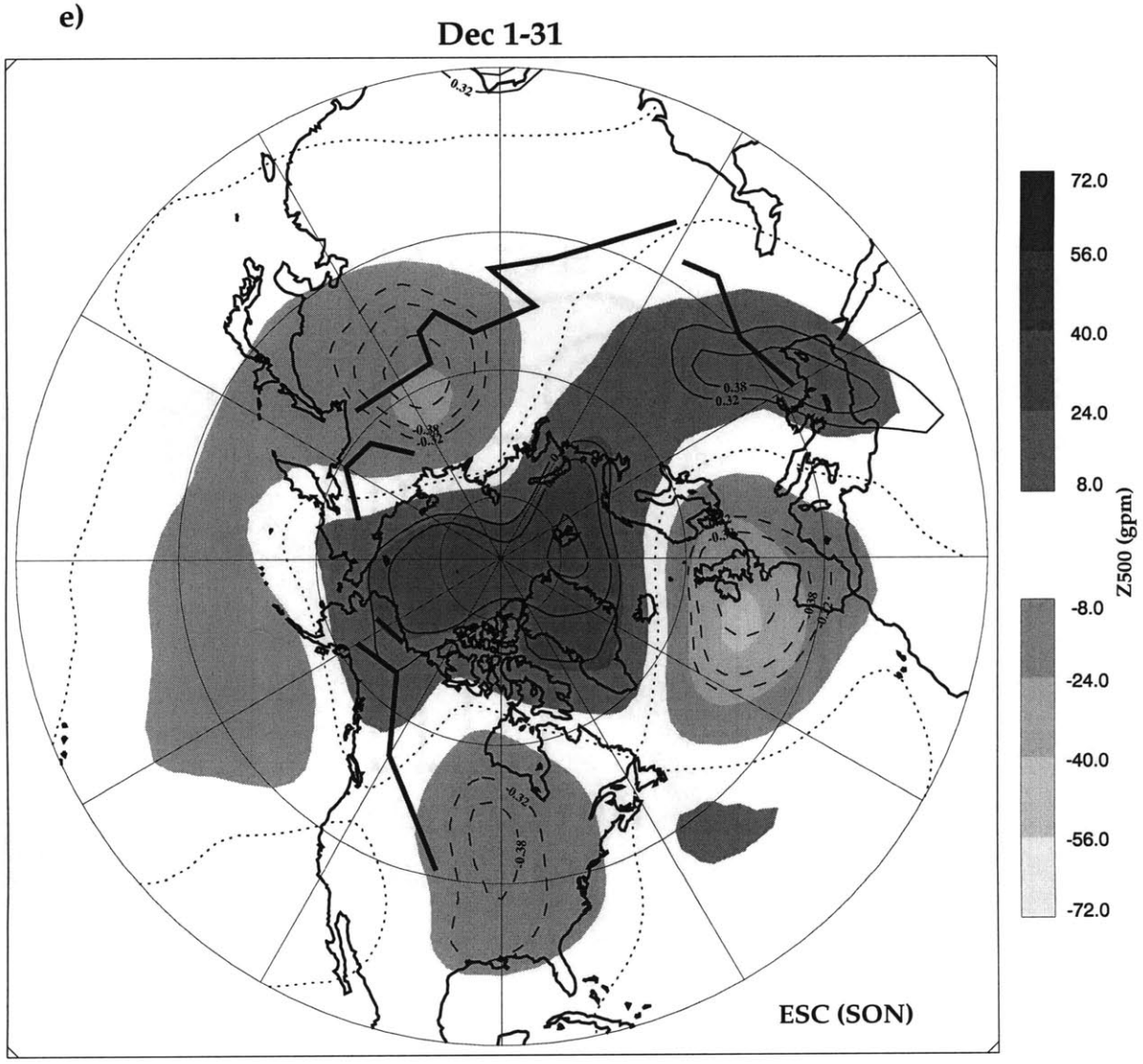

Figure B.2: *(Continued)*

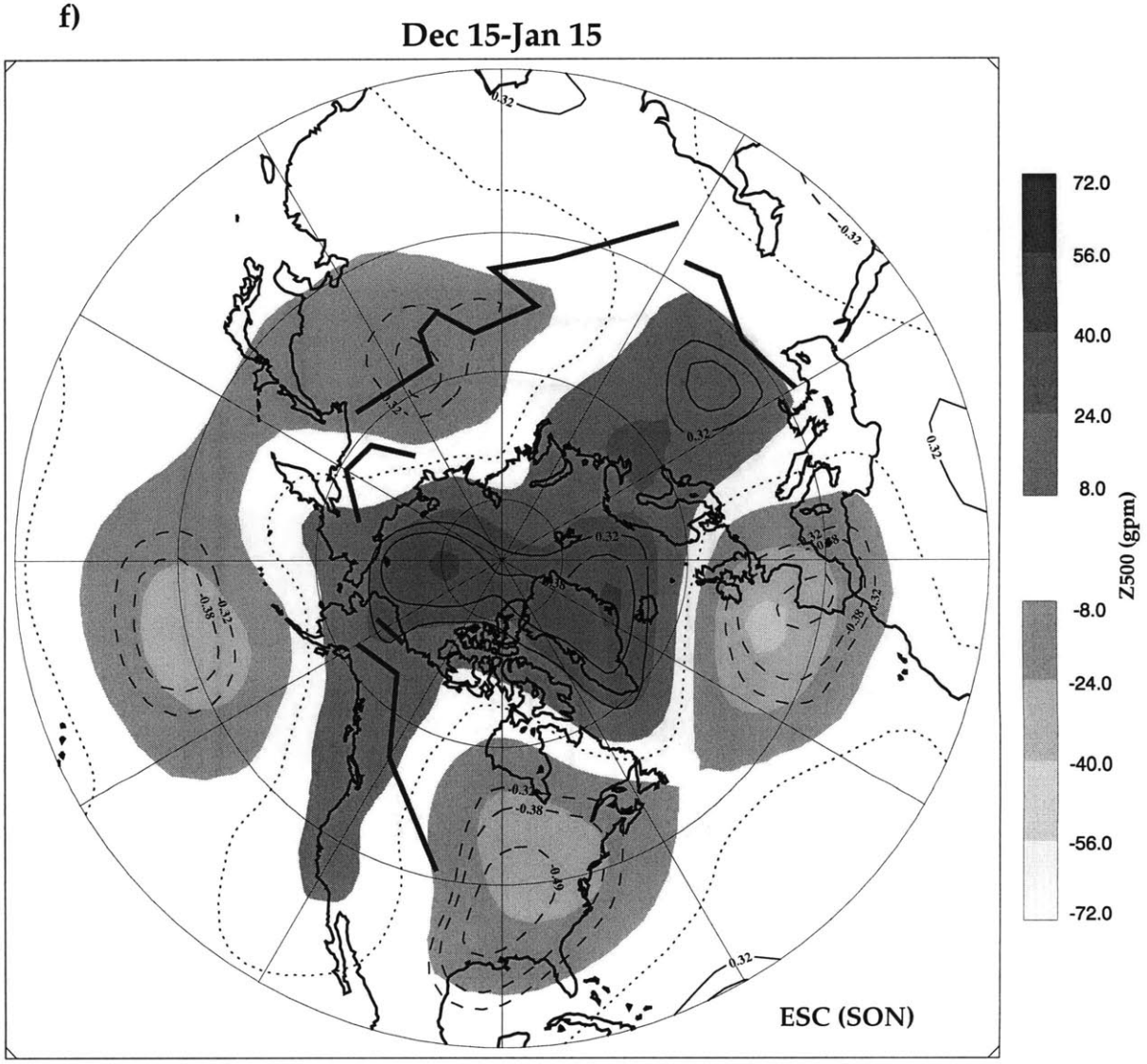

Figure B.2: *(Continued)*

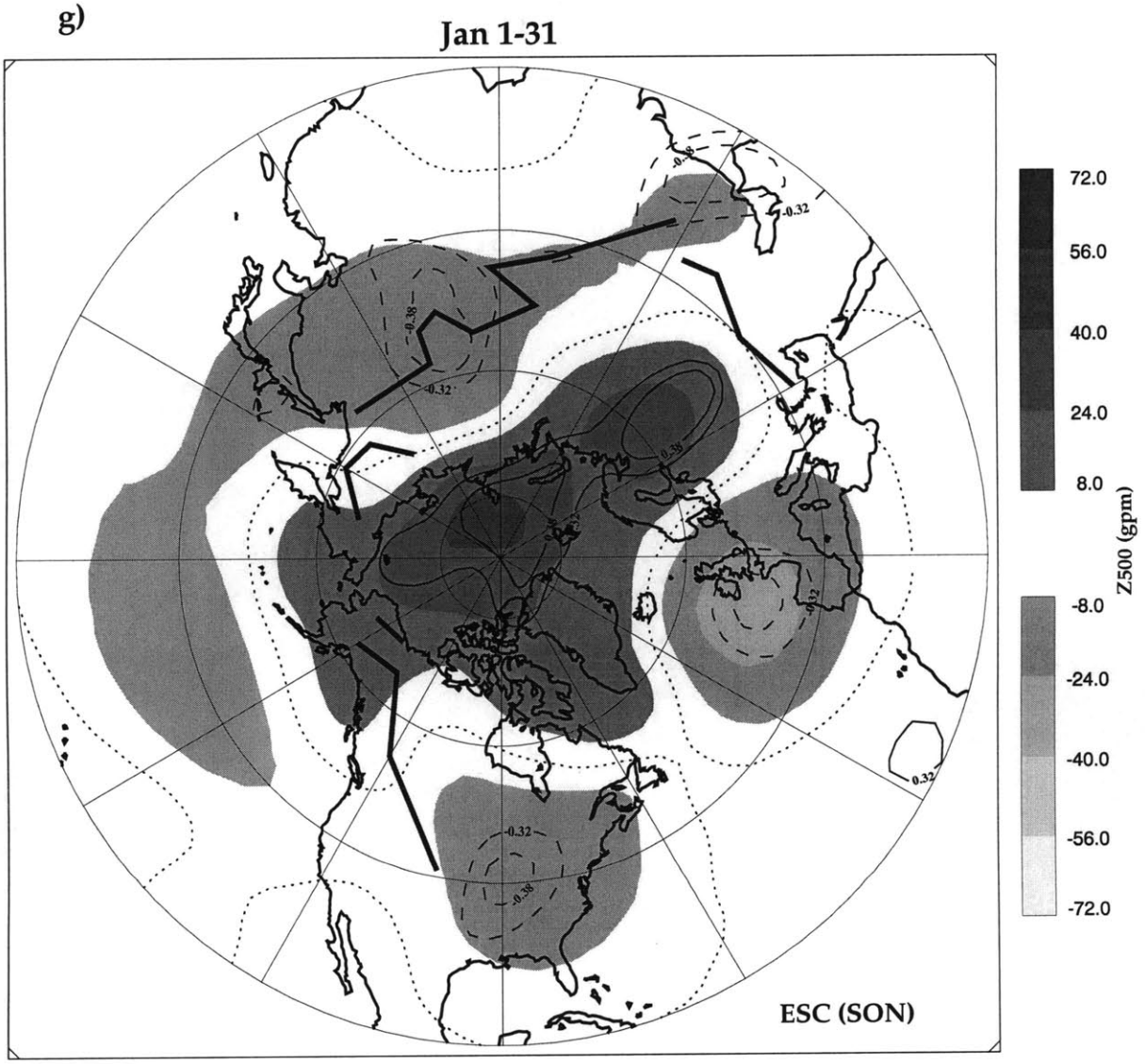

Figure B.2: *(Continued)*

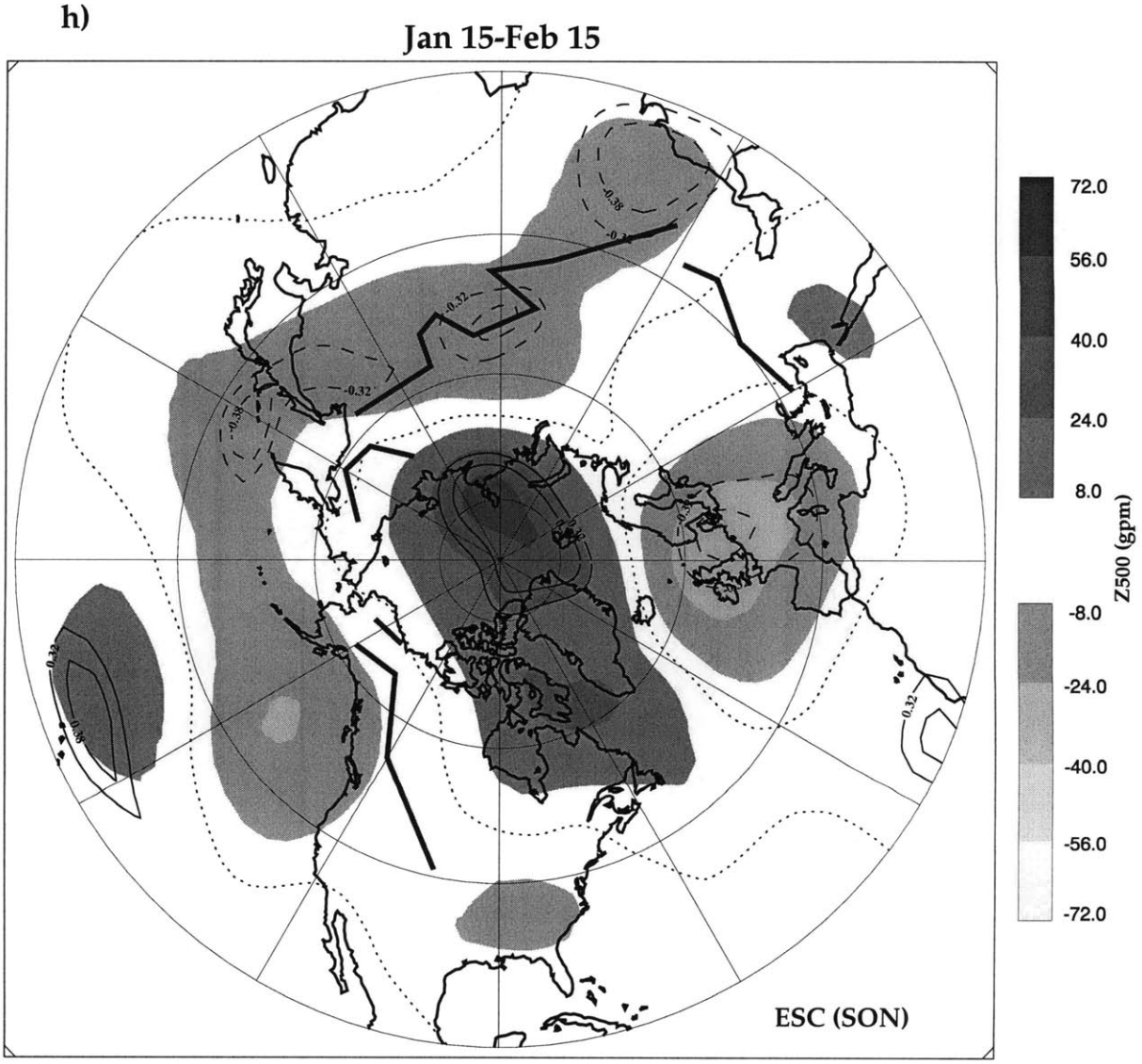

Figure B.2: *(Continued)*

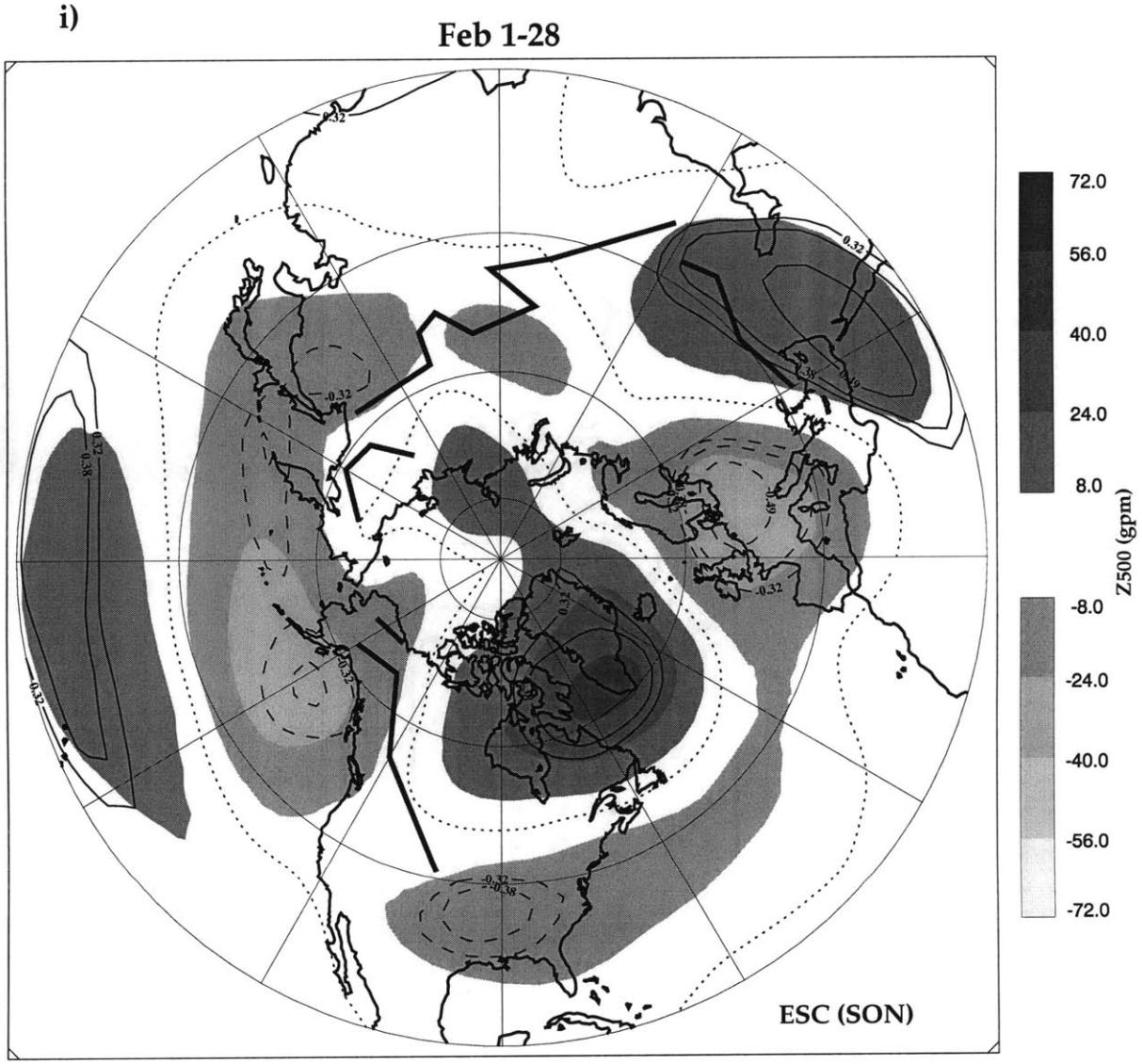

Figure B.2: *(Continued)*

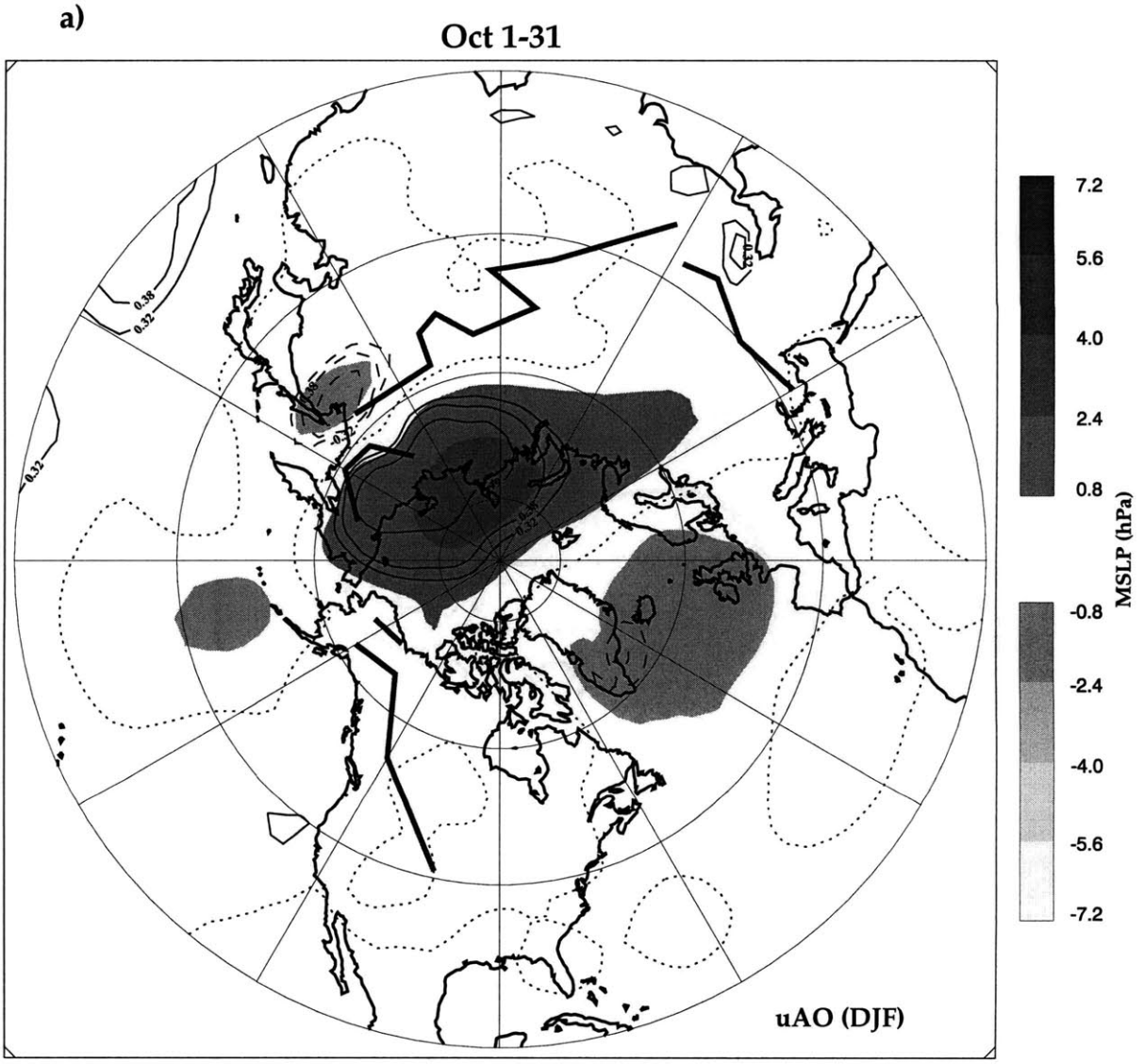

Figure B.3: Same as figure B.1 except for regressed onto the DJF uAO

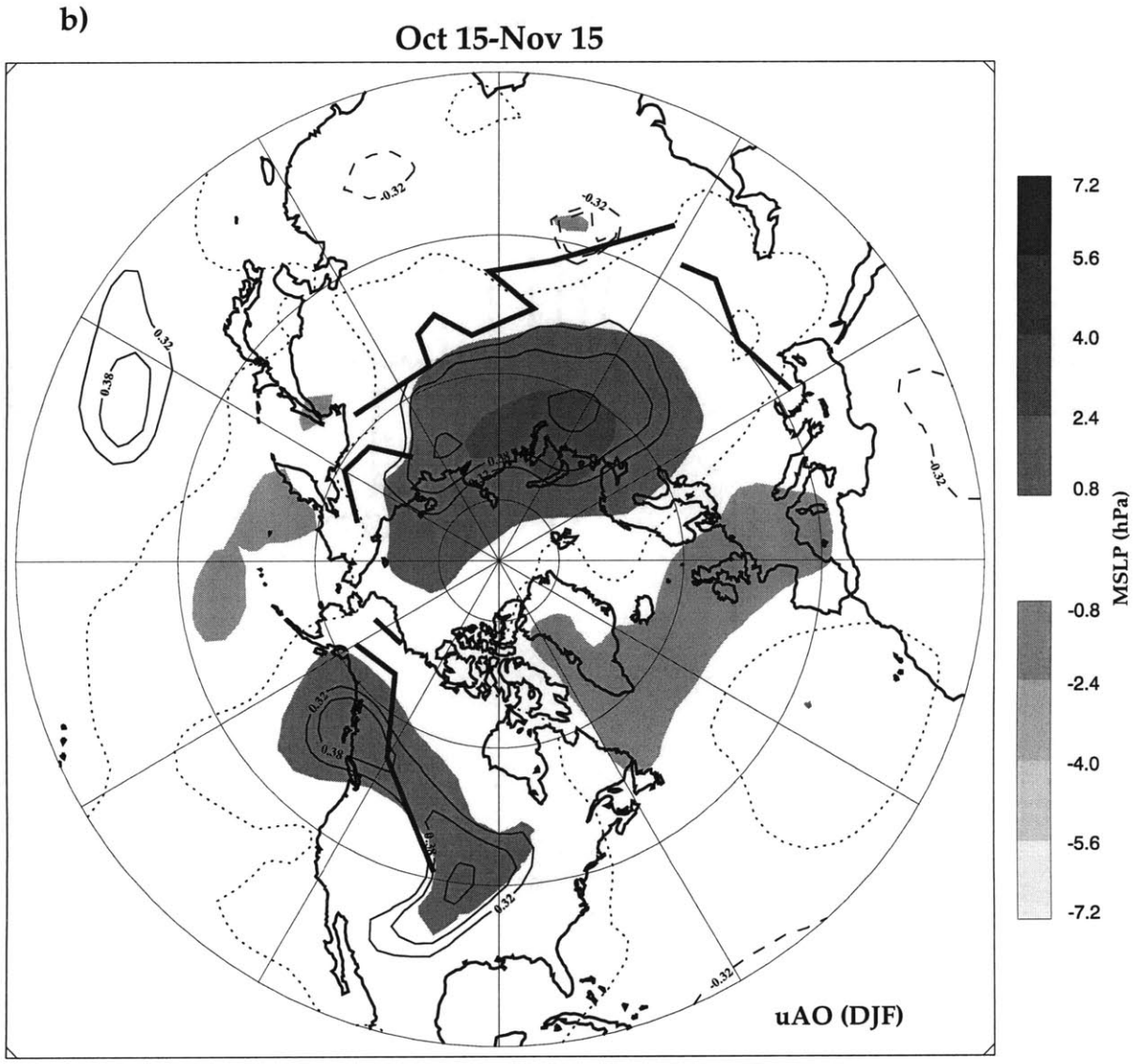

Figure B.3: *(Continued)*

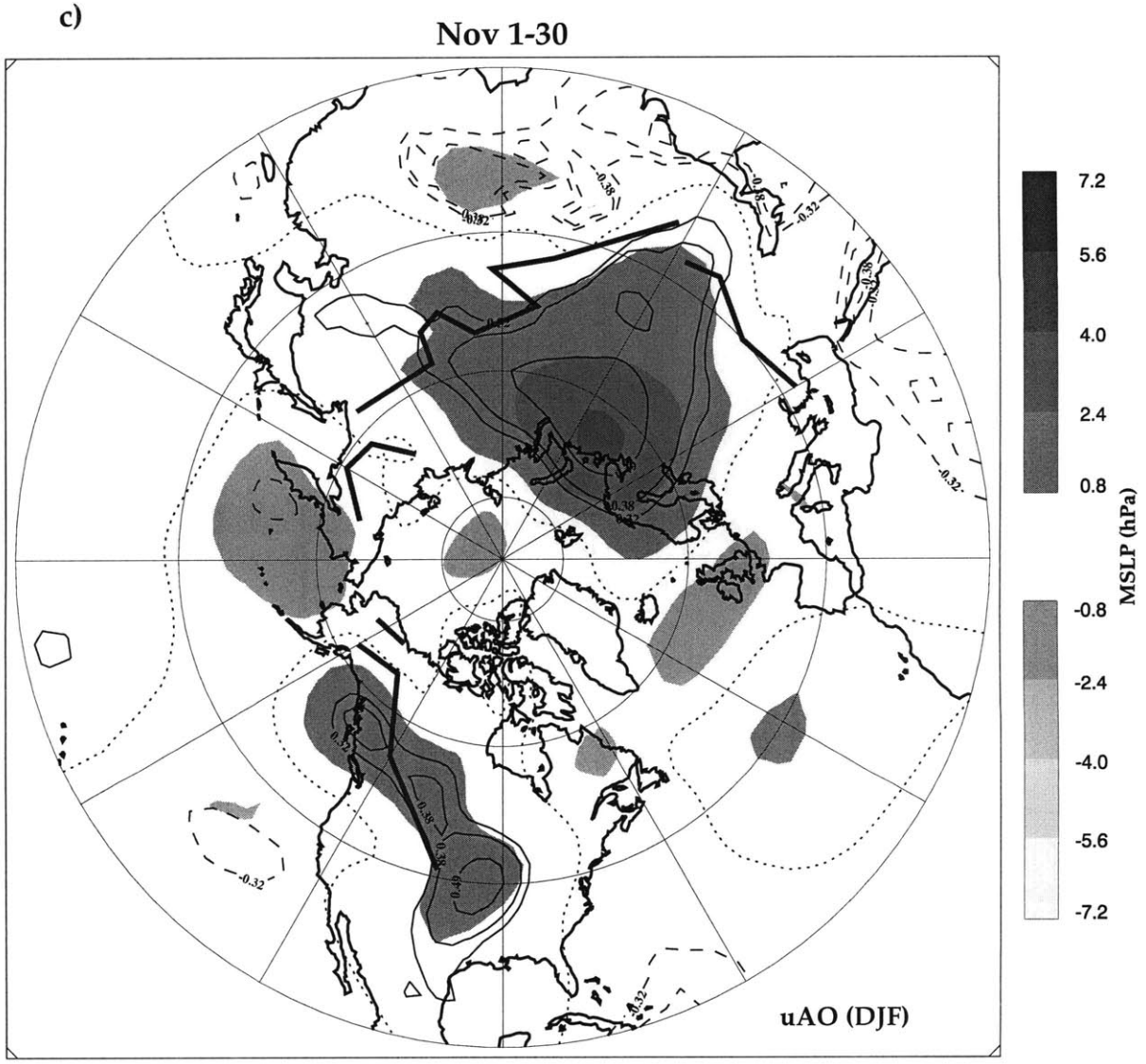

Figure B.3: *(Continued)*

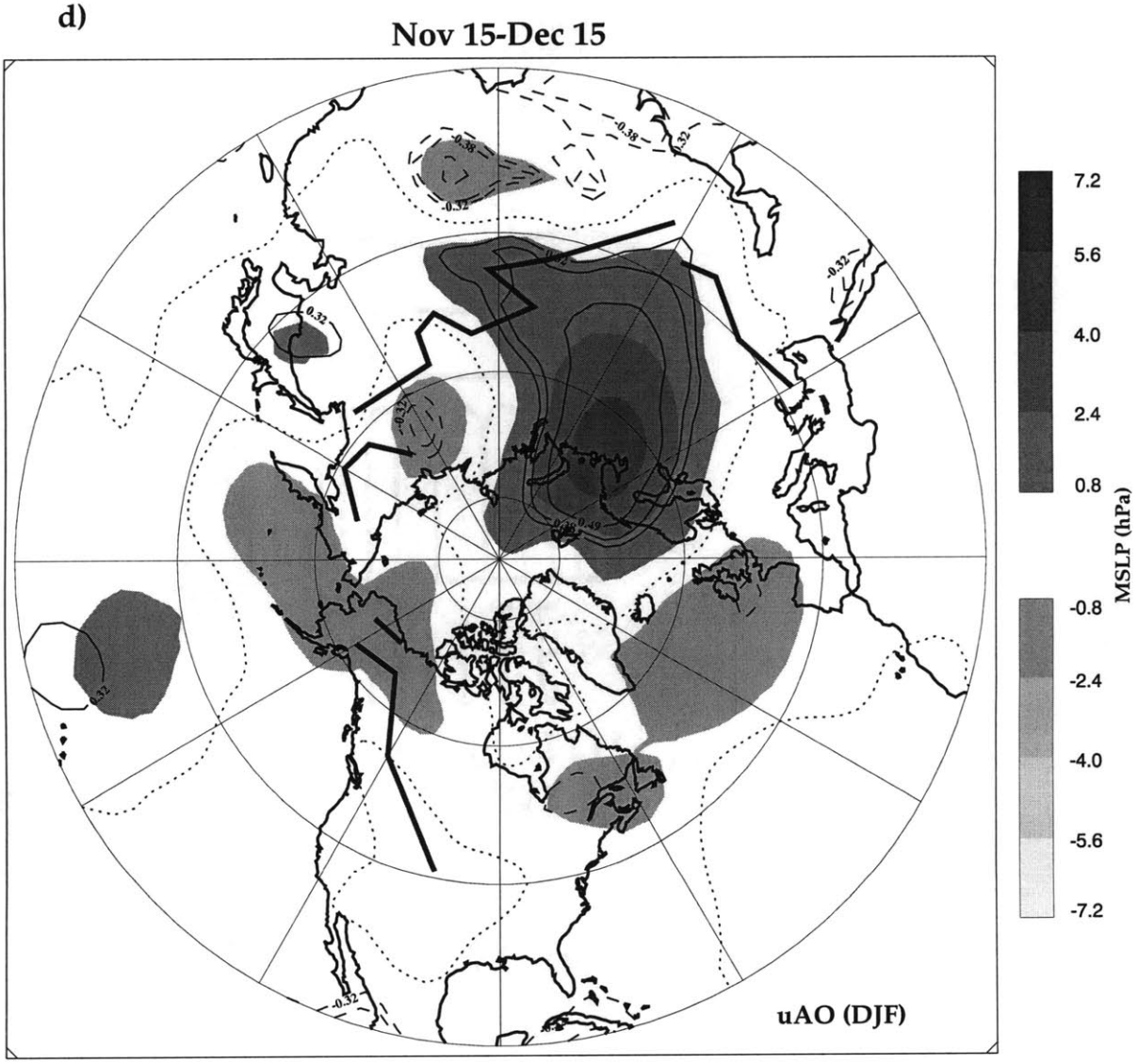

Figure B.3: *(Continued)*

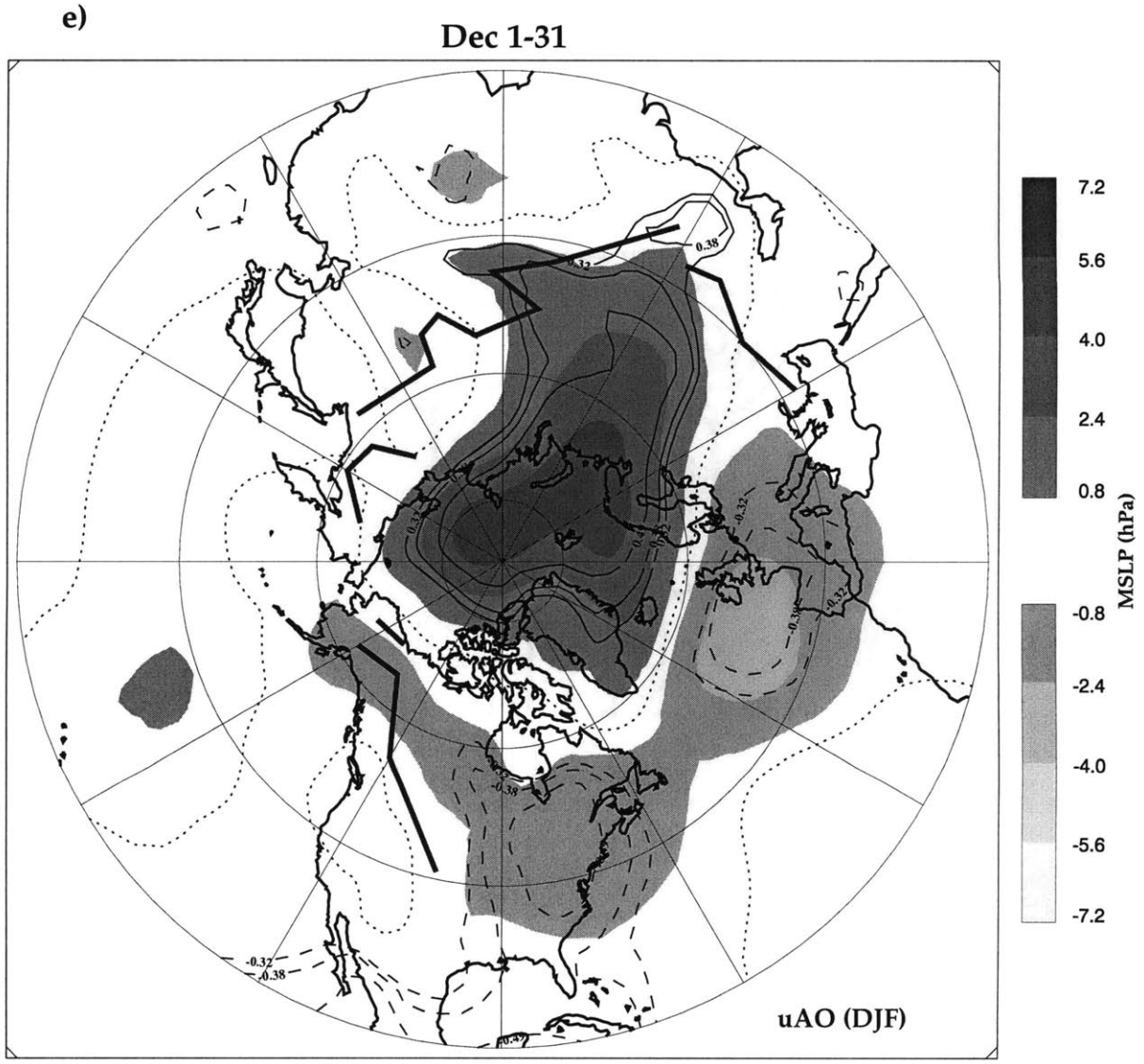

Figure B.3: *(Continued)*

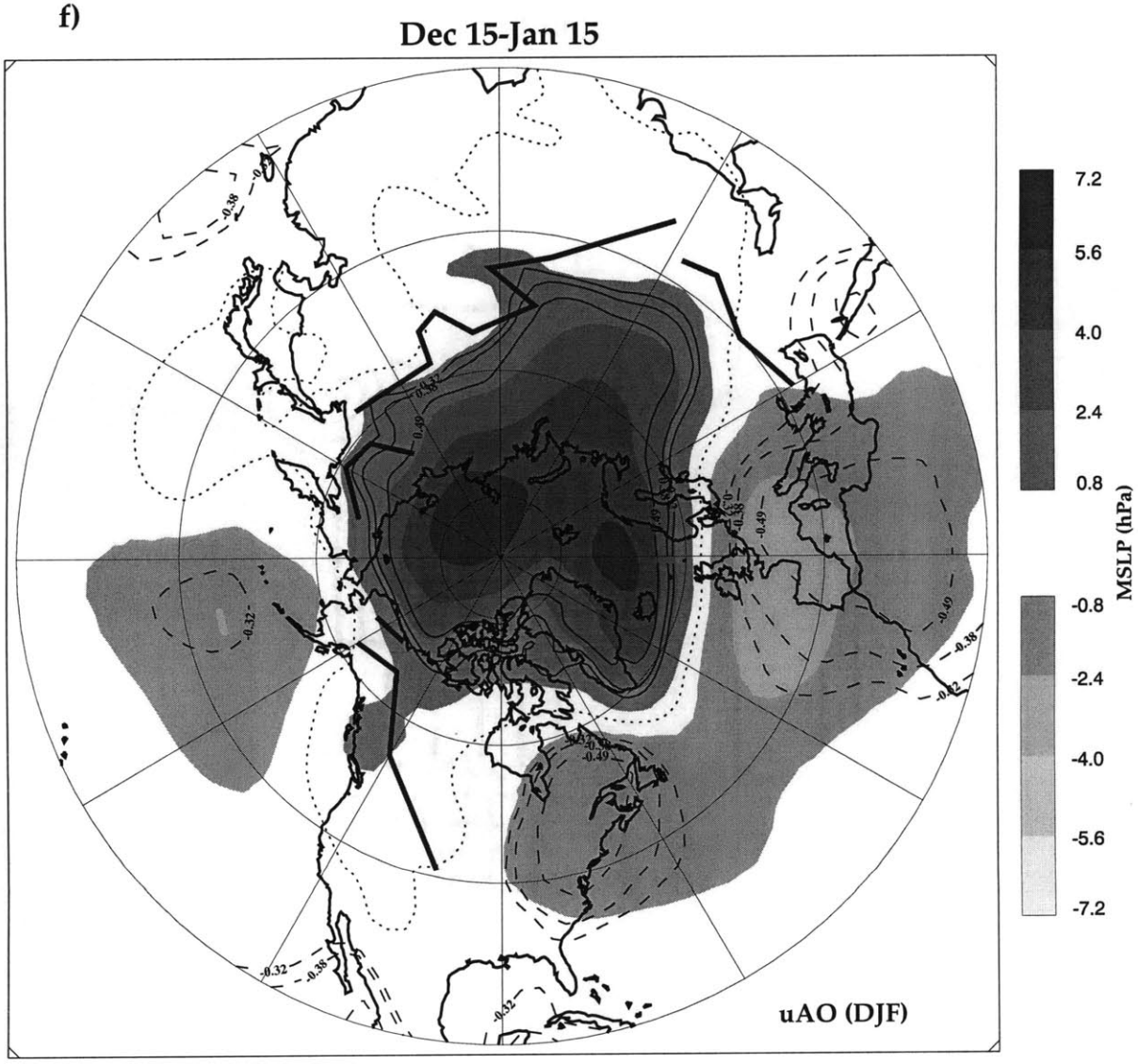

Figure B.3: *(Continued)*

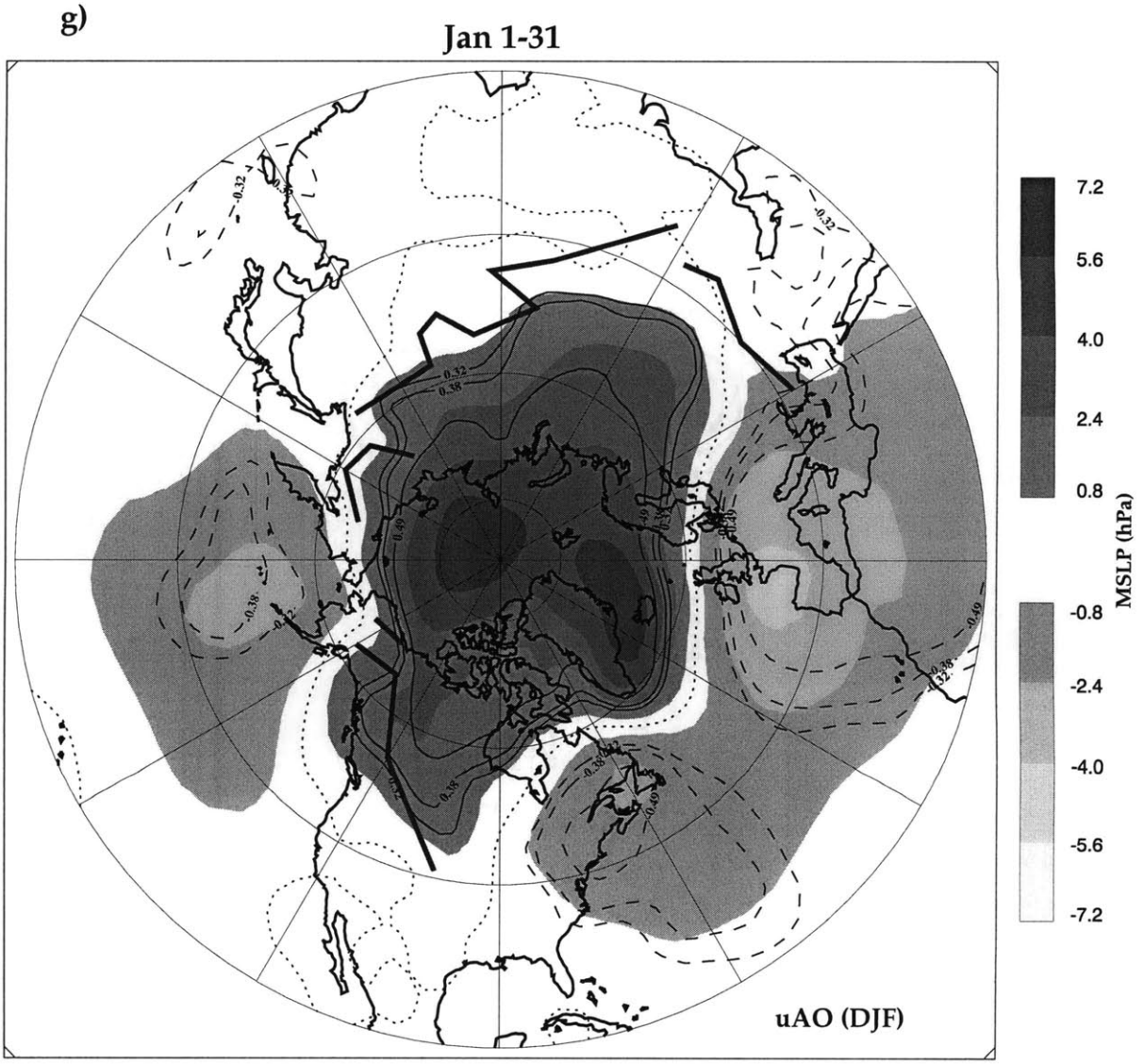

Figure B.3: *(Continued)*

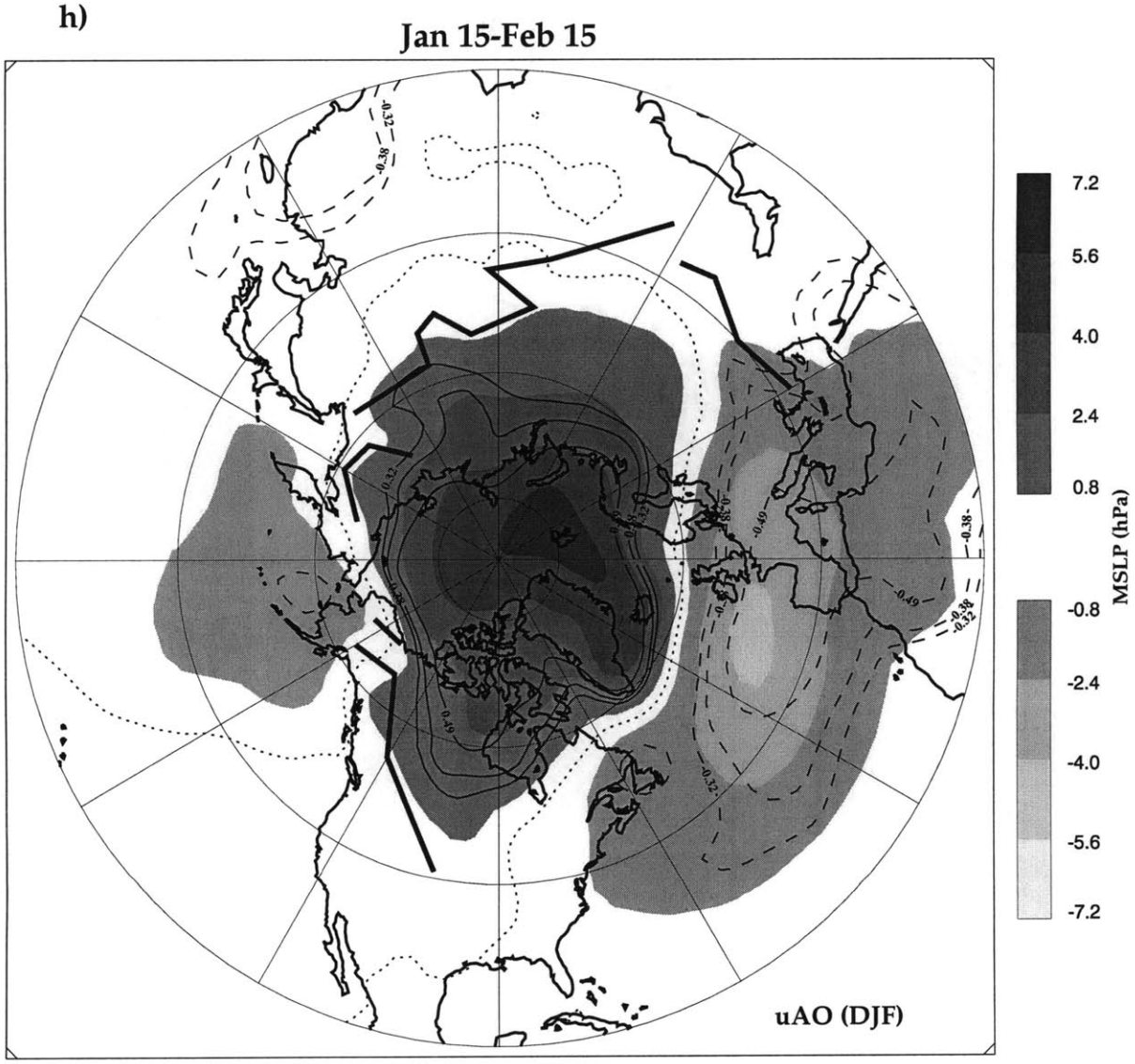

Figure B.3: *(Continued)*

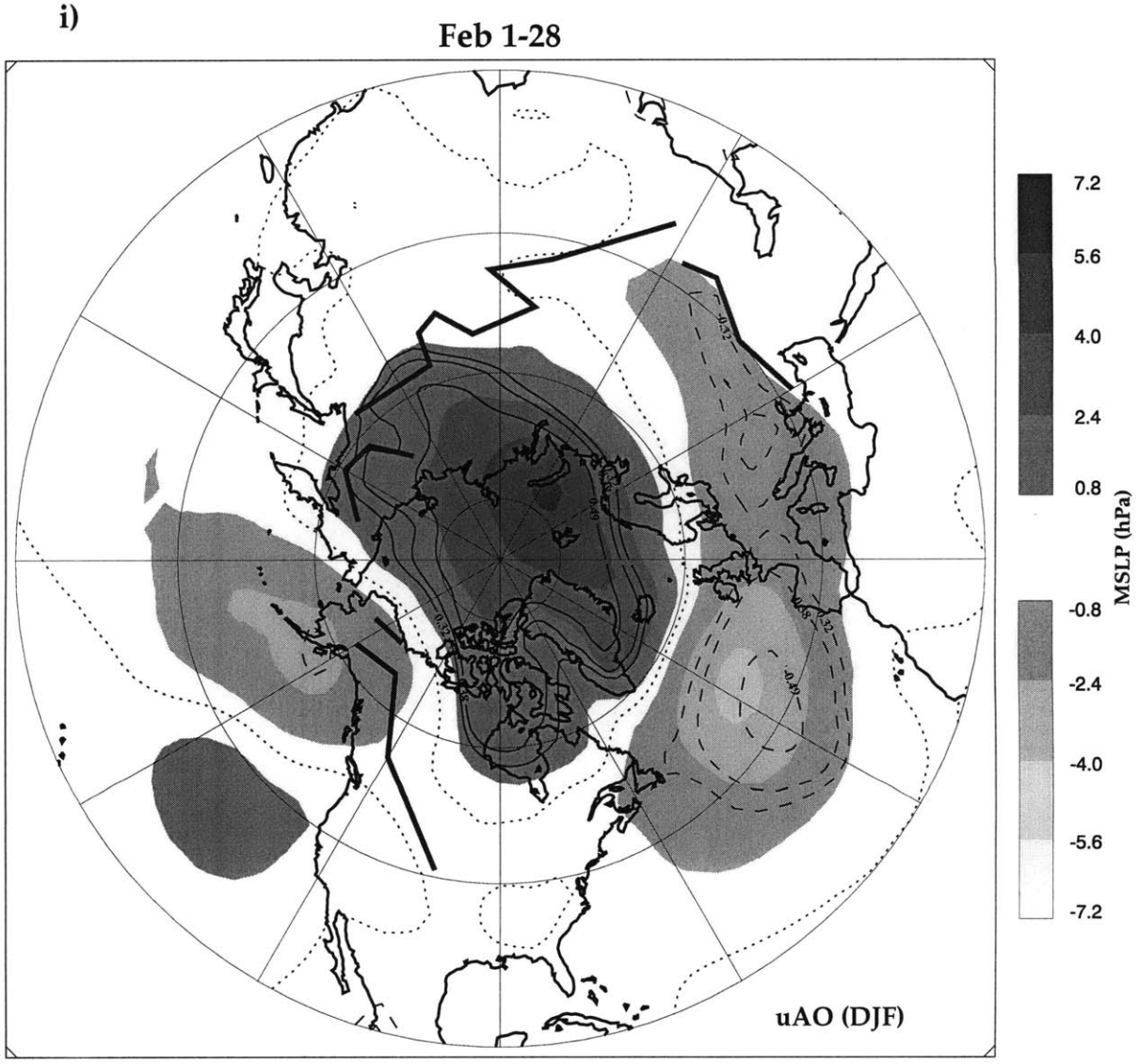

Figure B.3: *(Continued)*

Bibliography

[1] Anderson, T. W., 1958. *An introduction to multivariate statistical analysis.* John Wiley & Sons, 374pp.

[2] Baldwin, M. P., and T. J. Dunkerton, 1999. Propagation of the Arctic Oscillation from the stratosphere to the troposphere. *J. Geophys. Res.,* **104**(D24), 30,937-30,946.

[3] Baldwin, M. P., W. Lahoz, and A. O'Neil, 1999. Downward propagation of the Arctic Oscillation Signature during recent stratospheric warming. *Proceedings of the American Geophysical Union 1999 Fall meeting, December 13-17 1999,* San Francisco, California, F214.

[4] Bamzai, A. S., 1999. AO-snow cover relationships on Interannual and decadal time scales. *Proceedings of the American Geophysical Union 1999 Fall meeting, December 13-17 1999,* San Francisco, California, F240.

[5] Bamzai, A. S. and J. Shukla, 1999. Relation between Eurasian snow cover, snow depth, and the Indian summer monsoon: An observational study. *J. Clim.,* **12,** 3117-3132.

[6] Barnett, T. P., L. Dümenil, U. Schlese, E. Roeckner, and M. Latif, 1989. The effect of Eurasian snow cover on regional and global climate variations. *J. Atmos. Sci.,* **46,** 661-685.

[7] Barnston, A. G., and R. E. Livezey, 1987. Classification, seasonality and persistence of low-frequency atmospheric circulation patterns. *Mon. Wea. Rev.,* **115,** 1083-1126.

[8] Boville, B. A., 1984. The influence of the polar night jet on the tropospheric circulation in a GCM, *J. Atmos. Sci.,* **41,** 1132-1142.

[9] Bretherton, C. S., and D. S. Battisti, 2000. An interpretation of the results from atmospheric general circulation models forced by the time history of the observed sea surface temperature distribution. *Geophys. Res. Lett.,* **27,** 767-770.

[10] Brown, R. D., 1997. Historical variability in Northern Hemisphere spring snow-covered data. *Ann. Glaciol.,* **25,** 340-346.

[11] Charney, J. G., and P. G. Drazin, 1961. Propagation of planetary-scale disturbances from the lower into the upper atmosphere. *J. Geophys. Res.,* **66,** 83-109.

[12] Cohen, J., 1994. Snow cover and climate. *Weather,* **49,** 150-156.

[13] Cohen, J., and D. Entekhabi, 1999. Eurasian snow cover variability and Northern Hemisphere climate predictability. *Geophys. Res. Lett.,* **26,** 345-348.

[14] Deser, C., 2000. On the teleconnectivity of the "Arctic Oscillation." *Geophys. Res. Lett.,* **27,** 779-782.

[15] Deser, C., and M. Blackmon, 1993. Surface climate variations over the North Atlantic Ocean during winter: 1900-1989. *J. Clim.,* **6,** 1743-1753.

[16] Ding, Y., and T. N. Krishnamurti, 1987. Heat budget of the Siberian High and the winter monsoon. *Mon. Wea. Rev.,* **115,** 2428-2449.

[17] Ding, Y., 1990. Build-up, air mass transformation and propagation of Siberian High and its relations to cold surge in East Asia. *Meteorol. Atmos. Phys.,* **44,** 281-292.

[18] Douville, H., and J.-F. Royer, 1996. Sensitivity of the Asian summer monsoon to an anomalous Eurasian snow cover within the Météo-France GCM. *Clim. Dyn.,* **12,** 449-466.

[19] Dunkerton, T. J., D. A. Ortland, and M. P. Baldwin, 1999. The response of the polar troposphere to stratospheric planetary-wave driving: implications for the Arctic Oscillation. *Proceedings of the American Geophysical Union 1999 Fall meeting, December 13-17 1999,* San Francisco, California, F241.

[20] Fallot, J.-M., R. G. Barry, and D. Hoogstrate, 1997. Variations of mean cold season temperature, precipitation and snow depths during the last 100 years in the former Soviet Union (FSU). *Hydrol. Sciences-J. Sci. Hydrol.,* **42,** 301-327.

[21] Frei, A., and D. A. Robinson, 1999. Northern Hemisphere snow extent: Regional variability 1972-1994. *Int. J. Clim.,* **19,** 1535-1560.

[22] Frei, A., D. A. Robinson, and M. G. Hughes, 1999. North American snow extent: 1900-1994. *Int. J. Clim.,* **19,** 1517-1534.

[23] Gandin, L. S., 1965. The objective analysis of meteorological fields. Leningrad, 1963. English translation, Israel Program for Scientific Translations, Jerusalem, 1965.

[24] Gutzler, D. S., and R. D. Rosen, 1992. Interannual variability of wintertime snow cover across the Northern Hemisphere. *J. Clim.,* **5,** 1441-1447.

[25] Hahn, D. G., and J. Shukla, 1976. Apparent relationship between Eurasian snow cover and Indian summer monsoon rainfall. *J. Atmos. Sci.,* , 2461-2462.

[26] Hurrell, J. W., 1995. Decadal trends in the North Atlantic Oscillation: Regional temperatures and precipitation. *Nature,* **269,** 676-679.

[27] Hurrell, J. W., 1996. Influence of variations in extratropical wintertime teleconnections on Northern Hemisphere temperature. *Geophys. Res. Lett.,* **23,** 665-668.

[28] International Arctic Buoy Programme.
http://www-nsidc.colorado.edu/NASA/GUIDE/docs/dataset_documents/iabp_dataset_doc.html.
Polar Science Center, Applied Physics Laboratory, University of Washington (*http://iabp.apl.washington.edu/*).

[29] Intergovernmental Panel on Climate Change, 1995. *Climate Change 1995,* The science of Climate Change, Cambridge University Press, 572pp.

[30] Johnson, M. A., A. Y. Proshutinsky, and I. V. Polyakov, 1999. Atmospheric patterns forcing two regimes of Arctic circulation: A return to anticyclonic conditions? *Geophys. Res. Lett.,* **26,** 1621-1624.

[31] Kalnay, E., M. Kanamitsu, R, Kistler, W. Collins, D. Deaven, L. Gandin, M. Iredell, S. Saha, G. White, J. Woollen, Y. Zhu, M. Chelliah, W. Ebisuzaki, W. Higgins, J. Janowiak, K. C. Mo, C. Ropelewski, J. Wang, A. Leetmaa, R. Reynolds, R. Jenne, and D. Joseph, 1996. The NCEP/NCAR 40-year reanalysis project. *Bull. Amer. Met. Soc.,* **77,** 437-471.

[32] Kanno, H., and J. Matsumoto, 1993. Seasonal phase lock of temporal and spatial variations of the lower cold air in the winter Northern Hemisphere. *J. Met. Soc. Japan,* **71,** 111-122.

[33] Kodera, K., and K. Yamazaki, 1994. A possible influence of the recent polar stratospheric coolings on the troposphere in the Northern Hemisphere winter. *Geophys. Res. Lett.,* **21,** 809-812.

[34] Kodera, K., M. Chiba, H. Koide, A. Kitoh, and Y. Nikaidou, 1996. Interannual variability of the winter stratosphere and troposphere in the Northern Hemisphere. *J. Met. Soc. Japan,* **74,** 365-382.

[35] Kodera, K., and H. Koide, 1997. Spatial and seasonal characteristics of recent decadal trends in the northern hemispheric troposphere and stratosphere. *J. Geophys. Res.,* **102,** 19,433-19,447.

[36] Kripalani, R. H., and A. Kuikarni, 1999. Climatology and variability of historical Soviet snow depth data: some new perspectives in snow – Indian monsoon teleconnections. *Clim. Dyn.,* **15,** 475-489.

[37] Kuhn, M, 1989. The role of land ice and snow in climate. In, A. Berger, R. E. Dickinson, and J. W. Kidson (eds.) *Understanding climate change,* American Geophysical union, 17-28.

[38] Kushnir, Y., 1994. Interdecadal variations in North Atlantic sea surface temperature and associated atmospheric conditions. *J. Clim.,* **7,** 141-157.

[39] Latif, M., K. Arpe, and E. Roeckner, 1999. Oceanic control of decadal North Atlantic sea level pressure variability in winter. *Report No. 292,* Max-Planck-Institüt für Meteorologie.

[40] Leathers, D. J., and D. A. Robinson, 1993. The association between extremes in North American snow cover extent and United States Temperature. *J. Clim.*, **6,** 1345-1355.

[41] Lydolph, P. E., 1977. *Climates of the Soviet Union.* World Survey of Climatology **7.,** Elsevier Scientific Publishing company, 443pp.

[42] Makrogiannis, T. J., B. D. Giles, and A. A. Flocas, 1981. The problem of the extension of the Siberian anticyclone towards Southeast Europe, and its relation to Atmospheric circulation anomalies over the Northern Hemisphere. *Arch. Met. Geophys. Biokl.,* **A30,** 185-196.

[43] Matsuno, T., 1970. Vertical propagation of stationary planetary waves in the winter Northern Hemisphere. *J. Atmos. Sci.,* **27,** 871-883.

[44] Mehta, V. M., M. J. Suarez, J. V. Manganello, and T. L. Delworth, 2000. Oceanic influence on the North Atlantic Oscillation and associated Northern Hemisphere climate variations: 1959-1993. *Geophys. Res. Lett.,* **27,** 121-124.

[45] Mysak, L. A., and S. A. Venegas, 1998. Decadal climate oscillations in the Arctic: A new feedback loop for atmosphere-ice-ocean interactions. *Geophys. Res. Lett.,* **25,** 3607-3610.

[46] North, G. R., T. L. Bell, R. F. Cahalan, and F. J. Moeng, 1982. Sampling errors in the estimation of empirical orthogonal function. *Mon. Wea. Rev.,* **110,** 699-706.

[47] Osborn, T. J., K. R. Briffa, S. F. B. Tett, P. D. Jones, and R. M. Trigo, 1999. Evaluation of the North Atlantic Oscillation as simulated by a coupled climate model. *Clim. Dyn.,* **15,** 685-702.

[48] Overland, J. E., J. M. Adams, and N. A. Bond, 1999. Decadal variability of the Aleutian Low and its relation to high-latitude circulation. *J. Clim.,* **12,** 1542-1548.

[49] Perlwitz, J., and H.-F. Graf, 1995. The statistical connection between tropospheric and stratospheric circulation of the Northern Hemisphere in winter. *J. Clim.,* **8,** 2281-2295.

[50] Perlwitz, J., H. F. Graf, and R. Voss, 2000. The leading variability mode of the coupled troposphere-stratosphere winter circulation in different climate regime. *J. Geophys. Res.,* in printing.

[51] Polyakov, I. V., A. Y. Proshutinsky, and M. A. Johnson, 1999. Seasonal cycles in two regimes of Arctic climate. *J. Geophys. Res.,* **104**(C11), 25,761-25,788.

[52] Proshutinsky, A. Y. and M. A. Johnson, 1997. Two circulation regimes of the wind-driven Arctic ocean. *J. Geophys. Res.,* **102**(C6), 12,493-12,514.

[53] Przybylak, R., 2000. Diurnal temperature ranges in the Arctic and its relation to hemispheric and Arctic circulation patterns. *Int. J. Clim.,* **20,** 231-253.

[54] Robertson, A. W., C. R. Mechoso, and Y.-J. Kim, 2000. The influence of Atlantic sea surface temperature anomalies on the North Atlantic Oscillation. *J. Clim.,* **13,** 122-138.

[55] Robinson, D. A., K. F. Dewey, and R. R. Heim, Jr., 1993. Global snow cover monitoring: An update. *Bull. Amer. Met. Soc.,* **74,** 1689-1696.

[56] Rodwell, M. J., D. P. Rowell, and C. K. Folland, 1999. Oceanic forcing of the wintertime North Atlantic Oscillation and European climate. *Nature,* **398,** 320-323.

[57] Rogers, J. C., 1990. Patterns of low-frequency monthly sea level pressure variability (1899-1986) and associated wave cyclone frequencies. *J. Clim.,* **3,** 1364-1379.

[58] Rogers, J. C., and E. Mosley-Thompson, 1995. Atlantic Arctic cyclones and the mild Siberian winters of the 1980s. *Geophys. Res. Lett.,* **22,** 799-802.

[59] Sahsamanoglou, H. S., Makrogiannis, and P. P. Kallimopoulos, 1991. Some aspects of the basic characteristics of the Siberian Anticyclone. *Int. J. Clim.,* **11,** 827-839.

[60] Serreze, M. C., F. Carse, and R. G. Barry, 1997. Icelandic Low cyclone activity: Climatological features, linkages with the NAO, and relationships with recent changes in the Northern Hemisphere circulation. *J. Clim.,* **10,** 453-464.

[61] Serreze, M. C., M. P. Clark, D. L. McGinnis, and D. A. Robinson, 1998. Characteristics of snowfall over the eastern half of the United States and relationships with principal modes of low-frequency atmospheric variability. *J. Clim.,* **11,** 234-250.

[62] Shindell, D. T., R. L. Miller, G. A. Schmidt, and L. Pandolfo, 1999. Simulation of recent northern winter climate trends by greenhouse-gas forcing. *Nature,* **399,** 452-455.

[63] Sutton, R. T., and M. R. Allen, 1997. Decadal predictability of North Atlantic sea surface temperature and climate. *Nature,* **388,** 563-567.

[64] Thompson, D. W. J., and J. M. Wallace, 1998. The Arctic Oscillation signature in the wintertime geopotential height and temperature fields. *Geophys. Res. Lett.,* **25,** 1297-1300.

[65] Thompson, D. W. J., J. M. Wallace, and G. C. Hegerl, 2000. Annular modes in the extratropical circulation. Part II: Trends. *J. Clim.,* **13,** 1018-1036.

[66] Ting M., M. P. Hoerling, T. Xu, and A. Kumar, 1996. Northern Hemisphere teleconnection patterns during extreme phases of the zonal-mean circulation. *J. Clim.,* **9,** 2614-2633.

[67] Ting M., M. P. Hoerling, T. Xu, and A. Kumar, 2000. Reply. *J. Clim.,* **13,** 1040-1043.

[68] Trenberth, K. E., and J. W. Hurrell, 1994. Decadal atmosphere-ocean variations in the Pacific. *Clim. Dyn.,* **9,** 303-319

[69] Vowinckel, E. and S. Orvig, 1970. The climate of the North Polar basin. In *Climates of the Polar regions.* World Survey of Climatology **14.,** Elsevier Scientific Publishing company, 129-252.

[70] Wallace, J. M., and P. V. Hobbs, 1977. *Atmospheric Science.* Academic Press, 467pp.

[71] Wallace, J. M., and D. S. Gutzler, 1981. Teleconnections in the geopotential height field during the Northern Hemisphere winter. *Mon. Wea. Rev.,* **109,** 784-812.

[72] Walland, D. J., and I. Simmonds, 1997. Modelled atmospheric response to changes in Northern Hemisphere snow cover. *Clim. Dyn.,* **13,** 25-34.

[73] Walsh, J. E., W. H. Jasperson, and B. Ross, 1985. Influences of snow cover and soil moisture on monthly air temperature. *Mon. Wea. Rev.,* **113,** 756-768.

[74] Watanabe, M., and T. Nitta, 1998. Relative impacts of snow and sea surface temperature anomalies on an extreme phase in the winter atmospheric circulation. *J. Clim.,* **11,** 2837-2857.

[75] Watanabe, M., and T. Nitta, 1999. Decadal changes in the atmospheric circulation and associated surface climate variations in the Northern Hemisphere winter. *J. Clim.,* **12,** 494-510.

[76] Watanabe, M., M. Kimoto, T. Nitta and M. Kachi, 1999. A comparison of decadal climate oscillations in the North Atlantic detected in observations and a coupled GCM. *J. Clim.,* **12,** 2920-2940.

[77] Wilks, D. S., 1995. *Statistical methods in the atmospheric sciences.* Academic Press, 464pp.

[78] Yamazaki, K., 1989. A study of the impact of soil moisture and surface albedo changes on global climate using the MRI GCM-I. *J. Met. Soc. Japan,* **67,** 123-146.

[79] Yasunari, T., A. Kitoh, and T. Tokioka, 1991. Local and remote responses to excessive snow mass over Eurasia appearing in the Northern spring and summer climate -A study with MRI GCM -. *J. Met. Soc. Japan,* **69,** 473-487.